THE EFFECT OF PIPE-SOIL INTERACTION ON THE RESPONSE OF BURIED PIPELINES TO STRIKE-SLIP FAULT

by

© Mozhgan Asgarihajifirouz

A Thesis Submitted to the
School of Graduate Studies

in partial fulfillment of the requirements for the degree of

Doctor of Philosophy

Faculty of Engineering and Applied Science

Memorial University of Newfoundland

Oct 2023

St. John's Newfoundland Canada

ABSTRACT

Steel pipelines are widely used as a reliable and efficient solution for transmitting oil, gas, water, and other fluids in large quantities. Pipelines are usually buried in the pre-excavated trenches for protection against environmental and functional loads but still threatened by permanent ground displacement caused by geohazards like strike-slip faults. Trenches are usually backfilled with pre-excavated material as the most cost-effective solution. Depending on trenching methodology, environmental loads, and construction strategy, the backfilling material is remolded to different extents. The different stiffness between the backfill and native soil may affect the failure mechanisms of the soil surrounding the pipeline and consequently the pipeline's structural response in the fault zone. Most of the research that have been conducted on the evaluation of pipeline-soil interaction effect on the pipe response has neglected the pipeline-backfill-trench wall interaction effects by assuming a wide trench filled with a uniform backfill. Therefore, a proper understanding of the pipeline structural response to the fault-induced lateral movement needs a deep understanding of pipeline-backfill-trench wall interaction. The pipeline-backfill-trench wall interaction is usually modelled by performing 2D planar large deformation finite element (LDFE) analysis using coupled Eulerian-Lagrangian (CEL) technic, where the pipe is assumed to be rigid. This approach which is usually enforced to minimize the computational effort downplays the significance of longitudinal structural response of the pipeline. Three-dimensional large deformation modelling of the anisotropic soil surrounding the pipeline along with structural deformations is currently not feasible because of needing extreme computations, difficulties in simulation of ground movement,

modelling the multi-contact bodies between the pipe, backfill and trench wall, etc. These difficulties have caused the researchers and engineers to assume a Lagrangian soil domain in 3D analyses and compromise the accuracy of the analysis because of mesh distortion in large deformations. Therefore, there is an industry need for a solution to incorporate the pipeline-backfill-trench wall interaction effects into the 3D analysis of the fault-induced pipeline deformations. In the present study, first the pipeline-backfill-trench wall interaction was incorporated into an analytical pipeline-fault interaction model to examine the strength of analytical methods in implementation of the soil interaction effects. Then a 3D pipeline-fault interaction model was developed using Lagrangian soil domain to investigate the limitations of this approach. Eventually, a new decoupled methodology was developed by combining the advanced continuum modelling of the pipeline-backfill-trench wall interaction using CEL analysis and a 3D beam-spring pipeline model to overcome the aforementioned limitations. The proposed decoupled method comprises to main steps. First a Coupled Eulerian-Lagrangian (CEL) model was used for LDFE analysis of the trenched/backfilled pipeline in a 2D planar fashion to obtain the lateral soil resistance (p-y curves) involving pipeline-backfill-trench interaction effects. Then the extracted lateral soil resistance for various displacements was transferred to a 3D beam-spring pipeline model to obtain the pipeline response to the fault-induced large displacements. The proposed methodology used the accuracy advantage of continuum CEL model with simplicity advantage of beam-spring model to create an efficient tool for incorporation of the pipeline-backfill-trench wall interaction effects into the structural analysis of the pipeline attached by strike-slip fault. Moreover, the results were compared with pre-developed Lagrangian model to assess the improved model performance. The study contributed to a deeper insight

into this challenging engineering problem showing the significance of incorporation of the pipeline-backfill-trench wall interaction effects into the structural analysis of pipelines attacked by fault. In addition, the study resulted in developing a set of analysis tools that can be effectively used in daily engineering practice by the pipeline industry.

STATEMENT OF AUTHORSHIP

I, Mozhgan Asgarihajifirouz, hereby declare that the present doctoral thesis entitled “The effect of pipe-soil interaction on the response of buried pipelines to strike-slip fault" is the original work completed by me under the guidance and supervision of Prof. Hodjat Shiri and co-supervision of Dr. Xiaoyu Dong. This statement encompasses the entirety of the research, analysis, interpretation, and conclusions presented in the thesis.

Following is a list of publications and manuscripts that resulted from this work:

- Asgarihajifirouz, Mozhgan, Xiaoyu Dong, and Hodjat Shiri. "Assessment of the Response of Trenched–Backfilled Pipelines to Strike-Slip Faults: An Analytical Approach." Geosciences 13, no. 2 (2023): 47.
- Asgarihajifirouz, M., Dong, X. and Shiri, H., 2023. “Structural response of the spiral-welded pipelines buried in different uniform soil types to the strike-slip fault”. Journal of Pipeline Science and Engineering, p.100142.
- Asgarihajifirouz, M., Dong, X. and Shiri, H., 2023 “ The pipeline-backfill-trench wall interaction effect on the accumulation of 2D lateral soil resistance against moving pipeline ” (under review as a journal manuscript).
- Asgarihajifirouz, M. and Shiri, H., 2023. “Incorporation of Pipeline-Backfill-Trench wall Interaction into the Structural Analysis of Fault-Induced Steel Pipeline Deformation using a Decoupled Approach” (under review as a journal manuscript).
- Asgarihajifirouz, M., Dong, X. and Shiri, H., 2022. “3D finite element modeling of spiral welded pipe response to strike-slip fault”. 75th Canadian Geotechnical Conference, Calgary, Alberta, Canada, October 2022.

- Asgarihajifirouz, M., Dong, X. and Shiri, H., 2023. "The effect of pipeline-seabed interaction on its response to the strike-slip fault". 33rd International Ocean and Polar Engineering Conference (ISOPE), Ottawa, Ontario, Canada, June 2023.

I acknowledge that any ideas, concepts, theories, methodologies, or findings derived from external sources are appropriately credited and referenced within the thesis. The contributions of others to this work, whether in the form of data, concepts, or intellectual guidance, have been diligently acknowledged and attributed.

I express my sincere gratitude to all individuals, institutions, and funding bodies that have supported and contributed to the successful completion of this research. Their assistance, guidance, and resources have been invaluable in shaping the direction and outcome of this study.

Mozhgan Asgarihajifirouz

October 2023

ACKNOWLEDGMENT

First and foremost, I would like to express my great gratitude to my supervisor, Prof. Hodjat Shiri, for guiding me throughout the research journey and providing me with opportunities for professional development.

Further, I would like to thank my co-supervisor, Dr. Xiaoyu Dong, for the thoughtful recommendations on this dissertation.

I gratefully acknowledge the financial support of Wood Group through establishing the Research Chair program in Arctic and Harsh Environment Engineering at the Memorial University of Newfoundland. Special thanks are extended to NSERC through the NSERC CRD program and DIET through RDC Collaborative fund for providing financial resources for conducting this research program.

I am also thankful to the Engineering Graduate Studies Office staff for their patience, willingness to help, and thoughtful guidance. My sincere thanks go to Dr. Eduardo Ribeiro Malta for scientific discussions in our research group.

I would like to thank my parents for supporting me. Without their endless love, encouragement, and spiritual support, I would not have been able to conduct and complete this research. I am genuinely thankful for having you in my life.

I dedicate this thesis to God Almighty, my creator, the source of wisdom, insight, and understanding.

My journey continues after this thesis.

Contents

List of Figures

List of Tables

List of Abbreviations and Symbols

Abbreviations

API	American Petroleum Institute
ASCE	American Society of Civil Engineers
CEL	Coupled Eulerian-Lagrangian
DNV	Det Norske Veritas
FE	Finite Element
FEA	Finite Element Analysis
FEM	Finite Element Model
HDPE	High-Density Polyethylene
LDFE	Large Deformation Finite Element
M-C	Mohr-Coulomb
PGD	Permanent ground displacement
PRCI	Pipeline Research Council International
TWI	The Welding institute
VUSDFLD	User subroutine to redefine field variables at a material point

Symbols

Chapter 1

β	Fault crossing angle

Chapter 2

Chapter 3

A	Cross section area of the pipe
D	Pipe diameter
E	Young's Modulus
H	burial depth of the pipe
J	inertia moment of the pipe cross section
L	total length of the deformed shape of the pipeline
L_i	distance between the fault and the inflection point
L_1	distance of the fault and the end point with bending moment equal to zero
L_2	distance of the fault and the end point with bending moment equal to zero
W	Trench width
b	Soil resistance ratio
d	value of ground-induced displacement
d_y	value of ground-induced displacement corresponding to pipeline first yielding
k	pipeline bending curvature
p_u	soil resistance per unit length in horizontal direction
q_{u1}	soil resistance per unit length in vertical direction corresponding to length L_1

q_{u2}	soil resistance per unit length in vertical direction corresponding to length L_2
t	Pipe thickness
β	Fault crossing angle
ε_b	maximum bending strain
ε_m	axial membrane strain

Chapter 4

D	Pipe diameter
H	Burial depth from the pipe center
L	Total length of pipeline
R	Base leg of the triangle
W	Width of the helix
d	Diameter of pipe before the fault rupture
$\acute{d}$	Diameter of pipe after the fault rupture
h	Height of the helix
t	Pipe thickness
β	Fault crossing angle

Chapter 5

D	Pipe diameter
E	Young's modulus
s_u	peak undrained shear strength
$s_{u,r}$	residual undrained shear strength

v	Poison's ratio
γ^p	accumulated plastic shear strain
γ_r^p	the value of γ^p to reduce the shear strength from peak to residual

Chapter 6

D	Pipe diameter
E	Young's modulus
H	Burial depth
L	Unanchored length
p	Pipe internal pressure
r	Ramberg-Osgood parameter
t	Pipe thickness
P_u	Maximum lateral soil friction force
Q_d	Maximum bearing soil friction force
Q_u	Maximum uplift soil friction force
T_u	Maximum axial soil friction force
k_o	Lateral soil pressure coefficient at rest
α	Ramberg-Osgood parameter
β	Fault crossing angle
$\bar{\gamma}$	Unit weight of the pipeline
δ	Fault displacement
Δ_p	Maximum lateral displacement

Δ_t	Maximum axial displacement
Δ_{qu}	Maximum uplift displacement
Δ_{qd}	Maximum bearing displacement
δ_x	Fault displacement in x direction
δ_y	Fault displacement in y direction
ε	strain
ε_{cr}	Critical strain
σ	stress
σ_h	Hoop stress
σ_u	Ultimate stress
σ_y	Yielding stress

Chapter 1

Introduction

1.1. Overview

This chapter provides an overview of this dissertation and describes the research problem and its contribution to the current engineering knowledge. Research objectives are discussed, and the outline of the research is summarized to provide a roadmap for the reader.

1.2. Background

Over the past several decades, buried steel pipelines have been very important infrastructures in the transmission and distribution of oil, gas, water, and other fluids in large quantities. There is no doubt that pipelines have made a significant contribution to the economic growth of communities throughout the world. Pipelines are usually buried for physical protection against the environmental and functional loads but are still threatened by permanent ground displacements (PGD). PGDs can be caused by several sources, including liquefaction-induced lateral spreading, landslides, faults, and seismic settling. Although faulting and landslides generate PGD in small areas of the buried pipeline, the damage risk is rather substantial since PGD causes significant deformation (O'Rourke and Palmer 1996, Tang 2000, Chen et al. 2002).

A significant amount of research has been conducted worldwide on how to increase pipeline safety against seismic hazards, and this topic continues to be a very important for the pipeline industry with a range of remaining knowledge gaps. Analytical methods is one

of the areas that has been used to investigate the structural safety and health of pipelines under faulting(e.g., Newmark and Hall 1975, Kennedy et al. 1977, Karamitros et al. 2011, Sarvanis and Karamanos 2017, Talebi and Kiyono 2020), numerical methods (Trifonov 2015, Vazouras et al. 2015, Demirci et al. 2018) and experimentally (Ha et al. 2010, Xie et al. 2013, O'Rourke et al. 2016, Sarvanis et al. (2018) and Tsatsis et al. 2019). The simplicity and fair accuracy of analytical methods make them an attractive solution for optimization studies, where a large number of simulations shall be done in a short period. Pipeline-soil interaction is probably one of the most challenging areas of pipeline engineering that is associated with a large number of uncertainties and has been widely investigated in the literature. However, the pipeline-backfill-trench wall interaction is even more complicated but less-explored and has a significant impact on the structural response of the pipeline to PGDs. Pipelines are usually buried in excavated trenches for protection against environmental loads (see Figure 1- 1). Depending on the methodology of trenching, environmental loads, and construction strategy, the backfilling material is remolded to different extents. The different stiffness between the backfill and native soil may affect the pipeline response in the fault zone.

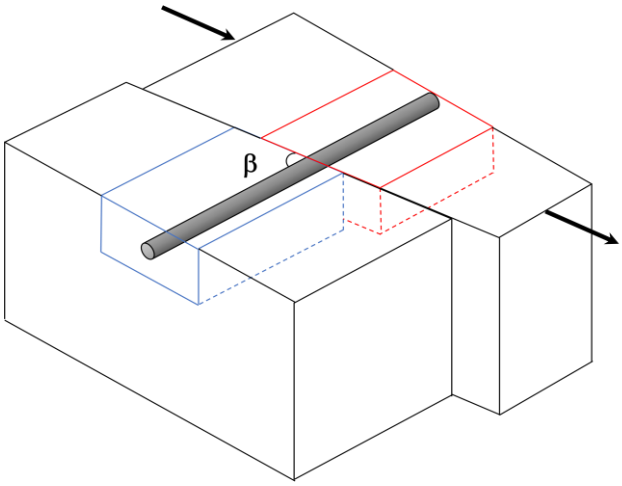

Figure 1- 1. Earthquake-induced ground rupture schematic shape for the strike-slip fault.

The mechanical behaviour of the pipeline because of fault crossing can be investigated numerically using continuum or beam-spring models (Xu et al. 2021). The pipeline's local buckling and the pipe-soil interaction can be assessed with a continuum model through the analysis of pipe-fault crossing. However, the model length is limited, and the trench geometry is typically ignored in the analysis. There are a number of limitations associated with the pipeline-backfill-trench interaction affecting fault-induced lateral pipeline displacements using the continuum model. However, the trench geometry is an essential issue in simulating the pipeline-backfill-trench interaction, as discussed by Trifonov 2015, Cheng et al. 2019, Shiri and Kianian 2020 and Kianian and Shiri 2021a and b.

1.3. Motivation for research

The main motivation of the present study is to first develop an accurate and cost-effective methodology to incorporate the pipeline-backfill-trench wall interaction effect into the structural analysis of pipeline affected by fault-induced lateral displacements, and second

to investigate its influence on pipeline response to strike-slip fault. This methodology is needed to overcome the limitations of the existing simulation methods such as extensive computational effort, difficulties in the simulation of ground movement in an LDFE analysis, proper modelling of the multi-contacts between the pipeline, backfill, and trench wall, etc. Usually, the large deformation finite element (LDFE) analysis of pipeline-backfill-trench interaction is conducted by assuming a rigid pipe in a plain-strain condition, which lacks providing any information about the 3D response of the buried pipeline to the large lateral displacements. Simultaneous continuum modelling of the 3D pipe and the surrounding non-uniform soil impose extreme computational costs and convergence problems. The current study is to investigate this challenging aspect and fill some of the existing knowledge gaps by developing a new analysis approach.

1.4. Key objectives

The specific objectives that underpin this research include short-term and long-term objectives. The short-term is to develop a simplified and robust methodology to incorporate the pipeline-backfill-trench interaction to the fault-induced structural analysis. The long-term objective is to improve the pipeline's integrity to protect society and the environment. Therefore, in this dissertation, the short-term objective is conducted as follows:

- Adopt an existing closed-form solution to analytically incorporate the trenching/backfilling effect on the lateral pipeline response to fault-induced displacements,

- Develop a 3D continuum model with Lagrangian soil domain to examine the functionality of the current approaches in analysis of the pipeline attacked by strike-slip fault,
- Use the Lagrangian soil model to investigate the performance of helical spiral welded pipe to strike-slip faults and determine the best helix angle when the trenching/backfilling effect is incorporated,
- Develop a Coupled Eulerian-Lagrangian (CEL) model to obtain the mobilized soil resistance (p-y curves) against the large lateral displacement of trenched/backfilled pipeline,
- Develop a decoupled method to incorporate the p-y curves obtained from CEL analysis into a 3D beam-spring model to investigate the pipeline response to lateral strike-slip faults,
- Conduct a parametric study using the developed decoupled method and provide practical recommendations for incorporation of the pipeline-backfill-trench wall interaction effects into the pipeline design for strike-slip faults.

1.5. Organization of the Thesis

The road plan for achieving the aforementioned research objectives is divided into seven chapters that have been prepared paper-based.

Chapter 1 presents an introduction to the problem statement, research motivation, and the novelty of conducted research work. Chapter 2 presents a summary of the literature review and describes the challenges of finite element methods on the pipe-backfill interaction due to strike-slip fault movement to provide well understanding of the 3D modelling of this

issue that an engineer might face. In addition, each chapter has its literature review as an independent journal manuscript. Chapter 3 is an investigation of pipeline-backfilling soil interaction using a modified analytical method. This chapter presents the incorporation of trenching/backfilling effect into the pipeline structural response. This chapter has been published as a journal paper in Geosciences. Chapter 4 is an investigation of the spiral-welded pipeline to the strike-slip fault using the Lagrangian method. This chapter tries to highlight the effects of soil types and fault intersection angles on the mechanical behaviour of the spiral-welded pipeline, considering different helical angles. The chapter is to show the limitations of the Lagrangian approach for modelling the soil and to compare the results in later stages with newly developed method. Chapter 5 presents the CEL 2D analysis of lateral pipeline-backfill-trench wall interaction and extraction of the lateral p-y curves that will be fed into the decoupled analysis in Chapter 6. This chapter has been submitted to a journal as a manuscript. Chapter 6 present the development of a decoupled method and the 3D beam-spring model and assesses the pipeline-backfill–trench wall interaction effect in pipeline structural analysis under fault action. Chapter 7 summarizes the key findings of the study and the recommendations for future studies.

1.6. Thesis outcomes

The following are the disseminated outcomes of this research including four journal papers, two published, two under review, and two published peer-reviewed conference papers:

Asgarihajifirouz, Mozhgan, Xiaoyu Dong, and Hodjat Shiri. "Assessment of the response of trenched–backfilled pipelines to strike-slip faults: an analytical approach." Geosciences 13, no. 2 (2023): 47.

Asgarihajifirouz, M., Dong, X. and Shiri, H., 2023. “Structural response of the spiral-welded pipelines buried in different uniform soil types to the strike-slip fault”. Journal of Pipeline Science and Engineering, p.100142.

Asgarihajifirouz, M., Dong, X. and Shiri, H., 2023 “ The pipeline-backfill-trench wall interaction effect on the accumulation of 2D lateral soil resistance against moving pipeline” (under review as a journal manuscript).

Asgarihajifirouz, M. and Shiri, H., 2023. “Incorporation of pipeline-backfill-trench wall interaction into the structural analysis of fault-induced steel pipeline deformation using a decoupled approach” (under review as a journal manuscript).

Asgarihajifirouz, M., Dong, X. and Shiri, H., 2022. “3D finite element modeling of spiral welded pipe response to strike-slip fault”. 75th Canadian Geotechnical Conference, Calgary, Alberta, Canada, October 2022.

Asgarihajifirouz, M., Dong, X. and Shiri, H., 2023. “The effect of pipeline-seabed interaction on its response to the strike-slip fault”. 33rd International Ocean and Polar Engineering Conference (ISOPE), Ottawa, Ontario, Canada, June 2023.

References

Chen, W.W., Shih, B.J., Chen, Y.C., Hung, J.H. and Hwang, H.H., 2002. Seismic response of natural gas and water pipelines in the Ji-Ji earthquake. Soil Dynamics and Earthquake Engineering, 22(9-12), pp.1209-1214.

Cheng, X., Ma, C., Huang, R., Huang, S. and Yang, W., 2019. Failure mode analysis of X80 buried steel pipeline under oblique-reverse fault. Soil Dynamics and Earthquake Engineering, 125, p.105723.

Demirci, H.E., Bhattacharya, S., Karamitros, D. and Alexander, N., 2018. Experimental and numerical modelling of buried pipelines crossing reverse faults. Soil Dynamics and Earthquake Engineering, 114, pp.198-214.

Ha, D., Abdoun, T.H., O'Rourke, M.J., Symans, M.D., O'Rourke, T.D., Palmer, M.C. and Stewart, H.E., 2010. Earthquake faulting effects on buried pipelines–case history and centrifuge study. Journal of earthquake engineering, 14(5), pp.646-669.

Karamitros, D.K., Bouckovalas, G.D., Kouretzis, G.P. and Gkesouli, V., 2011. An analytical method for strength verification of buried steel pipelines at normal fault crossings. Soil Dynamics and Earthquake Engineering, 31(11), pp.1452-1464.

Kennedy, R., Chow, A., and Williamson, R. 1977. Fault Movement Effects on Buried Oil Pipeline. Transportation Engineering Journal of ASCE, 103, 617-633.

Kianian M, Shiri H. The effect of backfilling stiffness on lateral response of the shallowly trenched-backfilled pipelines in clay. Marine Georesources & Geotechnology. 2021 May 4;39(5):610-22.

Kianian M, Shiri H. Experimental study of trench effect on lateral failure mechanisms around the pipeline buried in clay. Journal of Pipeline Science and Engineering. 2021 Jun 1;1(2):198-211.

Shiri H, Kianian M. Constructional and operational considerations in assessing the lateral response of buried subsea pipelines. In Proceeding, 14th Int. Symp. on Frontiers in Offshore Geotechnics. Reston, VA: ASCE 2020.

Newmark, N.M. and Hall, W.J., 1975. Pipeline design to resist large fault displacement. In Proceedings of US national conference on earthquake engineering (Vol. 1975, pp. 416-425).

O'Rourke, T.D. and Palmer, M.C., 1996. Earthquake performance of gas transmission pipelines. Earthquake Spectra, 12(3), pp.493-527.

O'Rourke, T.D., Jung, J.K. and Argyrou, C., 2016. Underground pipeline response to earthquake-induced ground deformation. Soil Dynamics and Earthquake Engineering, 91, pp.272-283.

Sarvanis, G.C. and Karamanos, S.A., 2017. Analytical model for the strain analysis of continuous buried pipelines in geohazard areas. Engineering structures, 152, pp.57-69.

Sarvanis, G.C., Karamanos, S.A., Vazouras, P., Mecozzi, E., Lucci, A. and Dakoulas, P., 2018. Permanent earthquake-induced actions in buried pipelines: numerical modeling and experimental verification. Earthquake Engineering & Structural Dynamics, 47(4), pp.966-987.

Talebi, F. and Kiyono, J., 2020. Introduction of the axial force terms to governing equation for buried pipeline subjected to strike-slip fault movements. Soil Dynamics and Earthquake Engineering, 133, p.106125.

Tang, A.K., 2000. Izmit (Kocaeli), Turkey, Earthquake of August 17, 1999 Including Duzce Earthquake of November 12, 1999: Lifeline Performance. ASCE Publications.

Tsatsis, A., Loli, M. and Gazetas, G., 2019. Pipeline in dense sand subjected to tectonic deformation from normal or reverse faulting. Soil Dynamics and Earthquake Engineering, 127, p.105780.

Trifonov, O.V., 2015. Numerical stress-strain analysis of buried steel pipelines crossing active strike-slip faults with an emphasis on fault modeling aspects. J. Pipeline Syst. Eng. Pract, 6(1), p.04014008.

Vazouras, P., Dakoulas, P. and Karamanos, S.A., 2015. Pipe–soil interaction and pipeline performance under strike–slip fault movements. Soil Dynamics and Earthquake Engineering, 72, pp.48-65.

Xie, X., Symans, M.D., O'Rourke, M.J., Abdoun, T.H., O'Rourke, T.D., Palmer, M.C. and Stewart, H.E., 2013. Numerical modeling of buried HDPE pipelines subjected to normal faulting: a case study. Earthquake Spectra, 29(2), pp.609-632.

Xu, R., R. Jiang, and T. Qu. 2021. Review of dynamic response of buried pipelines. J. Pipeline Syst. Eng. Pract. 12 (2): 03120003.

Chapter 2

Literature Review

2.1. Overview

This chapter attempts to provide a brief review of what has been published in this field so far. There are few studies that investigated the pipe-soil interaction due to the strike-slip fault. The studies can be divided into three main categories: analytical, finite element, and experimental studies, all of which are discussed in the following sections.

2.2. Introduction

Major permanent ground displacement (PGD) types include liquefaction-induced lateral spreading, landslides, faulting, and seismic settling. Although the PGD generated by seismic events such as faulting and landslides is limited to small area in the piping system, the damage possibility is rather considerable because PGD exerts significant deformation on the pipelines. The PGD may induce tensile, compressive, and bending strains along the pipeline. Figure 2-1 shows the different types of fault ruptures.

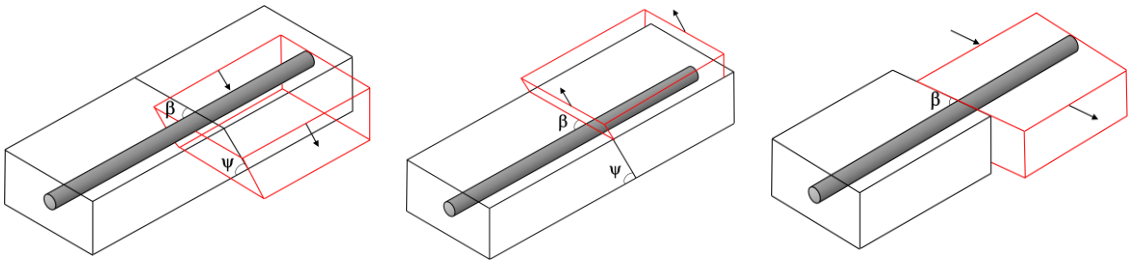

(a) (b) (c)

Figure 2-1. Schematic shape of different types of fault ruptures, (a) normal, (b) reverse, (c) strike-slip fault.

Strike-slip fault movements typically result in pipeline bending due to the shear stress generated by the lateral movement of the two fault blocks (O'Rourke and Liu 2012). The extent of bending depends on several factors, including the pipeline-fault intersection angle. A positive intersection angle (β) typically leads to compression and bending, whereas a negative angle results in tension and bending of the pipeline (Xie et al., 2011).

Normal fault movements typically induce tensile stress in the pipeline, which could result in longitudinal stretching and/or bending of the pipeline (O'Rourke and Bonneau, 2007). In contrast, reverse fault movements lead to compressive stresses, which could cause buckling or wrinkling of the pipeline. The concentrated compressive strain on the cross-section of the pipeline leads to the initiation of wrinkles (Karamanos (2002); Houliara and Karamanos (2006); Kyriakides, and Corona (2007)).

In general, pipelines are designed to withstand a certain amount of bending, tensile, and compressive stress. However, if the stress or strain exceeds the pipeline's design limits, it can result in deformation, buckling, rupture, or other types of failure. Therefore, it is essential to evaluate the pipeline's response to different types of fault movements and design the pipeline accordingly to ensure its safety and reliability. In this chapter, the existing methods and studies will be discussed.

2.3. Methodology

2.3.1. Analytical methods

The structural safety assessment under fault movement can be investigated by analytical methods. Different analytical models have been proposed to evaluate the performance of pipelines at crossing areas. The analytical methods are particularly time-efficient and

helpful for the initial designing of pipelines supposed to fault movements. This analysis can be considered as a confidence check for more complicated analytical results. They can provide insights into stress concentrations, bending moments, and deformation characteristics near the fault. These models often consider soil-structure interaction, pipe-soil interaction, and external load effects.

The first study of the lifeline earthquake project started after the San Fernando earthquake in 1971; then, further research was conducted to evaluate the response of pipelines in the seismic zone. Newmark and Hall (1975) established a simplified analytical model for pipelines subjected to tensile strain due to right-lateral strike-slip fault actions to study the failure mechanisms of the pipeline. The pipeline elongation was calculated using the small deflection theory. The passive soil pressure was neglected in this analytical model, and the elastic-plastic model was used to define the pipeline material. Kennedy et al. (1977) extended Newmark and Hall's model (1975) using the large deflection theory and considering the interaction effect between the pipeline and surrounding soil laterally and longitudinally. The entire pipeline was hypothesized to yield in the transitional region (high curvature region), and it was assumed that the pipeline would perform like a flexible cable without flexural strength in the transition zone. The proposed model has been presented in Figure 2-2.

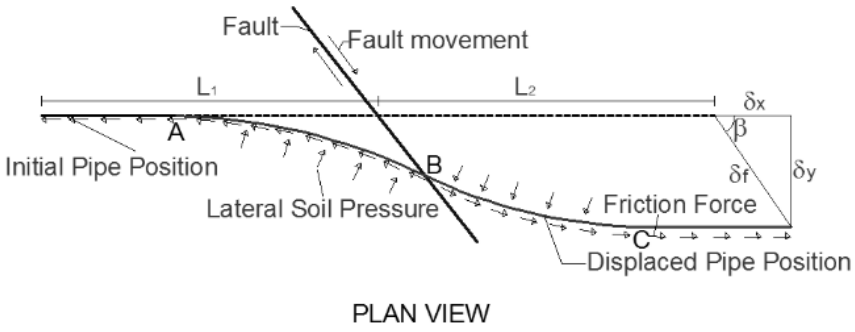

Figure 2-2. The analytical model proposed by Kennedy et al. (1977).

Wang and Yeh (1985) improved Kennedy et al.'s model (1977) and proposed a closed-form solution based on the elastic foundation theory to solve the pipe-soil interaction problem. In their study, the effect of large axial strain and the pipe-soil lateral interaction on the bending stiffness of pipelines were considered. Figure 2-3 represents the proposed analytical model by Wang and Yeh (1985).

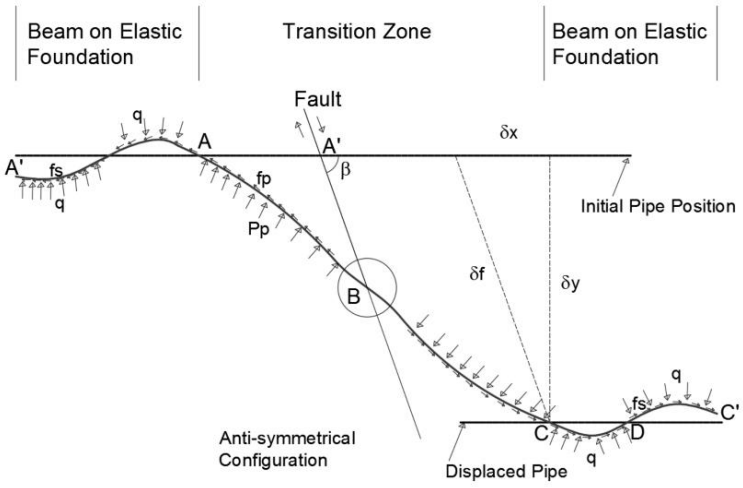

Figure 2-3. The analytical model in Wang and Yeh (1985).

The semi-analytical models were developed in the subsequence of these publications by Takada et al. (2001), Karamitros et al. (2007), and Trifonov and Cherniy (2010). Takada et al. (2001) used a beam-shell hybrid model to investigate the failure mechanism of pipelines. They developed the analytical methods considering the large deformation of the pipe cross-section. The maximum compressive and tensile strains were computed by conducting finite element analysis and implementing the simplified equations proposed by Kennedy et al. (1987). Figure 2-4 illustrates the analytical model proposed by Takada et al. (2001). In this method, initially, the bending point location is founded by Kennedy et al.'s equations (1987), then the distance between the fault crossing line and the bending point is calculated.

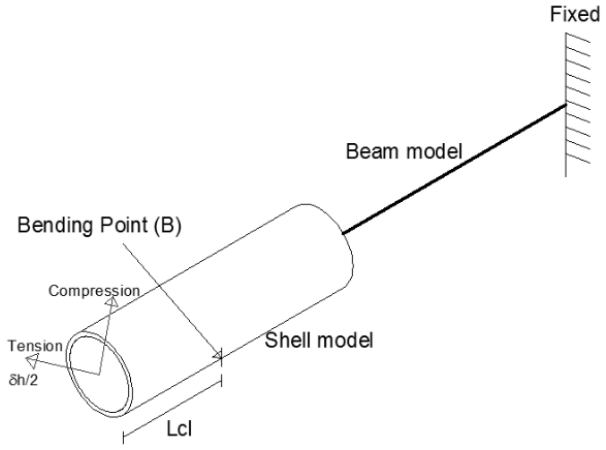

Figure 2-4. The analytical model proposed by Takada et al. (2001).

Karamitros et al. (2007) modified the previous analytical methods to adapt it to a wider range of applications. To measure the influence of axial strain on the pipeline curvature, they employed the equation given by Kennedy et al. (1977). In this model, the geometrical second-order effect was taken into account considering the influence of axial force on pipeline curvature. The modified elastic-plastic cross-section of the pipeline has been

presented in Figure 2-5. The yielding of the pipe wall is shown in red regions on the pipeline cross-section. Karamitros et al. (2007) calculated the overall axial force by integrating the stresses across the pipeline cross-section.

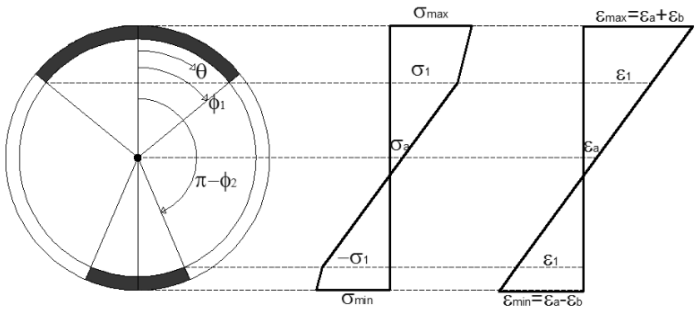

Figure 2-5. Modified elastic-plastic strain distribution on the cross-section of pipeline (Karamitros et al. (2007)).

Trifonov and Cherniy (2010) developed the proposed analytical technique by Karamitros et al. (2007) to investigate the pipelines' response crossing normal faults. In the modified method, the bending effect on the axial strain is considered. Besides, there is no symmetry requirement condition to achieve different forms of fault movement mechanisms (see Figure 2-6). Moreover, the axial force is directly considered in the equations of motion in the transitional region.

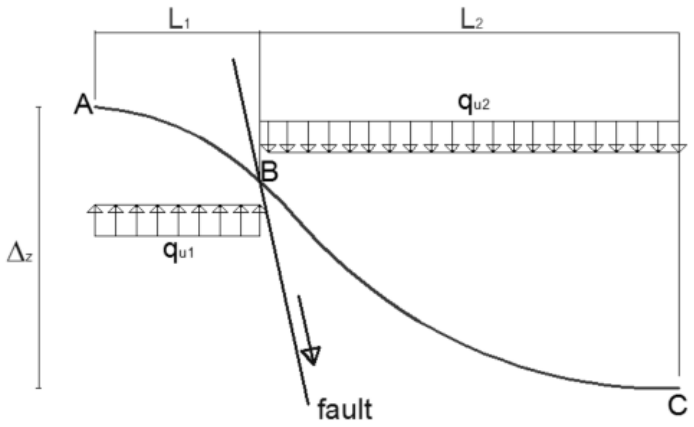

Figure 2-6. The transitional zone in Trifonov and Cherniy (2010) study.

Sarvanis and Karamanos (2017) developed an analytical method to calculate pipeline strains due to permanent ground displacements. In this method, the maximum pipeline strains are calculated using a closed-form solution. In the proposed method, the assumed shape function for pipeline deflection was suited for any kind of fault movement when pipelines are exposed to bending and tension. The length of the deformed pipeline is calculated using an equivalent static method.

Suggested analytical methods in the literature cannot well evaluate the response of pipelines exposed to considerable compressive strain because they do not consider the effects of local buckling and section distortion caused by compressive strain in the pipelines. Besides, pipelines are usually buried in excavated trenches for protection against environmental loads. The different stiffness between the backfill and native soil may affect the pipeline response in the fault zone. The previously proposed analytical methods ignore the effect of pipe-backfilling soil interaction.

2.3.2. Numerical methods

In recent decades, the numerical method has been considered very popular in solving engineering problems, especially for civil engineering analysis. Numerical modelling is a highly effective technique for modelling physical problems. The benefit of using the numerical model is applying various changes to boundary conditions, geometry, and material nonlinearity. Therefore, this method is one of the most effective approaches for investigating the reaction of pipes exposed to PGD.

The pipeline mechanical behaviour can be simulated numerically using beam-type and continuum models. The details of these numerical methods are presented below briefly.

- Beam-type model

In this model, the pipeline is meshed using beam elements. The strains and stresses are calculated at the integration points. The soil is modelled using four different nonlinear springs (axial, transverse horizontal, vertical downward, and vertical upward springs). The properties of these springs and the implementation of this method can be found in ASCE Guidelines, ALA Guidelines, CSA Guidelines, and EN 1998-4 to assess the pipeline behaviour.

- Continuum model

In this method, the pipeline is meshed by shell finite element, and the surrounding soil is modelled by 3D solid elements. Besides, the pipe-soil interaction is simulated by contact elements. This method is typically used to estimate the pipe-soil interaction in a more

accurate manner. Although some approximations are involved, it can accurately represent the behaviour of pipeline response to fault crossing.

Lim et al. (2001) developed a model using FE method to simulate the pipe-soil interaction. The developed model was based on the beam on the elastic foundation theory. In this study, beam elements were used to model the pipe, and soil springs for the soil-pipe interaction. An elastoplastic behaviour was considered to model the pipeline behaviour. The soil-pipeline contact was modelled using the relationship between soil stiffness and shear modulus. Consequently, they determined the maximum magnitude and length of lateral displacement that can cause local buckling failure.

Hybrid models are another type of FE method. Several research has been conducted using hybrid model to simulate the nonlinear response of pipelines under PGD (Yoshizaki et al. (2001), Takada et al. (2001), and Karamitros et al. (2007)). In this model, shell elements were implemented to model bending deformation and local buckling of the pipeline in the large deformation area and beam elements were used in the area with small deformations. The beam and shell elements were linked with rigid elements. The pipe-soil interaction was modelled using discrete spring elements in both the longitudinal and circumferential orientations for the beam and shell elements.

Takada et al. (2001) determined the relationship between bending angle and maximum strain for various pipeline. Yoshizaki et al. (2001) using low-angle elbows simulated large-scale buried pipelines and conformed that using hybrid model for FE analysis induces results that are in a good agreement with experimental study.

Liu et al. (2004) created a novel numerical approach, the equivalent boundary technique, to reduce the amount of memory required and the computation time. To simulate the local

buckling and large section deformation in the pipe, the pipeline section near the fault was simulated by shell element. In contrast to the hybrid model, nonlinear spring elements were implemented at the shell model's boundaries rather than beam elements. Both sides of the shell model were given equivalent boundaries. The fixed boundary shell model was used to validate the equal boundary element method. It is observed that using boundary springs reduces memory and computation time by shortening the model length.

Vazouras et al. (2010, 2012, 2015) used an extended prismatic model to model buried pipelines. The pipe was modelled using shell components. To model soil behaviour, an elastic- perfectly plastic Mohr-Coulomb model was used. A contact algorithm was used to model the soil-pipeline interaction. Tangential contact was implemented as a penalty frictional contact with a friction coefficient of 0.3. Normal contact was regarded as hard contact because it allowed the pipe and soil to separate. Vazouras et al. (2010) examined the mechanical behaviour of buried steel pipes subjected to strike-slip faulting, taking into account steel pipes with varying diameter-to-thickness ratios and steel types. They were particularly interested in the impacts of different soil and pipeline parameters on the behaviour of buried pipes exposed to strike-slip faulting. They observed that in cohesive soils, stiff ground characteristics reduced critical fault movement while softer ground environments increase pipeline deformation capacity under fault crossing. A similar finding was reached for cohesionless soils: loose sand increased critical fault motions, and pipelines placed in compact sands had lower deformation capacity than pipelines placed in loose sands. They also discovered that the interior pressure of the pipe decrease pipeline deformation capacity because of initial pipe material yielding. It was determined that improving the pipe material quality enhanced the pipe deformation capacity under fault

movements. At fault crossings, thick-walled pipelines were proposed because they minimized the buckling risk of buried pipelines crossing active faults.

Vazouras et al. (2012) expanded their study that had been done in 2010 on buried steel pipes crossing the fault considering various angles. They explored the influence of interior pressure on pipeline response. FEA was used to establish and evaluate strain-based performance criteria such as tensile failure, local buckling, and ovalisation. The performance factors that control various fault crossing angles were also investigated. As buried pipelines were compressed and bent, they observed that local buckling was the common performance criterion. The controlling mechanisms of pipelines under tension loading were ovalisation and tensile failure. They reached a conclusion that, like Vazouras et al. (2010), softer ground soil led to a greater deformation capacity of the pipeline. It was also shown that the ovalisation efficiency of pipes might improve when internal pipe pressure is noticeable.

Vazouras et al. (2015) studied the influence of boundary conditions on the response of buried pipelines to oblique strike-slip fault movement. To describe the elasticity of the end sections, they devised closed-form approaches for straight buried pipelines exposed to pure tension. The pipeline performance parameters for pipeline crossing strike-slip faults at various angles were explored, including ovalisation, local buckling, and tensile rupture. Considering the end circumstances, a simple formulation for illustrating the possibility of local buckling was provided. They conducted that the suggested closed-form nonlinear force-displacement equations for buried pipes under tension accurately approximated axial strains and pipeline displacements. Using the suggested closed-form nonlinear force-displacement equations, equivalent boundary springs at pipe ends can be obtained.

Using the finite element software ABAQUS, Liu et al. (2016) simulated the pipeline response to reverse fault crossing. The pipe was simulated as shell elements in their research, and nonlinear soil springs were employed to describe pipe-soil interaction. In this research, the influence of yield strength and strain hardening parameters on buckling behaviour was studied. They showed that increasing the steel grade (for example, from X-80 to X-90) enhanced the critical fault movement for local buckling because increasing the steel grade improved the pipe steel's yield strength and strain hardening parameter. As a result, upgrading the steel grade may be a viable option for the seismic engineering of buried pipes intersecting active faults.

Ozcebe et al. (2017) created a 3D numerical model in order to model the relationship of buried pipes with large diameters under high pressures where they cross normal faults. Shell elements were employed to depict the pipeline behaviour, while solid continuum elements were employed to simulate the soil around it.

2.3.3. Experimental method

The finite element approach is not only adequate for evaluating the behaviour of buried pipelines, but it is also necessary to verify finite element analysis results utilizing case histories to acquire accurate results. However, there is only a limited quantity of verified case studies available to validate FEA results. Centrifuge-based simulation, 1g scaled tests, and large-scale laboratory testing of buried pipelines are practical approaches for validation and calibration of numerical and analytical outcomes analysis.

Cornell University conducted a large-scale split-box experimental studies to investigate pipe-soil interaction during strike-slip faulting (Palmer et al. (2006), O'Rourke and

Bonneau (2007)). Figure 2-7 depicts the large-scale research facilities that have been implemented at Cornell University.

Figure 2-7. Cornell University Large-Scale Experiment Setup (O'Rourke and Bonneau, 2007).

Large-scale laboratory experiments of buried pipeline reaction to faulting are only achievable at a few locations across the world. Furthermore, large-scale experimentation has limitations owing to practical considerations such as price and size. To physically simulate ground faulting impacts on buried pipelines, O'Rourke et al. (2003, 2005) presented a centrifuge-based technique. They utilized the Rensselaer Geotechnical Centrifuge to create a split container to replicate horizontal fault offsets. Numerous centrifuge experiments were conducted by Ha et al. (2008), Abdoun et al. (2009), Ha et al. (2010), and Xie et al. (2011) to study the reaction of continuous buried pipes exposed to strike-slip faulting. O'Rourke et al. (2003) and (2005) suggested a novel notion based on a centrifuge to evaluate the reaction of a continuous pipeline exposed to strike-slip faults and

compare observed stresses to finite element findings. The analysis revealed that for modest fault deformation where the material of the pipe stayed elastic, the consistency between pipe strains estimated by FE modelling and those observed by centrifuge tests was good. They highlighted that for FE modelling of substantial fault deformations when the pipe material encounters plastic stresses, the actual stress behaviour of the pipe material should be employed.

To examine the influence of the pipe-fault alignment angle on the behaviour of pipes exposed to PGD, Ha et al. (2008) conducted four centrifuge experiments on submerged HDPE pipelines intersecting strike-slip faults. The findings of the analytical simulation presented by Kennedy et al. (1977) were used to compare the observed pipe strains. Combining data from tactile pressure sensor and strain gauges produced transverse force-deformation (p-y) relationships. p-y relationships were compared to ASCE Guidelines (1984) and Turner's suggestion for moist sand in 2004. They discovered a stiffer p-y connection near the fault and a smoother p-y correlation further away from the fault. They determined that the centrifuge experiment results largely follow the trend indicated by Kennedy et al. (1977) analytical simulation, as opposed to recorded peak bending strain quantities that are substantially lower than those anticipated by the Kennedy model. In the centrifuge testing, the force value for plastic p-y behaviour was determined to be reasonably compatible with the ASCE Guidelines (1984). The pipe-fault alignment angle was shown to have a significant impact on axial pipe strain, but only a moderate impact on pipe bending strain.

Abdoun et al. (2009) utilized five pairs of centrifuge experiments to explore the influences of soil moisture content, relative burial depth (H / D), fault offset rate, and pipe size on the

reaction of buried High-Density Polyethylene (HDPE) pipes subjected to strike-slip faulting. They found that the magnitude and positions of peak stresses and peak lateral forces on the pipe are unaffected by fault offset rate (the speed of fault displacement expressed in a unit of displacement per time, such as m/s) or the moisture content of soil. The magnitude and positions of peak strains inside the pipe were found to be significantly influenced by the relative burial depth (H / D). They concluded that the pipeline size to thickness ratio (D / t) has a significant impact on the soil-pipe interface. The maximal lateral force recorded using tactile pressure sensor was found to be close to the levels specified by the ASCE Guidelines (1984).

Ha et al. (2010) employed centrifuge-based method to model the 1999 Izmit Earthquake and compared the findings with a case history of pipe collapse from the 1999 Izmit. They also explored how the faulting direction affected buried HDPE pipelines that crossed strike-slip faults. The centrifuge experiments were conducted to measure the reaction of a pipeline intersecting a strike-slip fault at an angle of 60° and -60°, respectively, with pipes in net tension or compression. The failing process of the buried pipeline undergoing net compression was clearly explained utilizing the experimental findings and comparisons with case studies. To alleviate longitudinal pipe stress, they advised designing the pipe with a 90° pipe-fault alignment angle. Because of their great ductile and flexible behaviour, HDPE pipes were recommended for usage near faults. The maximum soil lateral force may be accurately predicted using the ASCE Guidelines (1984) p-y values.

The impacts of offset rate, pipe size, moisture content, H / D ratio, and fault angle on the response of buried pipelines during strike-slip faulting were investigated using twelve centrifuge experiments by Xie et al. (2011). They compared the recorded axial and bending

strain via experimental with numerical analysis findings generated from FE analysis to investigate the efficacy of the soil spring simulation suggested in the ASCE Guidelines for different values of H / D which is based on the ASCE Guidelines' soil spring simulation. Measurements and numerical analysis were used to verify the analytical methodologies. They stated that the 1D beam simulation is sufficient for acquiring the pipe response to faulting, and that selecting the variables for the soil springs model is critical for accurate pipe response estimations. The maximum lateral soil force recorded using tactile pressure sensor was found to be generally compatible with the ASCE Guidelines' values (1984). However, it was seen that the yield displacement in ASCE and centrifuge experiments differed significantly. They came to the conclusion that numerical modelling using FE Analysis are the ideal method for acquiring precise predictions of the behaviour of HDPE pipelines whose response is greatly impacted by both material and geometric nonlinearities, while analytical models are confined to anticipating the pipeline response owing to the complicated behaviour of the material and geometric nonlinearities. It was discovered that applying the ASCE (1984) soil springs in numerical analysis results in greater peak pipe stresses.

Sim et al. (2012) developed a novel measurement device that can simulate pipelines crossing a strike-slip fault. The faulting and seismic horizontal shake testing apparatus were attached to the shaking table at the same time. They discovered that faulting and shaking at the same time lowered soil shear strength, resulting in lower pipe strains and stresses. They discovered that when the pipe-fault crossing angle dropped, the bending moment within the pipe dropped. They revealed that the difference in the relative density of soil

around pipes caused greater stresses and bending moments in the pipeline. Table 2-1 summarizes the study subjects examined in previous experimental investigations.

Table 2-1. Summaries of conducted experimental studies.

Research	Experiment	Key subjects
O'Rourke et al. (2003)	Centrifuge Tests	• Investigation of the response of buried continuous pipelines to PGD. • The comparison of the measured strains and finite element results.
O'Rourke et al. (2005)	Centrifuge Tests	• Estimation of pipe strains under PGD. • The comparison of the measured strains and finite element results for larger and smaller offsets.
Palmer et al. (2006)	Large-Scale Tests	• The description of the large-scale testing facility at Cornell University. • The description of an experimental plan for evaluating pipeline response systematically. • The working principle of the large-scale testing setup. • Engineering properties of soil used in the experiments.
O'Rourke et al. (2007)	Large-Scale Tests	• Evaluation of steel gas distribution pipeline performance with 90°elbows. • Effects of ground rupture on HDPE pipelines. • Lateral soil-pipe interaction during ground failure.
Ha et al. (2008)	centrifuge Tests	• The effects of the pipe-fault orientation angle on the response of pipe.

		• The comparison of measured pipe strains and results predicted by the Kennedy model. • The evaluation of p-y relations proposed in the ASCE Guidelines.
Abdoun et al. (2009)	Centrifuge Tests	• The effects of moisture content, fault offset rate, relative burial depth (H / D), D / t and pipe diameter on the response of pipe subjected to strike-slip faulting. • The evaluation of p-y relations proposed in the ASCE Guidelines.
Ha et al. (2010)	Centrifuge Tests	• The comparison of results measured by centrifuge model tests and the results observed in a case history of pipe failure in 1999 Izmit. • The effects of the fault crossing angle on the pipeline behaviour. • The evaluation of p-y relations proposed in the ASCE Guidelines.
Xie et al. (2011)	Centrifuge Tests	• The effects of offset rate, moisture content, H / D ratio, pipe diameter, pipe-fault angle on the response of pipelines under strike-slip faulting. • The evaluation of soil spring model in ASCE Guidelines. The evaluation of analytical models.
Sim et al. (2012)	1g-Shake Table Tests	• A new testing setup which can simulate the behaviour of buried pipelines crossing strike-slip faults. • The behaviour of buried pipelines subjected to simultaneous fault movement and shaking.

2.4. Pipe-backfill-trench interaction

The trenching/backfilling effect has not been considered by existing pipeline design codes (e.g., DNVGL-RP-F114, 2017; PRCI, 2009; ALA, 2005; and ASCE committee, 2014). This is because there has been limited exploration of the pipeline-backfill-trench interaction and its impact on soil failure mechanisms.

Although previous studies on pipelines under fault crossings have neglected this interaction, some 2D experimental studies have shown that it is important to consider the difference in stiffness between backfill soil and native ground (i.e., trench wall and bed). Research conducted by Poorooshasb et al. (1994), Paulin (1998), C-CORE et al. (2003), Kouretzis et al. (2013), Chaloulos et al. (2015), Kianian et al. (2018), and Kianian and Shiri (2021a, b, c) demonstrate that lateral soil resistance can be significantly affected by the interaction between pipe-backfill-trench. In 1998, Paulin conducted centrifuge tests to study pipeline-clayey soil lateral interactions, focusing on trench width, burial depth, relative displacement rate, backfill properties, and stress history. Unfortunately, the physical model tests did not allow clear visualization of the failure mechanisms of the backfill and native soils due to the lack of suitable visualization techniques at that time. More recently, Kianian et al. (2018) and Kianian and Shiri (2021a, b) have conducted improved centrifuge tests. These tests incorporated transparent acrylic sheets, digital cameras, and particle image velocimetry (PIV) techniques to visualize progressive and interactive failure mechanisms of the backfill and native soils.

A limited number of numerical studies have also been conducted in the literature to investigate the impact of trenching/backfilling on the lateral soil resistance to moving pipelines (Phillips et al. 2004; Kouretzis et al. 2013; Chaloulos et al. 2015).

Since the problem involves large deformations, it has been extremely difficult to obtain reliable results. A more recent numerical study conducted by Dong et al. (2021) investigated this challenging problem by performing a large deformation finite element analysis using the ABAQUS software package. Two different LDFE approaches were used to develop and compare the models: the first one was remeshing and interpolation technique with small strain analysis (RITSS, Hu and Randolph 1998), and the second one was the Coupled Eulerian-Lagrangian (CEL) analysis. According to the research conducted, the difference in strength between backfill soil and native seabed soil significantly affects the pipes-soil interactions. These numerical modelling results are more in agreement with those obtained from experimental studies.

2.5. Conclusion

Most of the research that has been conducted on the evaluation of pipeline-soil interaction under fault crossing has not considered the backfilling effect. In the previous studies and current design codes like ALA (2001) and PRCI (2009), the pipelines are designed inside a uniform seabed, and the effects of trenching are neglected (the geometry and material properties). Backfilling material is remolded because of trenching, environmental loads, and construction strategy. Therefore, the backfilling material stiffness is less than in native soils. This difference impacts the failure mechanisms of soils surrounding the pipeline. Consequently, it influences the structural response of the pipeline.

The significance of trenching and backfilling on the pipe-backfill-trench interaction has been acknowledged by previous studies. However, this effect has been ignored in the 3D LDFE modelling and large-scale experimental studies. An accurate understanding of the

pipe-backfill-trench interactions using LDFE analysis involves several challenges, including significant computation work, difficulties in simulating fault movement, modelling the contact between the pipeline, backfill, and trench wall, and so on. Because of these reasons, the industry is looking for a more straightforward method to consider this effect.

References

Abdoun TH, Ha D, O'Rourke MJ, Symans MD, O'Rourke TD, Palmer MC, Stewart HE. Factors influencing the behavior of buried pipelines subjected to earthquake faulting. Soil Dynamics and Earthquake Engineering. 2009 Mar 1;29(3):415-27.

ALA, American Lifelines Alliance Guidelines for the Design of Buried Steel Pipes, 2005.

ASCE, Guidelines for the seismic design of oil and gas pipeline systems. New York: ASCE. 1984.

C-CORE, Honegger, Doug, D. G. Honegger Consulting. Extended Model for Pipe Soil Interaction. 2003. Technical Toolboxes, Houston, Texas.

CSA (Canadian Standards Association). Oil and gas pipeline systems. 2019. Z662:19. Etobicoke, Canada: CSA.

Chaloulos YK, Bouckovalas GD, Zervos SD, Zampas AL. Lateral soil–pipeline interaction in sand backfill: effect of trench dimensions. Computers and Geotechnics. 2015 Sep 1;69:442-51.

European Committee for Standardization. Eurocode 8—Design of structures for earthquake resistance—Part 4: Silos, tanks and pipelines. 2006. EN 1998-4:2006. Brussels, Belgium: CEN.

Ha D, Abdoun TH, O'Rourke MJ, Symans MD, O'Rourke TD, Palmer MC, Stewart HE. Buried high-density polyethylene pipelines subjected to normal and strike-slip faulting—a centrifuge investigation. Canadian Geotechnical Journal. 2008 Dec;45(12):1733-42.

Ha D, Abdoun TH, O'Rourke MJ, Symans MD, O'Rourke TD, Palmer MC, Stewart HE. Earthquake faulting effects on buried pipelines–case history and centrifuge study. Journal of earthquake engineering. 2010 May 20;14(5):646-69.

Houliara S, Karamanos SA. Buckling and post-buckling of long pressurized elastic thin-walled tubes under in-plane bending. International Journal of Non-Linear Mechanics. 2006 May 1;41(4):491-511.

Karamanos SA. Bending instabilities of elastic tubes. International Journal of Solids and Structures. 2002 Apr 1;39(8):2059-85.

Karamitros DK, Bouckovalas GD, Kouretzis GP. Stress analysis of buried steel pipelines at strike-slip fault crossings. Soil Dynamics and Earthquake Engineering. 2007 Mar 1;27(3):200-11.

Kianian M, Esmaeilzadeh M, Shiri H. Lateral response of trenched pipelines to large deformations in clay. InOffshore Technology Conference 2018 Apr 30 (p.

D032S092R009). OTC.

Kianian M, Shiri H. The effect of backfilling stiffness on lateral response of the shallowly trenched-backfilled pipelines in clay. Marine Georesources & Geotechnology. 2021 May 4;39(5):610-22.

Kianian M, Shiri H. Experimental study of trench effect on lateral failure mechanisms around the pipeline buried in clay. Journal of Pipeline Science and Engineering. 2021 Jun 1;1(2):198-211.

Shiri H, Kianian M. Constructional and operational considerations in assessing the lateral response of buried subsea pipelines. In Proceeding, 14th Int. Symp. on Frontiers in Offshore Geotechnics. Reston, VA: ASCE 2020.

Kouretzis GP, Sheng D, Sloan SW. Sand–pipeline–trench lateral interaction effects for shallow buried pipelines. Computers and Geotechnics. 2013 Oct 1;54:53-9.

Kyriakides S, Corona E. Mechanics of Offshore Pipelines, Volume 1: Volume 1 Buckling and Collapse.

Kennedy RP, Williamson RA, Chow AM. Fault movement effects on buried oil pipeline. Transportation Engineering Journal of ASCE. 1977 Sep;103(5):617-33.

Lim YM, Kim MK, Kim TW, Jang JW. The behavior analysis of buried pipeline: Considering longitudinal permanent ground deformation. InPipelines 2001: Advances in Pipelines Engineering and Construction 2001 (pp. 1-11).

Liu AW, Hu YX, Zhao FX, Li XJ, Takada S, Zhao L. An equivalent-boundary method for the shell analysis of buried pipelines under fault movement. Acta Seismologica Sinica. 2004 Nov;17:150-6.

Liu X, Zhang H, Han Y, Xia M, Zheng W. A semi-empirical model for peak strain prediction of buried X80 steel pipelines under compression and bending at strike-slip fault crossings. Journal of Natural Gas Science and Engineering. 2016 May 1;32:465-75.

Newmark NM, Hall WJ. Pipeline design to resist large fault displacement. In Proceedings of US national conference on earthquake engineering 1975 Jun 18 (Vol. 1975, pp. 416-425).

O'Rourke M, Gadicherla V, Abdoun T. Centrifuge modeling of PGD response of buried pipe. Earthquake Engineering and Engineering Vibration. 2005 Jun;4:69-73.

O'Rourke TD, Bonneau AL. Lifeline performance under extreme loading during earthquakes. InEarthquake Geotechnical Engineering: 4th International Conference on Earthquake Geotechnical Engineering-Invited Lectures 2007 (pp. 407-432). Dordrecht: Springer Netherlands.

O'Rourke MJ, Liu X. Seismic design of buried and offshore pipelines. MCEER Monograph MCEER-12-MN04. 2012 Nov;380.

Özcebe AG, Paolucci R, Mariani S. Numerical modeling of the interaction of pressurized large diameter gas buried pipelines with normal fault ruptures. Soil Dynamics and Earthquake Engineering. 2017 Oct 1;101:105-15.

Palmer DF, Henyey TL. San Fernando earthquake of 9 February 1971: pattern of faulting. Science. 1971 May 14;172(3984):712-5.

Palmer A, Touhey M, Holder S, Anderson M, Booth S. Full-scale impact tests on pipelines. International journal of impact engineering. 2006 Aug 1;32(8):1267-83.

Phillips R, Nobahar A, Zhou J. Trench effects on pipe-soil interaction. InInternational Pipeline Conference 2004 Jan 1 (Vol. 41766, pp. 321-327).

Poorooshasb F, Paulin MJ, Rizkalla M, Clark JI. Centrifuge modeling of laterally loaded pipelines. 1994.

PRCI, 2009. Guidelines for constructing natural gas and liquid hydrocarbon pipelines through areas prone to landslide and subsidence hazards. In Pipeline Research Council International

Sarvanis GC, Karamanos SA. Analytical model for the strain analysis of continuous buried pipelines in geohazard areas. Engineering structures. 2017 Dec 1;152:57-69.

Sim WW, Towhata I, Yamada S. One-g shaking-table experiments on buried pipelines crossing a strike-slip fault. Geotechnique. 2012 Dec;62(12):1067-79.

Takada S, Hassani N, Fukuda K. A new proposal for simplified design of buried steel pipes crossing active faults. Earthquake engineering & structural dynamics. 2001 Aug;30(8):1243-57.

Trifonov OV, Cherniy VP. A semi-analytical approach to a nonlinear stress–strain analysis of buried steel pipelines crossing active faults. Soil Dynamics and Earthquake Engineering. 2010 Nov 1;30(11):1298-308.

Trifonov OV, Cherniy VP. Elastoplastic stress–strain analysis of buried steel pipelines subjected to fault displacements with account for service loads. Soil Dynamics and Earthquake Engineering. 2012 Feb 1;33(1):54-62.

Vazouras P, Karamanos SA, Dakoulas P. Finite element analysis of buried steel pipelines under strike-slip fault displacements. Soil Dynamics and Earthquake Engineering. 2010 Nov 1;30(11):1361-76.

Vazouras P, Karamanos SA, Dakoulas P. Mechanical behavior of buried steel pipes crossing active strike-slip faults. Soil Dynamics and Earthquake Engineering. 2012 Oct 1;41:164-80.

Vazouras P, Dakoulas P, Karamanos SA. Pipe–soil interaction and pipeline performance under strike–slip fault movements. Soil Dynamics and Earthquake Engineering. 2015 May 1;72:48-65.

Wang LR, Yeh YH. A refined seismic analysis and design of buried pipeline for fault movement. Earthquake engineering & structural dynamics. 1985 Jan;13(1):75-96.

Wang YY, Cheng W, Horsley D. Tensile strain limits of buried defects in pipeline girth welds. InInternational Pipeline Conference 2004 Jan 1 (Vol. 41766, pp. 1607-1614).

Xie X, Symans MD, O'Rourke MJ, Abdoun TH, O'Rourke TD, Palmer MC, Stewart HE. Numerical modeling of buried HDPE pipelines subjected to strike-slip faulting. Journal of Earthquake Engineering. 2011 Dec 1;15(8):1273-96.

YOSHIZAKI K, O'ROURKE TD, HAMADA M. Large deformation behavior of buried pipelines with low-angle elbows subjected to permanent ground deformation. Doboku Gakkai Ronbunshu. 2001 Apr 21;2001(675):41-52.

Yoshizaki K, O'Rourke TD, Hamada M. Large scale experiments of buried steel pipelines with elbows subjected to permanent ground deformation. Structural Engineering/Earthquake Engineering. 2003;20(1):1s-1s.

Yoshizaki K, Sakanoue T. Analytical study on soil-pipeline interaction due to large ground deformation. In13th World Conference on Earthquake Engineering 2004 Aug 1.

Chapter 3

Assessment of the Response of Trenched–Backfilled Pipelines to Strike-Slip Faults: An Analytical Approach

Mozhgan Asgarihajifirouz[1], Xiaoyu Dong[2], Hodjat Shiri[3]

1: Department of Civil Engineering
Memorial University of Newfoundland

2: Post-doctoral Fellow, Department of Civil Engineering
Memorial University of Newfoundland

3: Associate Professor, Department of Civil Engineering
Memorial University of Newfoundland

This chapter has been published as a journal paper.

3.1. Abstract

Trenched pipelines may experience significant lateral displacement due to natural geohazards such as strike slip-fault movements, landslides, etc. Using pre-excavated soil to backfill the trench is a cost-effective option to protect pipelines against large deformations. These backfilling materials are heavily remolded and therefore softer than the native ground. Therefore, the shear strength difference between the backfill and native ground may affect the pipeline-backfill-trench interaction and the failure mechanism of the surrounding soil. By assuming a simplified uniform soil domain, the influence of softer pre-excavated backfilling material on the pipeline-backfill-trench interaction is neglected in the analytical methods that are usually used in the structural health monitoring of buried pipelines. In this study, the effect of trenching and backfilling was incorporated into an analytical solution for a fast assessment of the pipeline response at the early stages of engineering design projects and structural health monitoring. In comparison to other methods, this methodology provides a convenient and efficient method for computing pipeline strain and deflection curves in geohazardous regions.

Keywords: trenched-backfilled pipeline; analytical method; strike-slip fault; native and backfill soil; deflection curve; axial strain

3.2. Introduction

Permanent ground displacement (PGD) caused by fault movement has long been considered to be one of the most significant threats to pipeline safety, serviceability, and economic operation of buried pipelines. Therefore, the structural damage of buried

pipelines caused by fault activities have been a point of attention of pipeline engineers and researchers. The assessment of the pipeline integrity particularly near the fault line requires calculation of the strains developed in the pipeline under the fault effect.

The analytical methods are particularly time-efficient and helpful for the initial design, optimization studies, and structural health monitoring of pipelines exposed to fault movements. The analytical methods can be also considered as a confidence check for more complicated numerical and experimental results.

Initially, the lifeline earthquake studies were developed after the San Fernando earthquake in 1971 to assess the response of pipelines to earthquakes in seismic zones. Newmark and Hall (1975) established a simplified analytical model for pipelines subjected to tensile strain due to right-lateral strike-slip fault actions to study the failure mechanisms of the pipelines. They calculated pipeline elongation using the small deflection theory. The passive soil pressure was neglected in this analytical model, and the elastic-plastic model was used to define the pipeline material. Kennedy (1977) extended the previous study conducted by Newmark and Hall (1975) using the large deflection theory and considering the interaction effect between the pipeline and surrounding soil. In this method, the entire pipeline was hypothesized to yield in the transitional region (high curvature region). The authors assumed that the pipeline would perform like a flexible cable without flexural strength in the transition zone. Vougioukas (1979) developed an analytical method that could be applied to both strike-slip and reverse fault movements. In this methodological approach, the buried pipeline was considered to be elastic beams. Furthermore, the effect of axial forces on flexural stiffness has been considered. In an attempt to understand how the buried gas and water pipelines were affected during the San Fernando earthquake,

McCaffrey and O'Rourke (1983) investigated the performance of gas and water pipelines. Wang and Yeh (1985) improved the Kennedy's model (1977) and proposed a closed-form solution based on the elastic foundation theory to solve the pipe-soil interaction problem. In their study, the effect of large axial strain and the pipe-soil lateral interaction on the bending stiffness of pipelines were considered.

In recent years, Karamitros (2007) developed an analytical method that could be applied to active normal fault-crossing problems. The methodology has been refined by introducing several improvements over the previous methodologies. The stress-strain analysis of buried steel pipelines was performed using simple material nonlinearities and second-order influences. As a result, the beam-on-elastic-foundation and elastic beam theories were combined to calculate the pipeline's bending moment and axial force. Vazouras et al. (2010) developed a simplified analytical formulation in conjunction with the development of rigorous finite element models for describing buried steel pipeline deformation under strike-slip faults. A finite element model was used to investigate the pipeline-soil interaction, which took into account the inelastic behavior of the soil surrounding the pipeline, as well as the large inelastic strains of the pipeline and the special contact between the pipeline and soil. In their study, the analytical model presented the counteracting influence of bending moment and axial tension force.

More recently, Vazouras et al. (2015) extended their previous study and proposed a simplified analytical closed-form solution to describe pipeline deformation under strike-slip faults. This study was a comprehensive study consisting of both closed-form solutions and finite element modeling of pipelines affected by strike-slip fault movement. The study was started by developing a closed-form solution for the force-displacement relationship

of buried pipelines exposed to tension load at both ends in cases where the pipelines have finite and infinite lengths. A refined finite element model was then developed using the closed-form solution in the form of non-linear springs at both ends of the pipeline for evaluating the response of the pipeline to a strike-slip fault. Sarvanis (2017) developed an analytical method to calculate pipeline strains due to permanent ground displacements. In this method, the maximum pipeline strains are calculated using a closed-form solution proposed by Vazouras et al. (2015), where the assumed shape function for pipeline deflection was adopted for any kind of fault movements when pipelines are exposed to bending and tension. The length of the deformed pipeline was calculated using an equivalent static method.

The semi-analytical models were developed in the subsequence of these publications by Takada (2001), Karamitros (2007), and Trifonov and Cherniy (2010). Takada (2001) used a beam-shell hybrid model to investigate the failure mechanism of pipelines. The developed semi-analytical model was able to consider the large deformation of the pipe cross-section. The maximum compressive and tensile strains were computed by conducting finite element analysis and implementing the simplified equations proposed by Kennedy (1987). Karamitros (2007) modified the previous analytical methods to adapt it to a wider range of applications. To measure the influence of axial strain on the pipeline curvature, they employed the equation given by Kennedy (1977). In this model, the geometrical second-order effect was taken into account considering the influence of axial force on pipeline curvature. Trifonov and Cherniy (2010) developed the proposed analytical technique by Karamitros (2007) to investigate the response of pipelines to normal faults. In the modified method, the bending effect on the axial strain was considered. Besides,

there was no symmetry requirement condition to achieve different forms of fault movement mechanisms. Moreover, the axial force was directly considered in the equations of motion in the transitional region.

The continuum numerical model is considered to be the most efficient method for modeling the pipe-fault crossing phenomenon and assessing the local buckling of pipelines. Vazouras et al. (2012) assessed the boundary conditions' effects on pipeline responses. In this study, they investigated the behavior of pipelines with limited and unlimited lengths subjected to different tensile loads. The results show that pipelines exhibit local strain when the fault displacement rate is low. Increasing fault displacement rates result in ovalization phenomena in the local strain spot. Demofonti et al. (2013) investigated the mechanical responses of steel pipelines subjected to a horizontal permanent ground motion under fault crossing experimentally and numerically in order to gain a better understanding of soil and pipe interaction and calibration of numerical models for predicting strain demand in buried pipelines. Zhang et al. (2015, 2016) investigated the buckling behavior of buried pipelines using the finite element method. In their study, they found that fault displacement has a significant impact on the location of the maximum strain in buried pipelines. Additionally, as the thickness of the wall increases, the deformation curve of the buried pipeline becomes smoother.

Neither of these studies have considered the effect of different stiffness of backfill and native soil. Pipelines are usually buried in the excavated trenches for protection against environmental loads, where pre-excavated soil is used to backfill the trench as a cost-effective method. The pre-excavated backfill material is usually heavily remolded and has a lower stiffness compared with native soil. The different stiffness between the backfill and

native soil may affect the pipeline response in the fault zone. Modeling a 3D trench pipeline through the Large Deformation Finite Element (LDFE) analysis faces several challenges, including an extensive computational effort, difficulties in the simulation of ground movement, modeling the contact between the pipe, backfill, and trench wall, etc. These difficulties have caused the researchers to assume a Lagrangian soil domain and compromise the accuracy of the analysis. The present work has investigated the effect of trenching-backfilling on structural response of pipeline to the fault by incorporating pipeline-backfill-trench interaction effects into an analytical solution.

3.3. Analytical model

In this study, the analytical model proposed by Sarvanis (2017) was used to calculate the strains induced in the pipeline due to PGD. The model was extended by incorporation of the trenching-backfilling effects. The PGDs were modelled by the differential motions of the two adjacent soil blocks traversed by the pipeline at the fault crossing line. The model works based on the use of an assumed-shape function for the deformed pipeline, which is the improved version of a simple analytical model previously proposed by Vazouras (2015), which is only applicable to the symmetric soil resistance. Furthermore, the assumed-shape function by Vazouras (2015) did not consider the zero-curvature criterion at the two ends of the deformed pipeline segment, and there was no systematic method for calculating the length of the deformed pipeline. It should be noted that this method might not correctly represent post-buckling pipeline configurations.

3.3.1. Analytical model for uniform seabed

Figure 3-1 shows a schematic view of the model configuration, where the buried pipeline passes a ground discontinuity plane at an angle of β considering uniform seabed. Throughout the following text, the "discontinuity plane" will be referred to as the "fault plane" or “fault”. The primary need for using this approach is that permanent ground deformation causes both tensile and bending deformation of the pipeline when the crossing angle is greater than 0° ($\beta > 0°$). In comparison to the ground on the left side of the fault, the ground on the right-side moves parallel to the fault direction by an amount d. The pipeline is subjected to bending and stretching because of the different ground motions and gets an S-shape configuration, as depicted in Figure 3-1. The lengths L_1 and L_2 in this figure correspond to the lengths of the deformed S-shape of the pipeline on either side of the fault, while L_i represents the distance between the inflection point (the point where the curvature changes sign) and the fault plane.

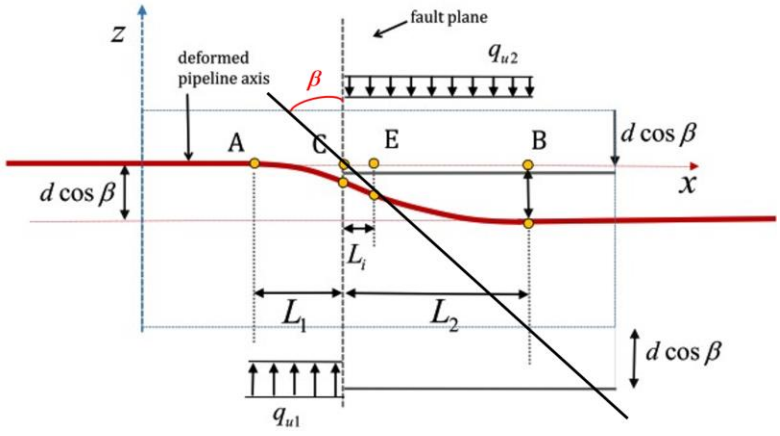

Figure 3-1. Schematic shape of pipeline curvature at active fault zone (Sarvanis (2017)).

As the pipeline moves in the fault zone, the pipeline deflection curve ($u(x)$) follows the equation below:

$$u(x) = \begin{cases} \hat{d}.(L_1 + L_i)cos\beta.\left[1 + \left[\frac{1}{4}\sin\left(\frac{\pi x}{L_1 + L_i}\right)\right] - \left(\frac{x}{L_1 + L_i}\right)\right] \\ 0 \le x \le L_1 + L_i \\ \hat{d}.(L_2 - L_i)cos\beta.\left[1 + \left[\frac{1}{4}\sin\left(\frac{\pi(-x + L_1 + L_i)}{L_2 - L_i}\right)\right] - \left(\frac{x + L_2 - L_1 - 2L_i}{L_2 - L_i}\right)\right] \\ L_1 + L_i \le x \le L \end{cases} \quad (3\text{-}1)$$

In this equation, the normalized ground displacement is $\hat{d} = d/(L_1 + L_2)$. Two ends of deformed shape of pipeline are located at $x = 0$ and $x = L_1 + L_2$; respectively. The proposed shape function ($u(x)$) can be used to both non-symmetric and symmetric circumstances (geometry and the surrounding soil resistance) with respect to the fault. The displacement and curvature continuity criteria at the inflection point. It can also describe pipeline material behaviour in both the elastic and plastic regions. The boundary conditions at both ends of the S-shape section in Figure 3-1 are

$$|u(0) - u(L_1 + L_2)| = dcos\beta \quad (3\text{-}2)$$

$$u''(0) = u''(L_1 + L_2) = 0 \quad (3\text{-}3)$$

The bending curvature k can be easily calculated by double differentiation of Eq. (3-1) as follows:

$$k(x) = -\frac{d^2u(x)}{dx^2} = \begin{cases} \frac{\pi^2 \hat{d} cos\beta}{4(L_1 + L_i)} \sin\left(\frac{\pi x}{(L_1 + L_i)}\right) & 0 \le x \le L_1 + L_i \\ \frac{\pi^2 \hat{d} cos\beta}{4(L_2 - L_i)} \sin\left(\frac{\pi(L_1 + L_i - x)}{(L_2 - L_1)}\right) & L_1 + L_i \le x \le L \end{cases} \quad (3\text{-}4)$$

The bending strain ($\varepsilon_b(x)$) of the deformed pipeline due to the lateral displacement $dcos\beta$ can be obtained using the beam bending theory and ignoring cross-sectional distortion or ovalisation as follows:

$$\varepsilon_b(x) = -\frac{d^2u(x)}{dx^2}\frac{D}{2} = \begin{cases} \frac{\pi^2 D \hat{d} cos\beta}{8(L_1 + L_i)} \sin\left(\frac{\pi x}{(L_1 + L_i)}\right) & 0 \le x \le L_1 + L_i \\ \frac{\pi^2 D \hat{d} cos\beta}{8(L_2 - L_i)} \sin\left(\frac{\pi(L_1 + L_i - x)}{(L_2 - L_1)}\right) & L_1 + L_i \le x \le L \end{cases} \quad (3\text{-}5)$$

Considering the maximum bending curvature, the maximum bending strain, ε_b , of the deformed pipeline can be calculated by the following equation:

$$\varepsilon_b = \frac{D}{2} k_{max} = \frac{\pi^2 D}{8(L_1 + L_i)} \hat{d} cos\beta \quad (3\text{-}6)$$

In the proposed method it was assumed that the total axial membrane strain, ε_m,is uniform in the pipeline section. The simplified axial membrane strain can be obtained by

$$\varepsilon_m = \left(\frac{(32 + \pi^2)}{64} \hat{d}^2 cos^2\beta + \hat{d} sin\beta\right)\left(\frac{\omega}{\omega + 1}\right) \quad (3\text{-}7)$$

In this equation, ω can be obtained by

$$\omega = \frac{\overline{K}_t L}{2EA} \tag{3-8}$$

Where E is Young's modulus of the pipeline and A is the pipeline cross-section area. $\overline{K}_t$ is the axial stiffness of the pipeline at the outside of the S-shape section on the pipeline. It can be obtained using the developed analytical methodology by Vazouras (2015).

The membrane strain ε_m is always tensile for the positive values of β, however, the bending strain ε_b might be either tensile or compressive, based on the direction of bending. The total pipeline strain is the summary of the membrane strain ε_m in Eq.(3-7) and the bending strain ε_b in Eq. (3-3).

As a result, the maximum tensile strain, ε_T, is computed as follows:

$$\varepsilon_T = \varepsilon_b + \varepsilon_m \tag{3-9}$$

and the maximum compressive strain, ε_C, is

$$\varepsilon_C = \varepsilon_b - \varepsilon_m \tag{3-10}$$

To obtain the deflection and strain curves, the existing lengths of the S-shape section of the pipeline should be calculated (See Figure 3-1). In this figure, the value of L_1, L_2 are the distributed load (the maximum soil resistance per unit length) length and L_{i} is the distance

between the inflection point and the fault. These lengths can be obtained by the general elastic static model. Considering non-symmetric condition with respect to the fault the length of L_1 is obtained as follow:

$$L_1 = \sqrt{\alpha}\left(\frac{24 d_y EJ}{q_{u2} + q_{u1}}\right)^{1/4} \tag{3-11}$$

Where α is the length ratio that can be found from Figure 3-2 using the value of the soil resistance ratio ($b = q_{u1}/q_{u2}$).

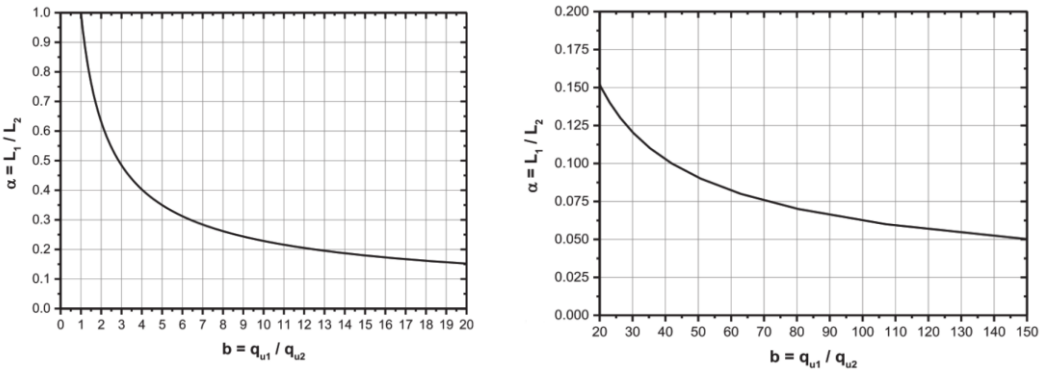

(a) (b)

Figure 3-2. Length ratio (a) diagram for b values between 0 and 20, (b) diagram for b values between 20 and 150 (Sarvanis (2017)).

In Eq. (3-11) the value of d_y is obtained by

$$\frac{d_y}{D} = \left(\frac{\sigma_y}{E}\right)\left(\frac{t}{D}\right)\left(\frac{D\sigma_y}{q_{u2}}\right)F(a) \tag{3-12}$$

In this equation, the value $F(a)$ can be obtained from Figure 3-3 based on the length ratio.

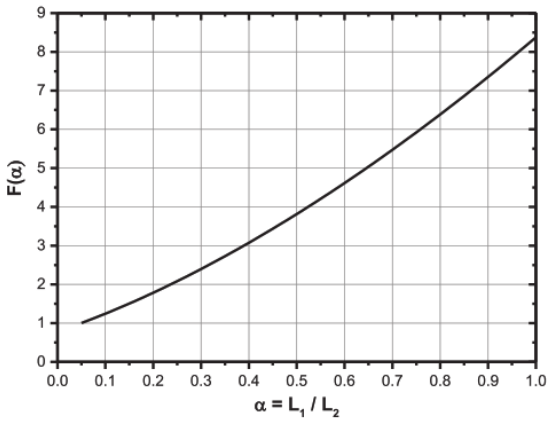

Figure 3-3. *F*(a) curve with respect to length ratio α (Sarvanis (2017)).

In the proposed method, the length between the fault and inflection point is obtained by Eq. (3-13) using static equilibrium in the moment diagram.

$$\left[\frac{q_{u2}}{2}\right]L_i^2 + \left[V_A - \frac{12EJd}{L^3} - (\alpha+1)q_{u2}L_1\right]L_i + \left[2\frac{L_1^2}{2}q_{u2}(1+\alpha)\right] = 0 \tag{3-13}$$

For the symmetric soil resistance condition, $q_{u1} = q_{u2} = p_u$ and $L_1 = L_2 = L/2$, $L_\mathrm{i} = 0$. Therefore, L can be obtained from the following simple equation:

$$L = 2\left(\frac{12d_yEJ}{p_u}\right)^{1/4} \tag{3-14}$$

Finally, yield displacement in the symmetric case can be expressed:

$$\frac{d_y}{D} = \frac{42}{5}\left(\frac{\sigma_y}{E}\right)\left(\frac{t}{D}\right)\left(\frac{D\sigma_y}{q_{u2}}\right) \quad (3\text{-}15)$$

3.3.2. Incorporation of Trenching-backfilling Effect into the Analytical Model

The majority of subsea pipelines installed under shallow water are buried in the trench as a means of protection against environmental loads. These buried pipelines may be subjected to large deformations due to permanent ground displacement (PGD). The pre-excavated soil is capable of being highly remolded when it is used as a backfilling material due to the effects of environmental loads. The use of pre-excavated soil consequently has a significant difference in the strength of the soil in comparison to the seabed soil. The stiffness difference effect has a significant influence on the force-displacement curves. However, due to the complexities in the pipeline-trench-backfill interaction problem, its influence was not investigated on the trenched pipeline subjected to fault crossing offsets before. In this section, the analytical method is modified in terms of soil strength variation for considering the effect of pipeline-trench backfill interaction in fault zones.

ASCE (1984) and ALA (2005) have elasto-plastic soil springs for dense to loose sand and stiff to soft clay. In practice, however, non-standardized soils such as intermediate soils and mixed soils that are not purely sand or clay can be found. In these cases, stress-strain properties of the soil must be used to obtain force-displacement values (p-y curves) for soil springs. In order to consider the influence of pipeline-trench-backfill interaction on the pipeline response, the p-y curves are divided into three zones (Zones 1, 2, and 3). Figure 3-4 schematically shows a pipeline displacement depending on the relative backfill/native soil stiffness. As shown in this figure, Zones 1 and 2 are located inside the backfill soil,

and Zone 3 is in the native soil. Using maximum soil resistance at different zones and considering symmetric conditions at both sides of the fault, the pipeline responses are extracted. The cumulative response of the pipeline at each point from the initial location point represents the axial strain distribution and the deflection curves of the pipeline.

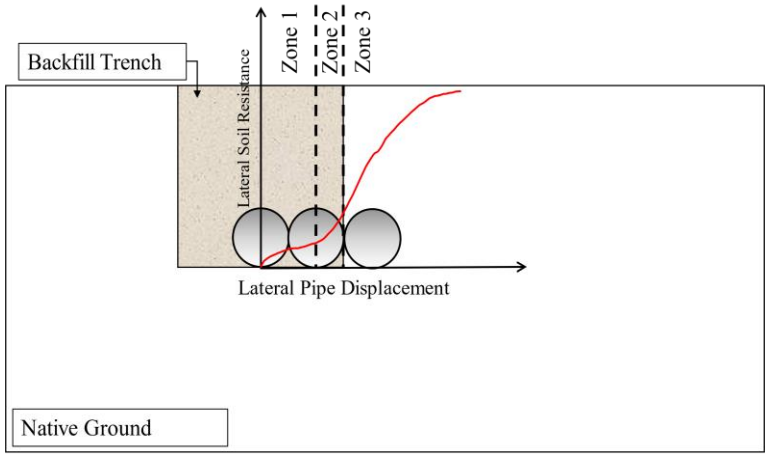

Figure 3-4. The lateral response of trenched and backfill pipeline to ground displacement.

To evaluate the trenched/backfilled pipelines interaction effect on the axial strain and deflection curves of pipelines, the p-y curves obtained from centrifuge tests were incorporated into the developed analytical methodology. The full details of the experimental studies can be found in Kianian. Table 3-1 summarizes the details of the experiments used in this section.

Table 3-1. Summary of experimental studies in clay (Kianian and Shiri (2021)).

Test Name	Trench Width	Burial Depth Ratio	Trench Wall Angle (°)	Trench Backfill Soil Type	γ'_{sat} (kN / m^3)	s_u (kPa)
T1P2	1.3D	4.1	90	Slurry	18.33	19
T3P1	1.0D	2.0	90	Slurry	18.51	17.5
T3P2	1.3D	2.0	90	Chunk		20
T4P1	1.3D	2.0	90	Slurry	18.45	17.5
T4P2	1.3D	2.0	30	Chunk		20
T5P1	0.75D	4.1	90	Slurry	18.43	17
T5P2	1.3D	4.1	30	Chunk		20.5

It should be noted that it was assumed that the friction angles of slurry and chunk backfilling are 0 and 36 degrees, respectively. The undrained shear strength of slurry was assumed to be $50\ Pa$. The unit weight of slurry and chunk soil were assumed $12.5\ kN/m^3$ and $17\ kN/m^3$, respectively. The total length (L) of the pipeline at the large deformation part was obtained by Eq. (3-14). The lengths L_1 and L_2 are both equal to half of the total length. Therefore, the value of L_i is zero.

3.4. Results and discussion

Several comparisons have been conducted between the developed analytical methodology for trench backfilling soil and the analytical model for the native seabed. In the first step,

the effect of slurry backfilling on deformation and the produced axial strain has been investigated. The strike-slip fault is assumed to be crossed with the angle of 0°.

The effect of slurry backfilling soil on the wide and narrow trench widths has been examined in two different comparisons. The first comparison was made using the p-y curves from T1P2 and T3P1 centrifuge tests. In these cases, the trench wall was vertical, and the native soils were in partially drained conditions. The trench depth ratios for T1P2 and T3P1 were 3.9 and 2.0 respectively and the trench width for both tests was $1.3D$.

The deflection and axial strain curves of buried pipeline in the wide width are presented in Figure 3-5. Figure 3-5(a) shows that the deflection of the pipeline decreases with the increasing of the trench depth. Besides, the comparison represents that the buried pipeline in the deep depth trench has an almost 10% smaller value of u(x) compared to the buried pipeline in shallow seabed soil. Therefore, when a pipeline is buried in the trench, the distance between the wrinkles increases. The effect of trench depth ratio on the distributed axial strain is presented in Figure 3-5(b). It shows that the axial strain of the pipeline will generally decrease with the presence of trenches and backfill soil, regardless of the depth of the trench.

The comparison of the axial strain curves of trenched pipelines shows that the axial strain of the deep depth trenched pipeline in the slurry is 27% smaller than the pipeline trenched in the shallow depth, while this value is 22% for pipeline buried in the seabed. Besides, as shown in this figure, the location of the maximum axial strain does not change significantly as the burial depth increases. However, when the pipeline is buried inside a trench change remarkably compared to the pipeline buried in the native seabed soil.

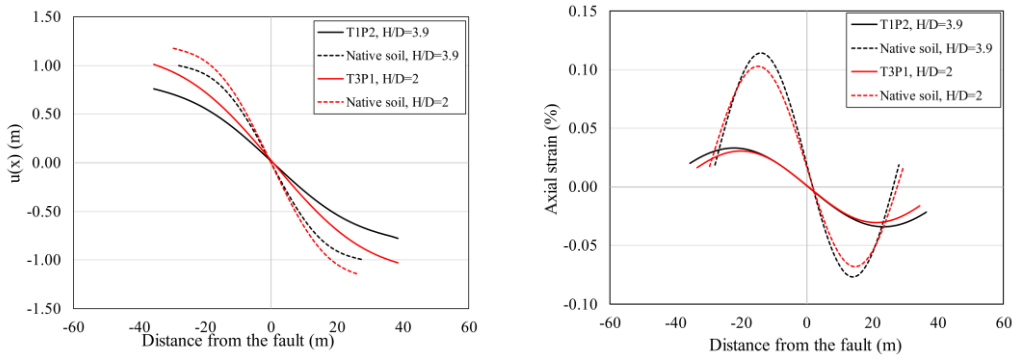

(a) (b)

Figure 3-5. Comparison between the developed analytical model for the trenched pipeline and the analytical model for the uniform seabed soil, T1P2 and T3P1 ($\beta = 0^{\circ}$): (a) Deformed pipeline shape, (b) Distribution of axial strains along the pipeline.

Figure 3-6 represents the second comparison of the buried pipeline responses in the slurry trench soil. In this comparison, the p-y curves of T4P1 and T5P1 were used. It should be noted that in the selected case studies, the trench widths are $1.3D$ and $0.75D$, the burial depth ratios are 2.0 and 4.1, respectively, and the trench wall is vertical. The native soil is in the drained conditions in these case studies. The results show that there is not significant change in the deflection curve of the buried pipeline in the seabed soil when the burial depth increases because in these two case studies, the soil shear strength at the pipeline depth is almost same. Besides, the deflection curve comparison shows that the wrinkles horizontal distance of the buried pipeline in a shallow trench (T4P1) is around 18% greater than a buried pipeline in a deep depth (T5P1). However, the vertical distance between the wrinkles is around 7% smaller (See Figure 3-6(a)). Figure 3-6(b) shows the distributed axial strain on the pipeline. This figure illustrates that using a trench with softer backfilling

soil decreases the axial strain. Besides, it shows that in the trench with wider width (T4P1), the axial strain curve is smoother than the axial strain of the buried pipeline in the narrow width (T5P1). The maximum axial strain of the buried pipeline in the T5P1 test is much more than T4P1 (around 50%) because it reaches the native soil earlier than T4P1. Also, the soil weight on the pipeline for T5P1 is greater than T4P1 due to the burial depth ratio. This figure again represents that the maximum axial strain's location doesn't change much as the burial depth increases. However, the comparison of solid lines that represent trenched pipelines' axial strains shows that the locations of the maximum axial strain change significantly with increasing the trench depth. It should be noted that the trench width of T4P1 is wider than T5P1. This observation represents the importance of the trench width in reducing the maximum axial strain and consequently increasing the distance between the maximum axial strain position.

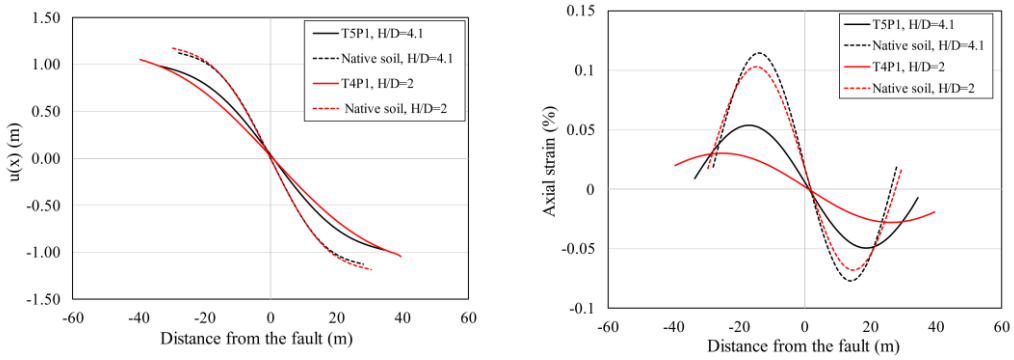

(a) (b)

Figure 3-6. Comparison between the developed analytical model for the trenched pipeline and the analytical model for the uniform seabed soil, T4P1 and T5P1 ($\beta = 0^{\circ}$): (a) Deformed pipeline shape, (b) Distribution of axial strains along the pipeline.

In the second step, the buried pipeline response to the strike-slip fault has been investigated, where the backfilling material was chucky clay (See Figure 3-7). The trench wall is not vertical in these two selected centrifuge tests (T4P2 and T5P2). The trench angle is 30° and the trench width is $1.3D$ in both tests. The native soil is in the drained condition and the soil properties are given in Table 3-1.

As shown in Figure 3-7(a), the deflection curve of the pipeline doesn't remarkably change as the depth doubles because of the same soil shear strength in the buried pipeline depth. Also, there is no significant change in the pipeline deflection for the buried pipeline in the trench considering different burial depth ratios. Although the horizontal distance between the wrinkles increases by around 13%, the vertical distance ($u(x)$) is almost 4%. Figure 3-7(b) illustrates the axial strain distribution in these two case studies.

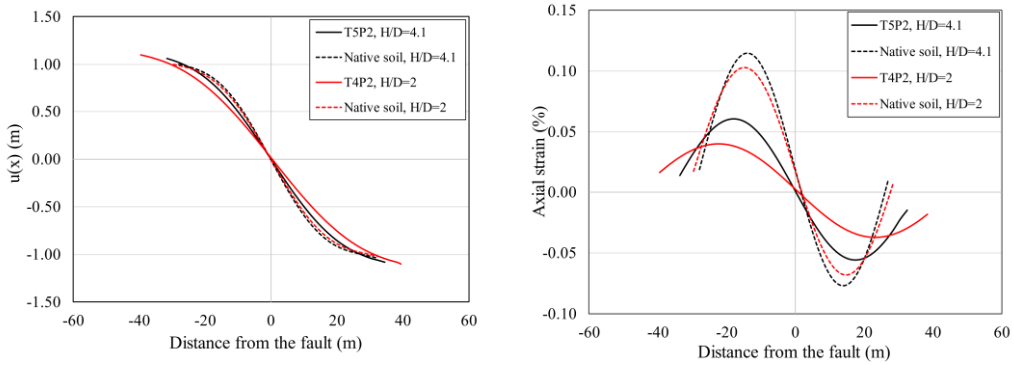

(a) (b)

Figure 3-7. Comparison between the developed analytical model for the trenched pipeline and the analytical model for the uniform seabed soil, T4P2 and T5P2 ($\beta = 0^{\circ}$): (a) Deformed pipeline shape, (b) Distribution of axial strains along the pipeline.

In this study, the effect of trench width on the pipeline responses has also been investigated as the pipeline moved in the soil because of strike-slip fault activities. Two different comparisons were made considering two different burial depth ratios (2 and$\sim$4). To investigate the trench width effect on the bending deformation of buried pipelines, centrifuge test results with similar trench depths (3.9 and 4.1) and backfilling soil (slurry) were selected (T1P2 and T5P1). The width of trench of T1P2 and T5P1 were $1.3D$ and $0.75D$, respectively. Figure 3-8(a) shows that the bending deformation decreases as the trench width increases. Besides, the distance between the wrinkles increases when the trench width rises. The comparison of axial strain distribution of the pipeline for these case studies are shown in Figure 3-8(b). This figure shows that as the trench width increases (doubled), the axial strain decreases (almost 50%). The comparison of the results of this figure shows that the maximum axial strain location depends on the trench width.

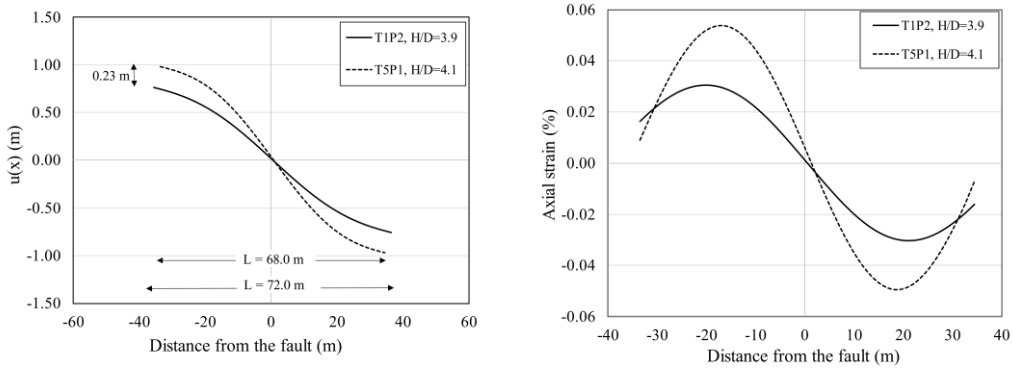

(a) (b)

Figure 3-8. Comparison between the developed analytical model for the trenched pipeline and the analytical model for the uniform seabed soil, T1P2 ($W = 1.3D$) and T5P1($W = 0.75D$) with ($\beta = 0^{\circ}$): (a) Deformed pipeline shape, (b) Distribution of axial strains along the pipeline.

Figure 3-9 shows the analytical results for T3P1 and T4P1. In these two case studies, the burial depth ratio is 2. The seabed soil drainage conditions are different in these case studies. The seabed soil in T3P1 is partially drained; however, in T4P1, it is drained conditions. Figure 3-9(a) represents that the bending deformation decreases as the trench width increases. Figure 3-9(b) shows the comparison of axial strain distribution in the large deformation part of T3P1 and T4P1 cases. This figure confirms the previous conclusion about the trench width effect on the axial strain although the seabed soil drainage conditions are different.

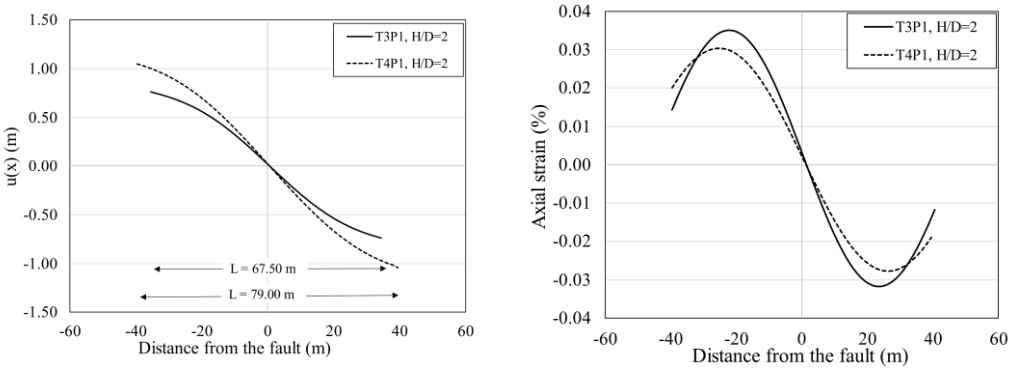

(a) (b)

Figure 3-9. Comparison between the developed analytical model for the trenched pipeline and the analytical model for the uniform seabed soil, T3P1 (W=D) and T4P1(W=1.3D) with ($\beta = 0^{\circ}$): (a) Deformed pipeline shape, (b) Distribution of axial strains along the pipeline.

3.5. Conclusion

In this study, the structural response of the buried pipeline to the strike-slip fault was studied by incorporation of the effects of backfilling soil properties and trench configuration into an analytical model. The deformed shapes and axial strain distribution curves were used to investigate the pipeline-backfill-trench interaction. The results showed that the impact of the pipe-soil interaction on pipe response can be significant during fault crossing. A parametric study was conducted to evaluate the pipe-backfill-trench interaction considering different burial depths and widths on the axial-lateral pipeline-soil interaction. The following conclusions were observed:

- In general, the properties of backfilling soil have a significant effect on the axial strain of the pipeline. Softer backfills induce around 50% less axial strains.
- The position of maximum axial strain does not considerably change as the trench depth increase. However, the trench width is an important factor that effects the location of the maximum axial strain.
- The deformed shape of the pipeline is significantly affected by trench geometry. As could be seen in the results, the distance between two major wrinkles increases on the buried pipeline in the trench as the trench width increases or the trench depth decreases.

Generally, better mechanical behavior of trenched pipelines in the softer material is evident. Increasing locally the trench width is suggested to protect buried steel pipelines against local buckling in the seismically active areas because of economic issues. It is recommended to extend the current study to advanced large deformation numerical simulations to further assess the reliability of the observations.

References

ALA. American Lifelines Alliance Guidelines for the Design of Buried Steel Pipes, 2005.

ASCE. Guidelines for the Seismic Design of Oil and Gas Pipeline Systems; ASCE: New York, NY, USA, 1984.

Demofonti, G.; Ferino, J.; Karamanos, S.A.; Vazouras, P.; Dakoulas, P. An integrated experimental-Numerical approach to predict strain demand for buried steel pipelines in geo-hazard areas. In Proceedings of the Rio Pipeline Conference, 24–26 September 2013.

Karamitros, D.K.; Bouckovalas, G.D.; Kouretzis, G.P. Stress analysis of buried steel pipelines at strike-slip fault crossings. Soil Dyn. Earthq. Eng. 2007, 27, 200–211.

Karamitros, D.K.; Bouckovalas, G.D.; Kouretzis, G.P. Stress analysis of buried steel pipelines at crossing fault zones, ASCE J. Geotech. Geoenviron. Eng. 2007, 134, 1501–1515.

Kennedy, R.; Chow, A.; Williamson, R. Fault Movement Effects on Buried Oil Pipeline. Transp. Eng. J. ASCE 1977, 103, 617–633.

Kianian, M., Allahbakhshi, M., Shiri, H. Centrifuge Testing of Lateral Pipeline-Soil Interaction Buried in Very Loose Sand. GeoEdmonton Conference; Edmonton, AB, Canada, 2018.

Kianian, M.; Esmaeilzadeh, M.; Shiri, H. Lateral response of trenched pipelines to large deformations in clay. In Proceedings of the Offshore Technology Conference. OnePetro, 2018.

Kianian, M.; Shiri, H. The influence of pipeline–trench bed interaction intensity on lateral soil resistance and failure mechanisms. Int. J. Geotech. Eng. 2019, 1–14.

Kianian, M.; Shiri, H. The effect of backfilling stiffness on lateral response of the shallowly trenched-backfilled pipelines in clay. Mar. Georesour. Geotechnol. 2020, 1–13.

Kianian, M.; Shiri, H. Experimental study of trench effect on lateral failure mechanisms around the pipeline buried in clay. J. Pipeline Sci. Eng. 2021, 1, 198–211.

MaCaffrey, M.A.; O'Rourke, T.D. Buried pipeline response to reverse faulting during the 1971 San Fernando Earthquake. In Proceeding. ASME PVP Conf. 1983, 77, 151–159.

Newmark, N.M.; Hall, W.J. Pipeline design to resist large fault displacement. In Proceeding US Natl. Conf. Earthq. Eng. 1975, 416-425.

Palmer, D.F.; Henyey, T.L. San Fernando earthquake of 9 February 1971: Pattern of faulting. Science 1971, 14, 712–715.

Sarvanis, G.C.; Karamanos, S.A. Analytical model for the strain analysis of continuous buried pipelines in geohazard areas. Eng. Struct. 2017, 152, 57–69.

Takada, S.; Hassani, N.; Fukuda, K. A new proposal for simplified design of buried steel pipes crossing active faults. Earthq. Eng. Struct. Dyn. 2001, 30, 1243–1257.

Trifonov, O.V.; Cherniy, V.P. A semi-analytical approach to a nonlinear stress–strain analysis of buried steel pipelines crossing active faults. Soil Dyn. Earthq. Eng. 2010, 30, 1298–1308.

Vazouras, P.; Karamanos, S.A.; Dakoulas, P. Finite element analysis of buried steel pipelines under strike-slip fault displacements. Soil Dynam Earthq. Eng. 2010, 30, 1361–1376.

Vazouras, P.; Karamanos, S.A.; Kakoulas, P. Mechanical behavior of buried steel pipes crossing active strike-slip faults. Soil Dyn. Earthq. Eng. 2012, 41, 164–180.

Vazouras, P.; Dakoulas, P.; Karamanos, S.A. Pipe–soil interaction and pipeline performance under strike–slip fault movements. Soil Dyn. Earthq. Eng. 2015, 72, 48–65.

Vougioukas, E.A.; Theodossis, C.; Carydis, P.G. Seismic analysis of buried pipelines subjected to vertical fault movement. ASCE J. Tech. Counc. 1979, 105, 432–441.

Wang, L.R.L.; Yeh, Y.H. A refined seismic analysis and design of buried pipeline for fault movement. Earthq. Eng. Struct. Dyn. 1985, 13, 75–96.

Zhang, J.; Liang, Z.; Han, C.J.; Zhang, H. Numerical simulation of buckling behavior of the buried steel pipeline under reverse fault displacement. Mech. Sci. 2015, 6, 203–210.

Zhang, J.; Liang, Z.; Zhang, H. Response analysis of buried pipeline subjected to reverse fault displacement in rock stratum. Trans. FAMENA 2016, 40, 91–100.

Chapter 4

Structural response of the spiral-welded pipelines buried in different uniform soil types to the strike-slip fault

Mozhgan Asgarihajifirouz[1], Xiaoyu Dong[2], Hodjat Shiri[3]

1: Department of Civil Engineering
Memorial University of Newfoundland

2: Post-doctoral Fellow, Department of Civil Engineering
Memorial University of Newfoundland

3: Associate Professor, Department of Civil Engineering
Memorial University of Newfoundland

This chapter has been published as a journal paper.

4.1. Abstract

Buried steel pipelines, which are widely used in, often face the threat of permanent ground deformations (PGD) caused by fault crossings. The structural response of the pipeline can be influenced by the pipe-trench-backfill interaction, resulting in various hoop strains, axial plastic strains, and consequently, formation of wrinkles at different locations in the fault zone. This chapter investigates the structural response of spiral-welded pipelines at strike-slip fault crossings by incorporating the burial effects in a range of different soil materials. A dynamic explicit analysis is used to address the convergence issue commonly encountered in the analysis of post-buckling problems. The helix angles and the burial depth effects in different soil types and pipeline-ground interaction angles are examined. The study provides valuable insights into the influence of burial conditions and corresponding helix angle on the performance of spiral-welded pipelines in strike-slip faults.

Keywords: Spiral-welded pipeline; trenching-backfilling; nonlinear dynamic analysis, strike-slip fault

4.2. Introduction

Buried pipelines are widely regarded as the most reliable means of transmitting oil, gas, water, and other fluids in large quantities, playing a vital role in the economic growth of communities. With the exploration and development of oil and gas, there is an increasing demand for various types of pipelines, including seamless, UOE (U-ing, O-ing, and Expanding), and spiral-welded pipelines. According to The Welding Institute (TWI), spiral

welded pipelines are expected to be 10-15% cheaper than UOE pipelines, leading to an increase in the production of spiral-welded pipelines.

Post-earthquake investigations have revealed that permanent ground deformation (PGD) resulting from fault movements, liquefaction, or landslides can cause severe damage to buried and surface structures (O'Rourke and Palmer, 1996; Tang, 2000; Chen et al., 2002). Buried pipelines and tunnels are among the most critical and vulnerable structures due to their crucial role in post-earthquake serviceability. According to the Central Intelligence Agency (CIA) World Factbook (2013), there is a pipeline network spanning over 3.5 million kilometers across 120 countries worldwide. Hence, it is crucial to investigate the performance of these structures to ensure safe operation and serviceability against fractures caused by PGD. Besides, current field studies on the buried steel pipelines indicate that fracturing of these structures is primarily attributed to PGD rather than wave propagations (Tang, 2000; Tsai et al., 2000; Ha et al., 2008; Vazouras et al., 2012). The significance and vulnerability of buried spiral-welded pipelines to fault movements have prompted research into their behaviour under fault movements. Excessive deformation of steel pipelines can lead to leakage, posing risks to human life and the environment. Therefore, the main objective of designing buried pipelines in fault crossing areas is to minimize the risk of damage. Thus, accurate prediction of strain demand on the pipeline, incorporating the effect of the surrounding soil, is essential for a successful pipeline design against the PGD. The behavior of buried pipelines affected by fault movement was initially investigated by Newmark and Hall (1975) using a cable model. They ignored the lateral soil strength and the flexural stiffness of pipeline. Subsequently, the model was further enhanced by incorporating the soil lateral pressure, pipe-soil interaction, and the pipe flexural stiffness

(e.g., Kennedy et al., 1977). The ASCE guidelines (1984) adopted the work conducted by Kennedy et al. (1977) for buried pipeline design. Kennedy et al. (1977) continued Newmark and Hall's work by considering the lateral strength of the soil while still neglecting the flexural stiffness of the pipe. Analytical developments in this field were continued by Wang and Yeh (1985), who introduced the contribution of the pipe flexural stiffness. They also considered the effects of soil-pipe lateral interaction and the large axial strains on the pipeline bending stiffness.

Kokavessis et al. (2006) developed a simplified finite element model to investigate the response of buried pipelines to PGD. They incorporated the soil and pipe interaction using contact elements. Liu et al. (2008) modeled the pipe and soil interaction using spring elements connected to a shell model to represent the pipelines crossing the active fault. Their study revealed that the fault movement creates localized axial strain during the early stage of loading, with the localized strain location depending on the loading fault mode.

O'Rourke et al. (2009) and Xie et al. (2011) investigated the mechanical behavior of polyethylene pipelines under fault crossing in different soil conditions. Demofonti et al. (2013) conducted experimental and numerical studies to explore the mechanical responses of steel pipelines subjected to horizontal ground movement. Their research improved the understanding of soil and pipe interaction and facilitated the calibration of numerical models for predicting strain demand in buried pipelines.

Zhang et al. (2015; 2016) employed the finite element method to examine the buckling behavior of buried pipelines. They demonstrated that the amplitude of fault displacement and pipe wall thickness significantly influence the maximum strain location. Vazouras et al. (2015) investigated the mechanical response of buried steel pipelines crossing active

strike-slip seismic faults for different fault angles and evaluated the critical fault offset based on various performance criteria.

Jalali et al. (2016) conducted experimental and numerical studies to show the dependence of the uplift force on the pipe diameter and its relative stiffness in a pipeline crossing a reverse fault. Their findings contradicted the guidelines of American Lifeline Alliance (ALA), which assume a constant uplift force for a given burial depth. Nekooei et al. (2019) performed experimental and numerical studies on a horizontally-bent buried pipeline crossing an active fault. They studied failure mechanisms, deflection of pipeline and soil surface inflation and deflation. Their study demonstrated that increasing the pipe diameter-to-wall thickness ratio (D/t) reduces pipe deformation, and the plastic hinge forms farther away from the fault.

The majority of the studies mentioned have considered seamless or UOE pipelines, while the effect of surrounding soil strength on the performance of spiral-welded pipes have been limitedly explored in the literature. For instance, Kaya et al. (2017) conducted a case study simulation to examine the performance of the spiral-welded steel pipes at the Kullar fault. The authors developed a 3D nonlinear continuum finite element model and simulated the pipeline-soil interaction considering the internal pressure effect with different boundary conditions. The results showed that the pipe behaviors under compressive strain is highly sensitive to the end boundary conditions, soil properties, and internal pressure.

The present study provides a thorough investigation of the nonlinear structural response of buried spiral-welded pipelines in terms of tensile and compressive strain capacity under various conditions. These conditions include different uniform soil types such as dense and loose sands and clay, varying burial depths, intersection angles, and helical angles. To

capture the pipeline-soil interaction effects, a 3D Lagrangian finite element model was developed. To validate the developed model, its results were compared against those obtained by Kaya et al. (2017) in their Kullar fault case study. Furthermore, a comprehensive parametric study was conducted to investigate the effects of backfilling properties, burial depth, pipeline geometry, intersection angles, and helical angles on the failure mechanism of spiral-welded pipelines. Through this extensive investigation, the study offers a more understanding of the performance of the buried spiral-welded pipelines under the strike-slip fault conditions.

4.3. Numerical model and material properties

The numerical model was developed in ABAQUS/Explicit, based on the model configuration presented in the study by Kaya et al. (2017), to facilitate the validation. The model represented a buried spiral-welded pipeline situated within a mixture of native soil (soft and stiff clay) with sand and gravel. The dimensions of the model were 100 m (length) × 20 m (width) × 5 m (height), as shown in Figure 4-1. The material of the spiral-welded pipeline was API Grade B steel with a minimum yield stress of 241 MPa. The diameter, thickness, and length of the pipeline were 2.20 m, 0.018 m, and 100.0 m, respectively. The soil and pipe elements were modeled using C3D8R (8-node linear brick (Hex) with reduced integration and hourglass control) and S4R (4-node shell element with reduced integration) shell elements available in the software library with properties presented in Table 4-1 and Table 4-2, respectively. The 3D continuum model encompassed a total of 33,488 solid elements and 18,038 shell elements.

Table 4-1. Soil properties (Kaya et al., 2017).

Soil type	Cohesion (kPa)	Young Modulus (MPa)
Soft	20	8
Stiff	40	16

Table 4-2. Steel pipeline properties.

Min Yield stress (MPa)	Min Tensile stress (MPa)	Young Modulus (GPa)	Min yield strain	Elongation (%)
241	414	210	0.002	23

The performance of pipelines can be significantly influenced by boundary conditions (BCs). Based on the findings of Kaya et al. (2017), it was observed that assuming fixed BCs at the ends of the pipelines resulted in better correlation with field observations compared to assuming free ends. Therefore, in this paper, fixed BCs are assumed to prevent pipeline slippage.

The loading process was divided into three steps. In the first step, geostatic loads were applied to account for the self-weight of the pipeline and soil. In the second step, the internal surface of the pipeline was subjected to an internal pressure of 10 bar. As part of the third step, one of the soil blocks was subjected to fault movements while the other block remained fixed. A maximum strike-slip fault displacement of 3.0 m was assumed in this study.

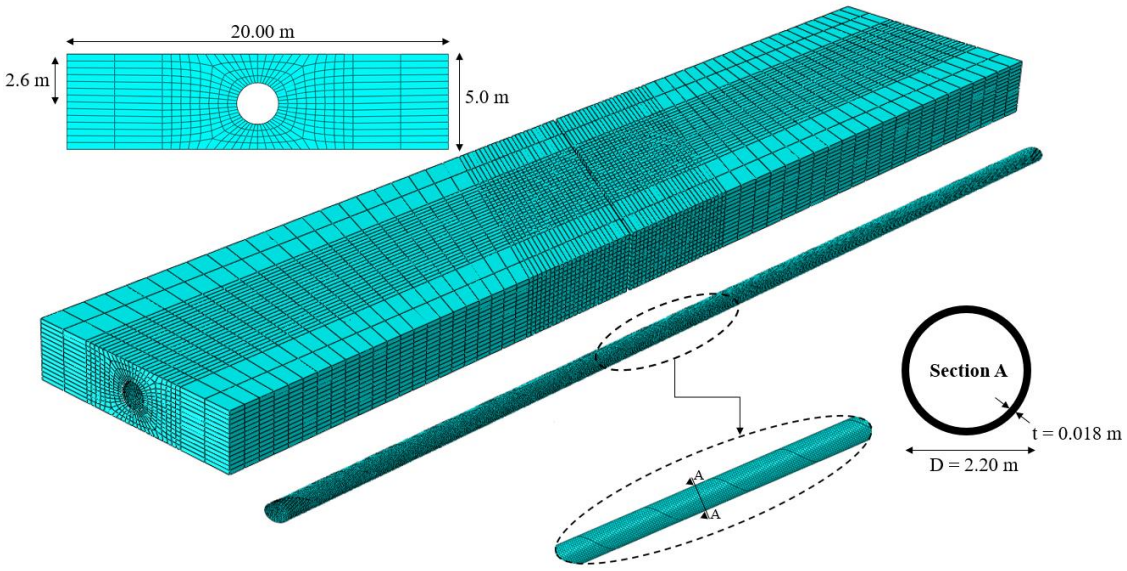

Figure 4-1. Finite element model, mesh, and dimensions.

4.3.1. Soil properties

A plastic Mohr-Coulomb (M-C) model that is suitable for soils under monotonic loading is used to model the soil behavior. The general equation of this model is as follow:

$$\tau_n = f(c, \varphi, \sigma_n) \tag{4-1}$$

Where, c is the cohesion factor of soil, φ is the internal friction angle, and σ_n is the positive stress on the yield surface. It should be noted that the M-C model does not consider the hydrostatic pressure and intermediate principal stress. However, it is well-suited for capturing the behaviour of soil and rock under tensile and compressive loads. A separation-allowed surface-to-surface contact definition is used to simulate the pipeline-soil interaction that is defined by friction coefficient.

4.3.2. Spiral-welded pipeline model

A spiral-welded pipeline is produced by twisting metal strips into a spiral shape and welding the edges where they join to form a seam. To create the spiral-welded pipe model, a Python script was developed to produce the configuration depicted schematically Figure 4-2. The spiral shape is not simply an extrusion of a circle; it requires a pitch to create a spiral circle composed of two arcs. The Python script used three points, including one center and two end points, to generate the arc. Moreover, the model incorporated two distinct types of materials: the shell and the weld. The width of the weld is significantly smaller than that of the shell. The script used the following set of equations to calculate the helix angle (α):

$$tan\alpha = \frac{W}{R} \tag{4-2}$$

where, R is the length of the adjacent side of the triangle and W represents the width of the helix, as illustrated in Figure 4-2. To calculate the total length of the strip used for the full length of the pipeline and the helix angle, R can be calculated as follows:

$$R = \sqrt{(\pi D)^2 - W^2} \tag{4-3}$$

where D is the pipe diameter. As shown in Figure 4-2, the total length of pipeline is obtained by the following equation, where L can be calculated using the cylinder area presented Eq. (4-4).

$$L = n\pi D - 2R \tag{4-4}$$

Where n is the number of turns.

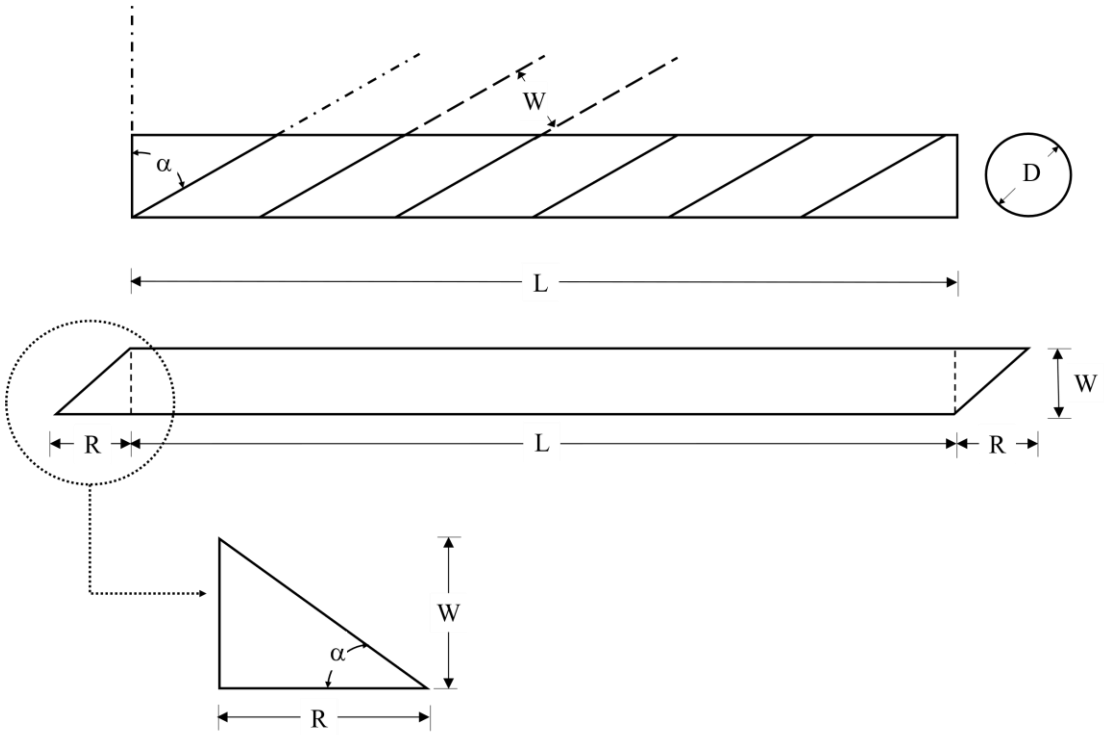

Figure 4-2. Basic dimensions of the spiral welded pipe.

The isotropic von Mises yield model from the library of ABAQUS was adopted for the spiral-welded pipe.

4.3.3. Pipeline failure criteria

The existing design codes, such as American Lifeline Alliance (ALA) and Pipeline Research Council International (PRCI), have established criteria for the buried pipelines that are subjected to significant ground deformation. These criteria are designed to cover different modes of deformation:

1. Limiting the axial tensile strains to prevent pipeline yielding.
2. Limiting axial compressive strains to prevent local buckling.
3. Limiting the cross-sectional distortion or ovalisation.

Based on the recommendations of ALA and PRCI, modern pipelines with high-quality welding should adhere to certain strain limits to achieve the desired performance. Specifically, for pipelines where the performance target is to maintain pressure integrity, ALA recommends a tensile strain limit of 4%, while PRCI recommends a range of 2-4%. However, if the performance target is immediate serviceability, such as post-event functionality, the recommended strain limit by ALA is 2%, while PRCI suggest a limit of 1-2%.

The compressive strength of the pipeline, which is associated with local buckling, depends on the geometry of the pipeline, material properties, initial imperfections, and internal pressure level. The failure process typically initiates with the formation of wrinkles, which then progress and cause the pipeline to fold in the wrinkled region. Ultimately, the deformation leads to the rupture of the pipeline wall. Wijewickreme (2006) recommends the following values of limit states to control the compressive ruptures:

For 10 % failure probability, Axial strain (ε_1) = 0.4 t / D = 0.33 % (4-5)

For 90 % failure probability, Axial strain (ε_2) = 2.4 t / D = 2 % (4-6)

The third failure mode occurs when the pipeline experiences a large bending moment, causing the cross-section to flatten, as illustrated in Figure 4-3. Gresnigt's (1986) proposed a criterion to prevent pipeline failure due to flattening, suggesting that the maximum change in pipe diameter should be kept below the $\frac{D - D'}{D} = 0.15$, where D and D' are the

diameters of the pipe before and after fault rupture, respectively. In this study, this criterion was adopted to assess the potential failure of the pipeline.

It should be noted that the Det Norske Veritas (DNV, 2017) standard for submarine pipelines imposes a maximum limit of 3% the ovalisation parameter. DNV (2017) defines the ovalisation parameter as the ratio of the difference between the maximum and minimum pipe diameter after being deformed to its initial diameter. The strict limitation on the ovalisation parameter of submarine pipes is crucial because the local ovalisation can lead to collapse under the high level of external hydrostatic pressure (Alrsai et al., 2018).

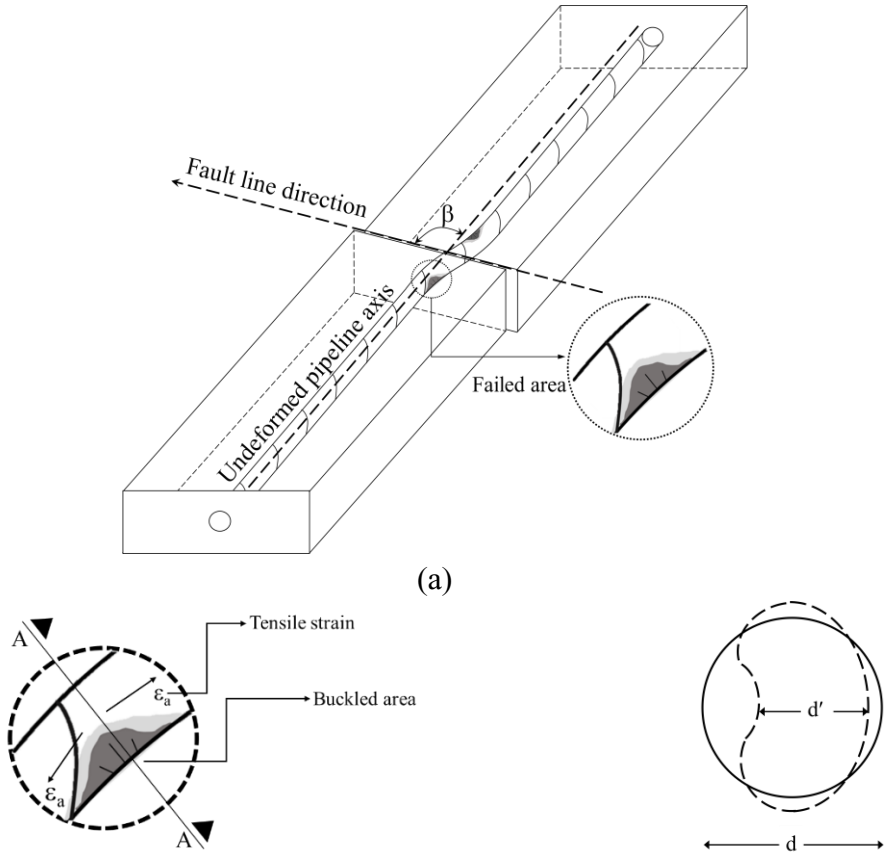

Figure 4-3. Schematic representation of a pipeline interaction with strike-slip fault rupture; (a) axial section, (b) failed area, (c) ovalisation.

4.3.4. Verification of the numerical model

The model's performance was validated against the data from a spiral-welded pipeline that was damaged crossing the North Anatolian fault activated by the Kocaeli earthquake in 1999 in Turkey. The analysis results, including the distance between major wrinkles, axial strain and rotation at wrinkles, location of the third minor wrinkle, as well as the wavelength and strain associated with local buckling were compared with both the field observations and an earlier simulation conducted by Kaya et al. (2017). The specific pipeline selected for validation was a main water transmission spiral-welded pipeline with an external diameter of 2.20 m that was ruptured and leaked. This pipeline, which had been installed one year prior to the earthquake, crossed the fault at an angle of 55°. It had experienced one minor and two major local buckles (see Figure 4-4).

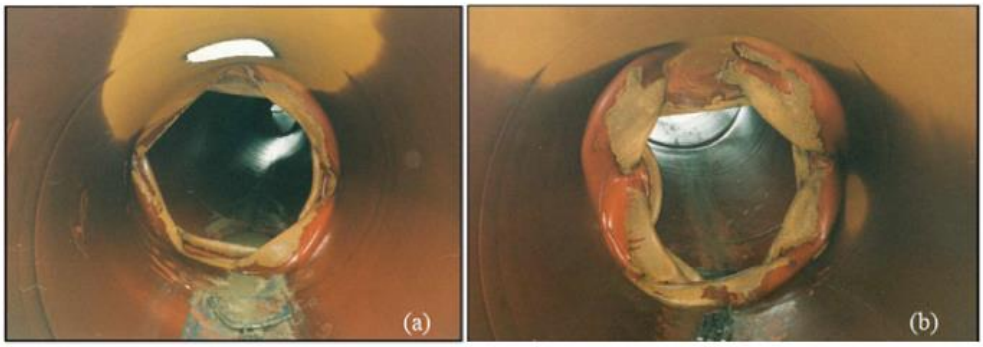

Figure 4-4. Two major wrinkles of main water transmission pipeline. (Eidinger and O'Rourke (2002)).

Table 4-3 presents a comparison between the results of the current numerical analysis, field observations, and those obtained by Kaya et al. (2017). The comparison demonstrates a

good agreement between the developed model and the available data, indicating the reliability of the model for conducting the subsequent parametric study.

Table 4-3. Comparison of validated numerical model results with field observations and the numerical model conducted by Kaya et al. (2017).

	Distance between wrinkles (m)	Average axial strain at wrinkles (1&2)	Rotation demands at wrinkles (1& 2) (degrees)	Location of the 3rd minor wrinkle (m)	Local buckling wavelength (cm)	Local buckling strain (%)
Field observation	17.1-17.6	15-20%	7.5-8.5°	13.0	50-60	-
Kaya **et al.** (2017)	16.5	15-20%	7.5-8.0°	13.1	50-55	0.21
Validated model	16.51	15-20%	7.1-8.9°	13.3	50-55	0.22

Figure 4-5 displays the deformed shapes of the pipeline in the validated model. The distance measured between the two major wrinkles in this model is 16.51 m, which exhibits a slight deviation of 3.5% from the field observation.

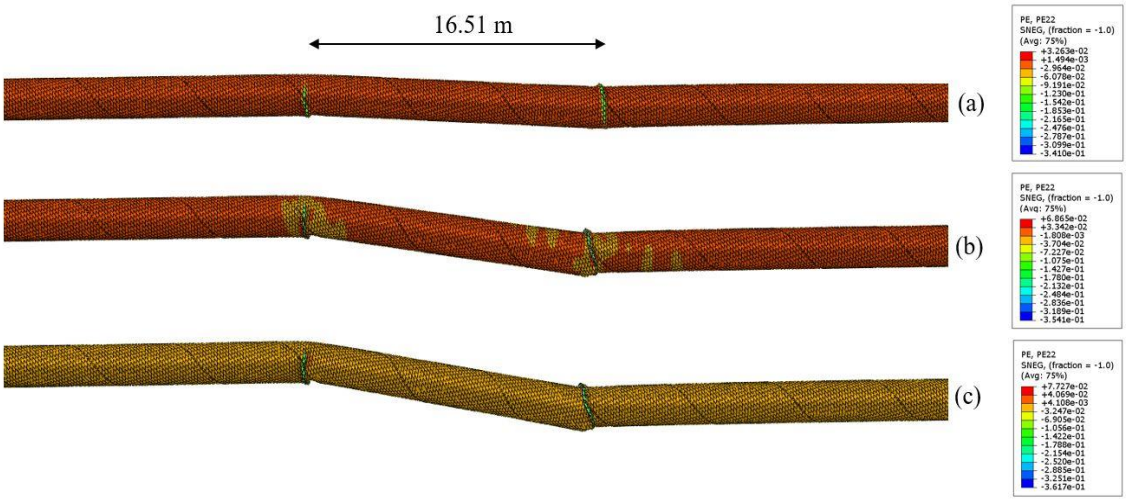

Figure 4-5. Deformed shapes of pipe (w/ internal pressure) and separation distance of wrinkles at fault displacements of (a) 1.0, (b) 2.0, and (c) 3.0 m (fixed end BC's) of the verified model.

The validated model was used to conduct a comprehensive parametric study, which aimed to investigate the effect of various crucial parameters, including the soil type, burial depth ratio, intersection angle, and helical angle, on the behavior of the pipeline. The outcomes of this parametric study will be presented and discussed in the next section.

4.4. Results and discussions

4.4.1. Effect of intersection angle

In this section, the effect of fault crossing angle on the behavior of the spiral-welded pipeline is investigated, considering the burial depth of 1.50 m from the highest point of

the pipeline. The properties of the soil blocks and the spiral-welded steel pipeline are presented in Table 4-1 and Table 4-2 respectively.

The deformed shape of pipeline and stress contour of the pipeline under two different crossing angles (55° and 90°) are presented in Figure 4-6. A comparison of the strain and stress distribution in Figure 4-6(a) and (b) shows that a fault intersection angle of 55° results in more severe deformation of the pipeline compared to a fault crossing angle of 90°. Figure 4-6(b) highlights the presence of high concentrated stress areas near the fault line. it can be observed that the maximum axial stress in the model with the fault crossing angle of 55° is significantly higher than that in the model with the fault crossing angle of 90° as the fault movement applies a high tension force in the axial direction. However, the fault with the angle of 90° tends to induce a pure bending mode on the pipeline due to the tensile strain reduction (see Figure 4-6(a)). The FEA results indicate that the distance between the two major wrinkles is 16.51 m in the model with the fault crossing angle of 55°, while it is 18.30 m when the angle is 90°.

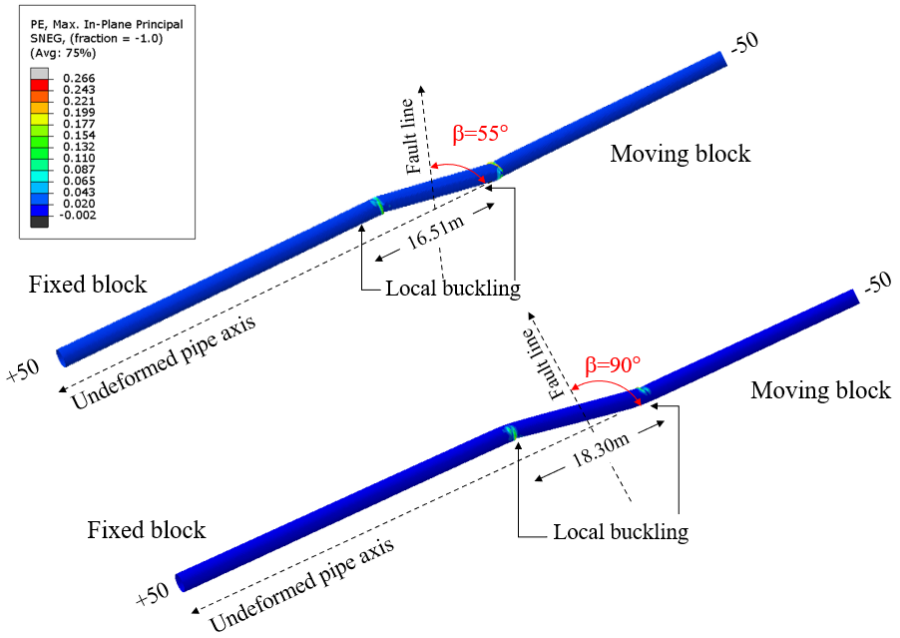

(a)

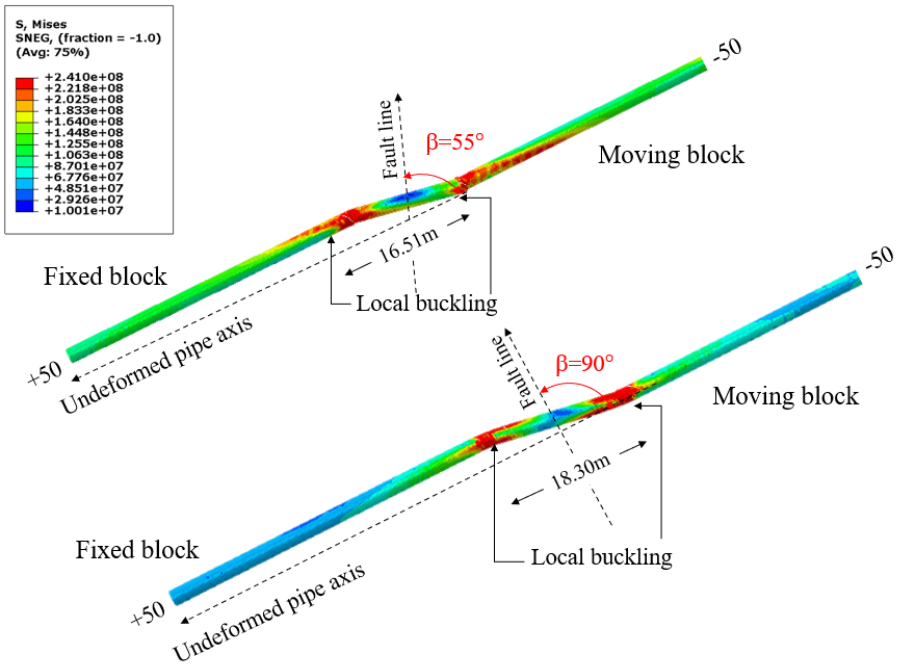

(b)

Figure 4-6. formed shapes of pipeline (w/internal pressure), (a) strain distribution, (b) stress distribution.

Figure 4-7 depicts the displacement curves and distributed axial strain along the spiral-welded steel pipeline. In Figure 4-7**Error! Reference source not found.**(a) it can be observed that the displacement curve trends of the two models are similar, indicating that the fault crossing angle does not significantly affect the trend of the displacement curve. Additionally, Figure 4-7(a) shows that a larger interaction angle results in a more significant displacement in the transverse direction. When the crossing angle is 90°, the horizontal displacement is applied to the model. On the other hand, as the crossing angle decreases, there are two displacement components in the horizontal and axial directions. Figure 4-7(b) illustrates the distribution of the (tensile) axial strain for the two different case studies when the fault movement is 1.0 m. In the model with a fault crossing angle of 55°, the fault movement generates a large tension force along the pipeline due to the axial displacement. Consequently, the pipeline experiences a larger tensile strain at both sides of the pipeline compared to the model with the crossing angle of 90°.

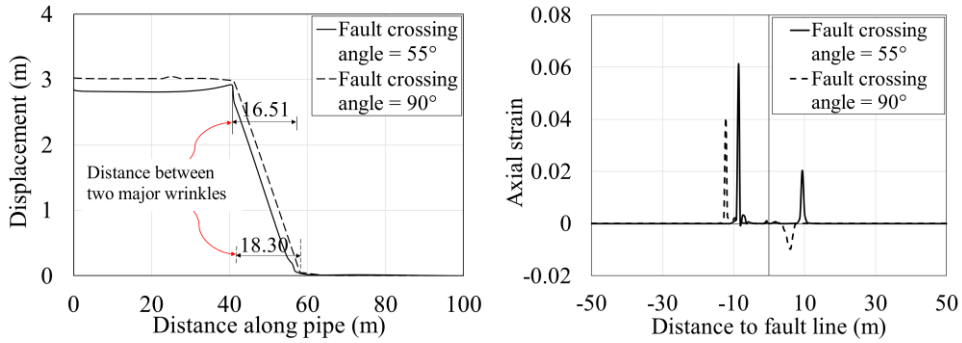

(a) (b)

Figure 4-7. Finite element results (a) Displacement curves, (b) axial strain curves.

Table 4-4 represents a comparison of results between validated models with different intersection angles. In the case of 90° intersection angle, which results in a pure bending

mode, two wrinkles are observed along the pipeline. However, as the intersection angle decreases, the probability of the formation of a third wrinkle increases. Additionally, the results indicate that the ovalisation parameter increases as the intersection angle decreases.

Table 4-4. Comparison of verified model with different intersection angles.

Intersection angle	Distance between wrinkles (m)	Average axial strain at wrinkles (1&2)	Rotation demands at wrinkles (1& 2) (degrees)	Location of the 3rd minor wrinkle (m)	Local buckling wavelength (cm)	Local buckling strain (%)	Ovalisation Parameter
55°	16.51	15-20%	7.1-8.9	13.3	50-55	0.22	0.126
90°	18.30	10-15%	4.5-6.3	-	60-65	0.13	0.061

4.4.2. Effect of burial depth ratio

In this section, the response of the spiral-welded pipeline to a strike-slip fault is examined at two different depths (1.50 m and 3.0 m) to determine how the pipeline's burial depth affects compression and axial strain. The soil properties used in the analysis are presented in Table 4-1.

Figure 4-8 illustrates the distribution of axial strain versus fault displacements at two major wrinkles of the pipeline. This figure illustrates how the maximum compressive strain and axial strain at wrinkles increase with increasing burial depth. As the burial depth increases, the gravity and frictional forces increase, and consequently, the axial and compressive force of the pipeline also increase. As a result, pipelines buried at greater depths are more prone to failure compared to those buried at shallower depths. Figure 4-8(b) represents the

maximum axial strain at wrinkle 2, which is in the soft soil block. A comparison of the results for the soft soil reveals that initially the axial strain is lower for shallow burial depths compared to deep burial depths. However, as the fault displacement increases, the pipeline tends to fold due to the lower friction force in the soft soil compared to the stiff soil. Thus, the axial strain increases abruptly after a displacement of 1.0 m. The effect of soil type on the behavior of spiral-welded steel pipeline is further investigated in the next sections.

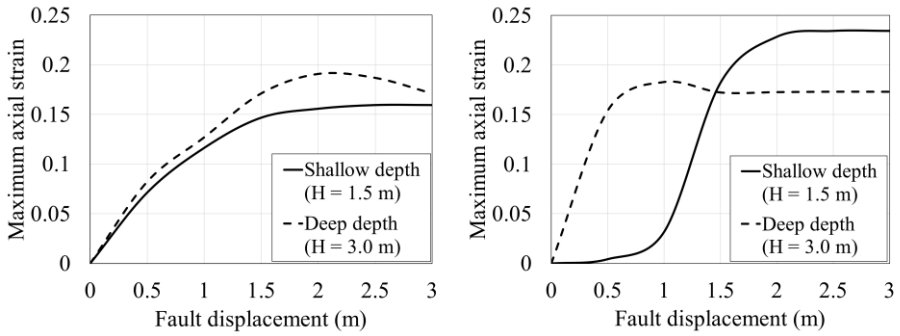

(a) (b)

Figure 4-8. Effect of burial depth on the maximum axial strain in the pipeline considering intersection angle = 55°, (a) wrinkle1, (b) wrinkle2.

The axial strain and stress distribution of the spiral-welded steel pipeline at different burial depths are displayed in Figure 4-9. As shown in Figure 4-9(a), the distance between the wrinkle decrease as the burial depth increases. Furthermore, Figure 4-9(b) shows the stress distribution along the pipeline. A comparison between Figure 4-9(a) and (b) reveals that as the burial depth increases, the maximum stress and strain become more concentrated in a small area. The distance between two major wrinkles in the buried pipeline at the greater depth is 8.30 m, whereas it is 16.51 m in the case of shallow burial depth.

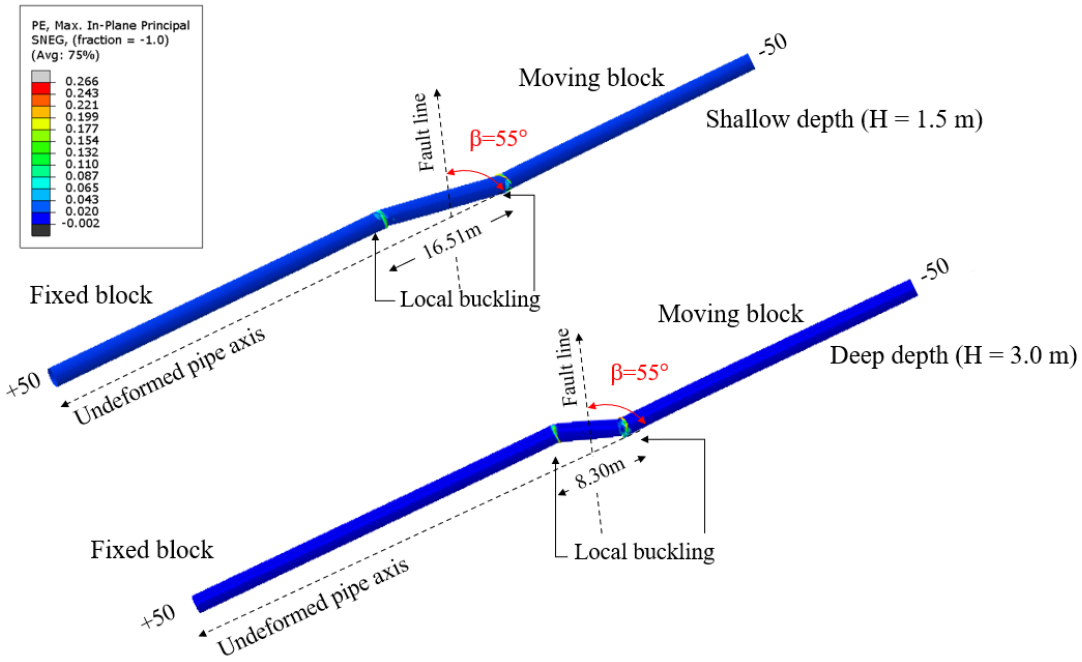

(a)

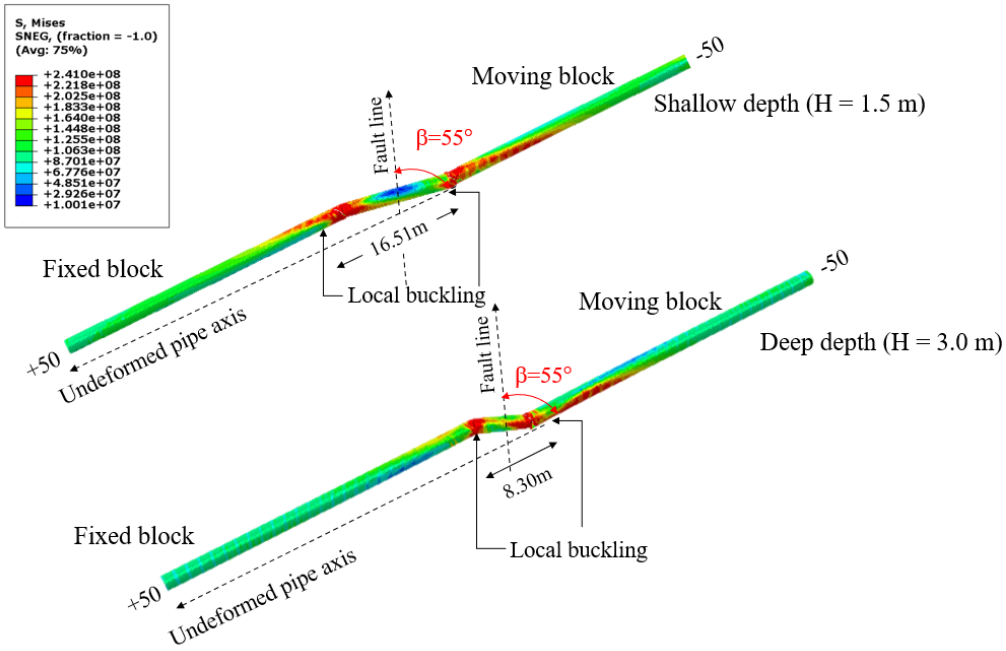

(b)

Figure 4-9. Deformed shapes of pipe (w/ internal pressure), intersection angle = 55° for different burial depths, (a) strain distribution, (b) stress distribution.

Figure 4-10 shows that the lateral displacement decreases with increasing burial depth. As mentioned before, as the burial depth increases, the soil weight increases, leading to an increase in the friction force. Consequently, the pipeline displacement decreases. The results of FEA for this section are presented in Table 4-5. The ovalisation parameter values of the pipeline are also presented in Table 4-5, assuming a fault movement of one meter. Comparing the ovalisation parameter between the two models indicates that in shallow burial depths, the local buckling of the pipeline is more severe due to the different soil properties on either side of fault.

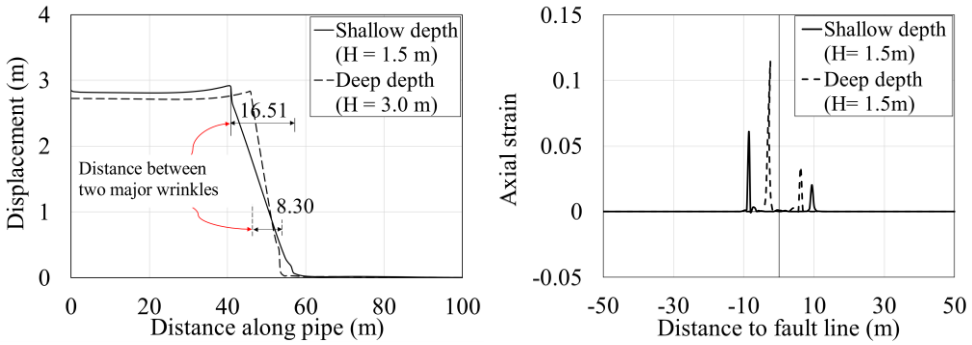

(a) (b)

Figure 4-10. Finite element results intersection angle = 55° for different burial depths (a) Displacement curves, (b) axial strain curves.

Table 4-5. Comparison of spiral-welded pipeline mechanical response considering different burial depth.

Burial depth (m)	Distance between wrinkles (m)	Average axial strain at wrinkles (1&2)	Rotation demands at wrinkles (1& 2) (degrees)	Location of the 3rd minor wrinkle (m)	Local buckling wavelength (cm)	Local buckling strain (%)	Ovalsation parameter
1.5	16.51	15-20%	7.1-8.9	13.3	50-55	0.22	0.126
3.0	8.30	12-20%	6.4-7.5	7.81	80-85	0.2	0.084

4.4.3. The influences of the helical angles of pipeline

In the numerical study conducted by Kaya et al. (2017), the effect of the helical angle on the pipeline response has been ignored. In this study, however, the influence of the helical angle on the behavior of a spiral-welded steel pipeline is investigated under different soil conditions (cohesive and non-cohesive) and two different intersection angles. The soil properties are presented in Table 4-6. An elastic-perfectly plastic Mohr-Coulomb model was used to represent the behavior of loose sand, dense sand, and clay. The finite element models used the same pipeline diameter, thickness, length, and burial depth as described in Figure 4-1. For this investigation, a total of four different helical angles (35°, 40°, 45°, and 55°) were used. To thoroughly analyze the finite element results, it is first necessary to first examine the deformed shape of the spiral-welded pipeline. Then, the strains in the critical cross-sections and the ovality of the pipeline are investigated to determine the influence of the helical angle on the behavior of the spiral-welded steel pipeline under a strike-slip fault.

Table 4-6. Soil properties for parametric studies (NAVFAC 1986).

Soil type	Cohesion (kPa)	Friction angle (°)	Young Modulus (MPa)	Density (kg/m^3)
Clay	50	20	25	2000
Loose Sand	18	30	20	1932
Dense Sand	20	35	45	2100

4.4.3.1. Intersection angle of 55 degrees

Figure 4-11 presents the deflection curves of the deformed spiral-welded steel pipelines under different soil conditions. Moreover, this figure depicts the distribution of axial strain on the pipelines. In this figure, the vertical axis represents the vertical component of the fault movement, and the horizontal axis represents the distance along the pipeline.

By comparing the deformed shapes, it is evident that soil properties have a significant impact on the deflection curve. Softer soils, such as loose sand, result in smaller axial strain, which leads to an increased distance between wrinkles in the pipeline.

Furthermore, the comparison of results reveals that wrinkle shapes are influenced by both soil properties and helical angle. For instance, in Figure 4-11(a), (b), and (c), the wrinkle shape of the pipeline with a helical angle of 40° demonstrates that in clayey soil, due to the cohesive force, local buckling occurs very close to the fault line, and the failure shape of the pipeline is more severe in clay compared to non-cohesive soils. Moreover, as depicted in Figure 4-11(a), the shape of the wrinkles indicates that, depending on the helical angle, the location and shape of critical cross-section changes. In general, different helical angles that have various welding lengths along the pipeline, make different plastic strains on the pipeline. Therefore, changing the helical angle may affect the amount of axial strain and

hoop strain. When a spiral-welded pipeline is subjected to a strike-slip fault with an intersection angle smaller than 90°, the pipeline is affected by two different displacement components in both vertical and horizontal directions. Consequently, as the fault moves, the amount of axial and hoop strains on the pipeline undergoes changes.

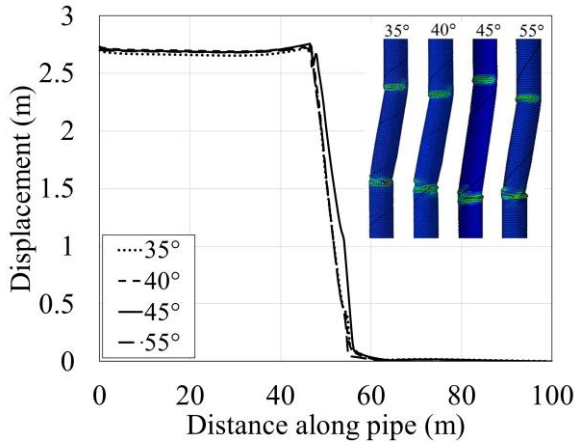

(a)

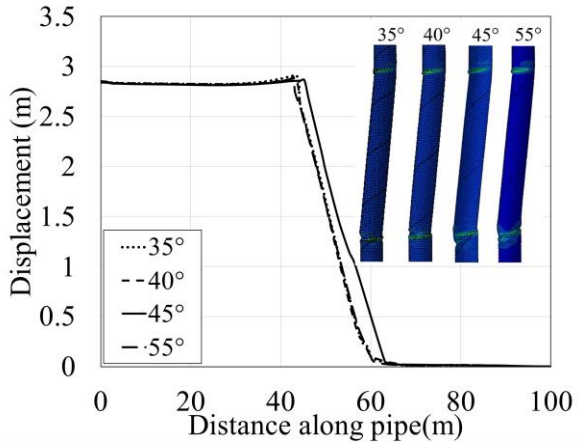

(b)

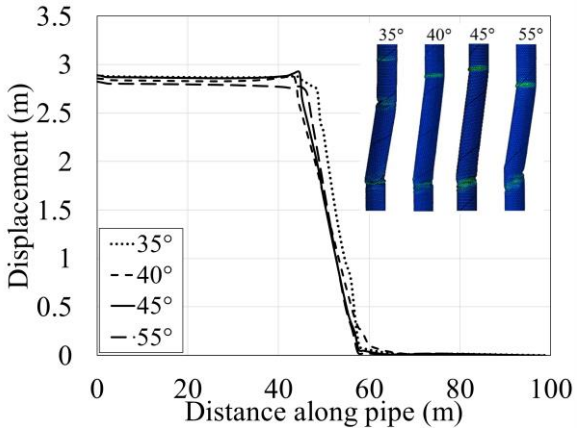

(c)

Figure 4-11. Deformed shape of pipeline considering different helical angle (a) clay, (b) loose sand, (c) dense sand.

The finite element results are summarized in Table 4-7. It is noteworthy that the distance between two wrinkles depends on the pipeline diameter, which is estimated to be 8D, 7D, and 5D for loose sand, dense sand, and clay, respectively. This distance is also affected by the helical angle of the pipeline.

As mentioned before, after conducting a thorough evaluation of pipeline behavior by comparing deformation curves, the critical cross-sections were investigated by analyzing strains.

Fault movement may result in a stress concentration in specific areas of the pipeline, potentially leading to localized deformation or even buckling. In buckled regions, wavy patterns manifest after the transition from smooth deformations along the critical cross-section. As displacement increases, one of the wrinkles becomes dominant, resulting in local buckling (Vazouras et al., 2011). Spiral-welded pipelines may experience excessive stresses in the welding area due to severe compressive strain in the critical section.

Therefore, the helical angle of the pipeline plays a crucial role in reducing strain and determining the distance between the two major wrinkles. When the intersection angle is less than 90°, fault movement involves both vertical and axial components. Consequently, both compressive and axial (tensile) strains may affect the pipeline response.

Table 4-7. Spiral-welded steel pipeline response under different soils and the intersection angle of 55°.

Pipe helix angle (°)	Soil type	Separation distance between wrinkles (m)	Average axial strain at wrinkles (1&2)	Location of the 3rd minor wrinkle (m)
35	Loose sand	16.57	15-17%	-
	Dense sand	14.26	18-19%	5.35
	Clay	8.95	14-27%	2.78
40	Loose sand	16.73	15-16%	-
	Dense sand	14.94	19-20%	9.43
	Clay	8.67	18-23%	8.41
45	Loose sand	17.61	12-15%	-
	Dense sand	14.70	17-18%	4.86
	Clay	10.48	18-22%	3.21
55	Loose sand	15.65	14-15%	-
	Dense sand	11.55	18-20%	2.5
	Clay	9.46	19-25%	3.01

The pipeline failure criteria were discussed in section 4.3.3. According to ALA and PRCI, the tensile strain capacities for high-quality pipeline are associated with defined

performance goals. The typical limitation of compressive strain in high-quality pipelines is 0.25%. Compressive limit states for compressive strains provided by Wijewickreme (2006) are 0.33% to 2%. However, these values are considered too low as higher compressive strains can cause permanent deformation of the pipeline, leading to reduced strength and durability of the pipeline, and potential failure. Comparing the average yielding strain of different pipelines with the considered limit states for such pipelines indicates that the chosen strain limits are conservative.

The numerical results in Figure 4-12 depict the strain distribution of spiral-welded steel pipelines buried in different types of soils with varying helical angles. The comparison of compressive strains in this figure (Figure 4-12(a), (b), and (c)) indicates that different helical angles result in different strains at the critical cross-section. Interstingly, a helical angle of 45° produces a smaller value of comressive strain compared to the other angles. In the case of the buried pipeline in dense sand with the helical angle of 35˚ (see Figure 4-12(c)), a smaller value of the compressive strain is observed due to the presence of a third wrinkle between the two major wrinkles. This third wrinkle becomes apparent after approximately 0.5 m of fault movement.

These figures show that a spiral-welded pipeline buried in clayey soil experiences failure at earlier stages of fault displacements compared to non-cohesive soils. This attributed to the larger cohesive forces exerted on the pipeline in clayey soil. Additionally, the figures show that, at the same displacements, the maximum axial strains are considerably lower than the maximum compressive strains, indicating the significance of compressive strains. The maximum strain at the critical cross-section of the pipeline increases as the fault

displaces. Once yielding occurs in the pipeline and wrinkles form, the strains remain relatively constant as the fault displacement increases.

The maximum axial strain results (See Figure 4-12(d), (e), and (f)) indicate that increasing the helical angles leads to an increase in the axial strain in cohesive soil, while it results in a decrease in non-cohesive soils. The distributions of axial strains along the spiral-welded pipeline are presented in Figure 4-12(g), (h) and (i). These figures depict the axial strain on the side of the pipeline where it is subjected to compression and the fault movement is 1.0 m. It is observed that the spiral-welded pipeline with a helix angle of 55° exhibits a larger strain, while the pipeline with the helix angle of 45° shows smaller values of avarage axial strain. The finite element results are summarized in Table 4-7.

The ovality limit for high-quality pipelines, such as spiral-welded pipelines, in DNV standards depends on various factors such as pipeline material, size, and intended use, as well as operating conditions. For example, according to DNVGL-ST-F101 Submarine Pipeline Systems, the maximum allowable ovality limit for high-strength carbon steel pipelines, including spiral-welded pipelines, is specified as 0.75% of the pipe diameter.

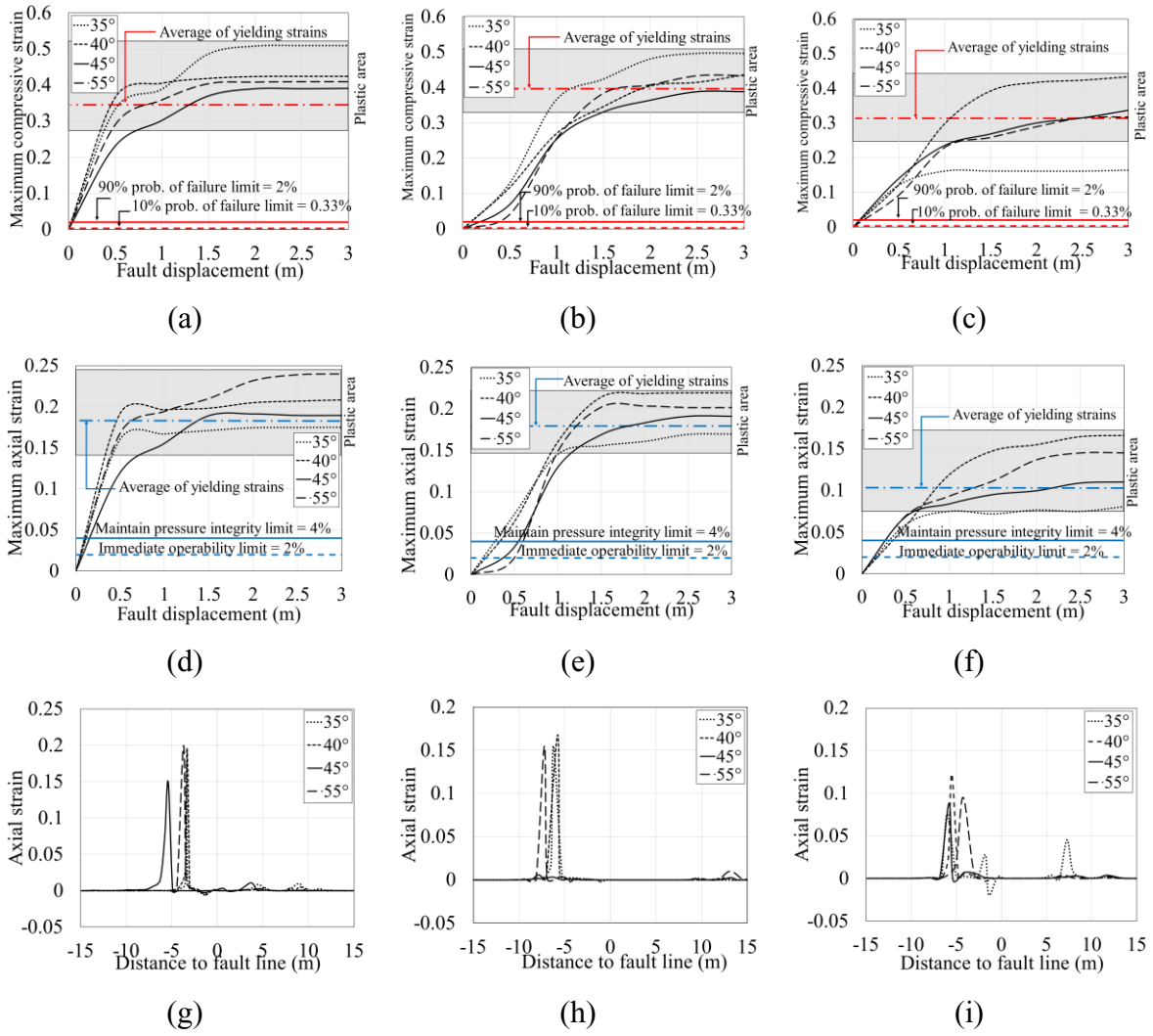

Figure 4-12. Effect of buried pipeline helical angle on the distribution of strain considering the intersection angle of 55°at critical cross-section of pipeline, (a) maximum compressive (buried in clay), (b) maximum compressive strain (buried in loose sand), (c) maximum compressive strain (buried dense sand), (d) maximum axial strain (buried in clay), (e) maximum axial strain (buried in loose sand), (f) maximum axial strain (buried in dense sand), (g) axial strain distribution along the pipeline (buried in clay), (h) axial strain distribution along the pipeline (buried in loose sand), (i) axial strain distribution along the pipeline (buried in dense sand).

Figure 4-13 shows the ovalisation parameter of the pipeline subjected to a strike-slip fault. As shown in this figure, the spiral-welded pipeline exceeds the allowable value of 0.15 when the fault displacement is 3.0m. The comparison of the results demonstrates that the ovalisation parameter is influenced by the helix angle of the pipeline and the soil type. Increasing the helix angle leads to an increase in the ovalization parameter, except for the case with a helix angle of 45°, which exhibits a smaller value. The results of these case studies show that the mechanical properties of soil (i.e. friction angle and cohesion) play a significant role in the formation of major wrinkles. Besides, in dense and clayey soil, the probability of the formation of a third wrinkle increases for different helix angles. In contrast, in the loose sand, the presence of a third wrinkle is not observed on the pipeline due to the lower friction and cohesive forces in such soil conditions.

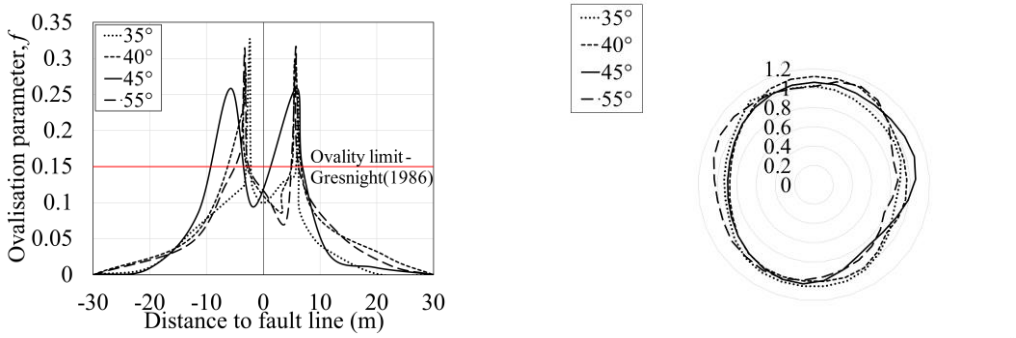

(a)

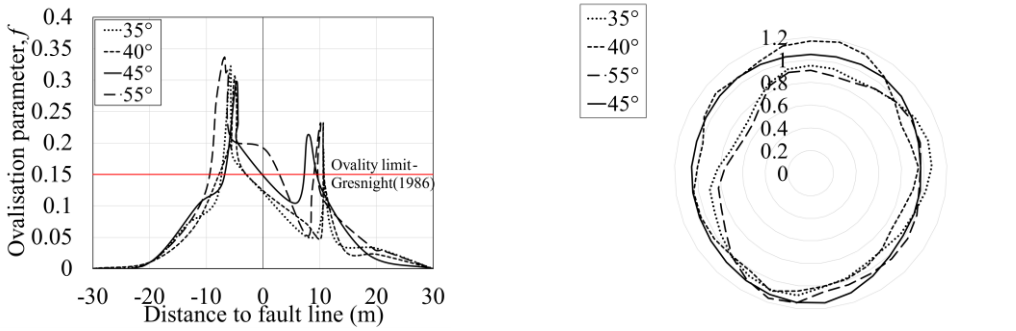

(b)

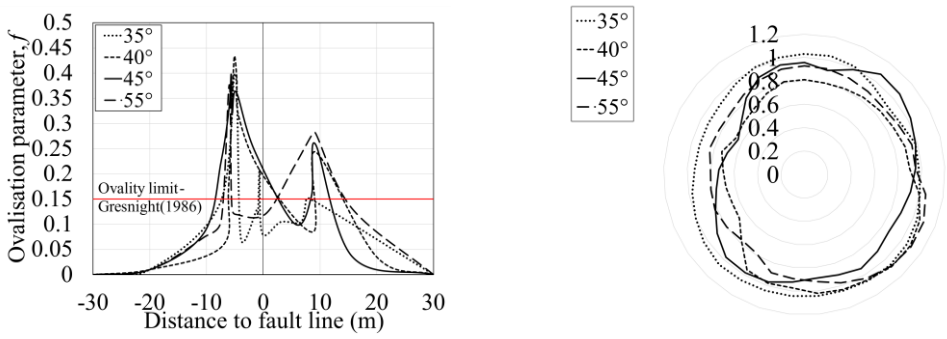

(c)

Figure 4-13. Ovalisation parameter for spiral-welded pipeline considering the intersection angle of 55°, (a) clay, (b)loose sand, (c)dense sand.

4.4.3.2. intersection angle of 90 degrees

In this section, the effect of helix angle on the spiral-welded pipeline behavior in the fault zone with an intersection angle of 90° is investigated. The structural response of the pipeline is depicted in Figure 4-14. The numerical model results are summarized in Table 4-8. A comparison of these finite element results with Table 4-7 indicates that the maximum strains experienced by the pipeline are significantly lower when subjected to fault movement with an intersection angle of 90° compared to the case with an intersection angle of 55°.

Figure 4-15 illustrates the distributed strain on the pipeline at both the critical cross-section and along the pipeline. As mentioned earlier, an increase in the helical angle results in a decrease in compressive strain while the axial strain increases. For a 90° intersection angle, it has been observed that the maximum axial strain can be minimized (Liu et al., 2008). Therefore, at a 90° intersection angle, the axial strain value is lower compared to the axial strain of the pipeline with an intersection angle smaller than 90°.

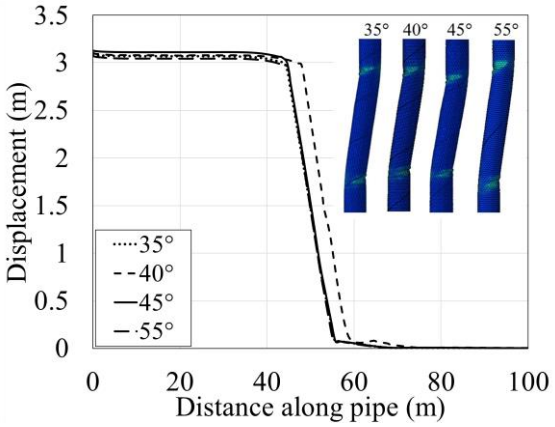

(a)

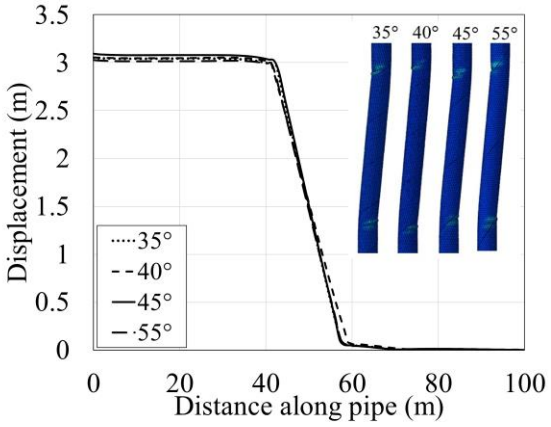

(b)

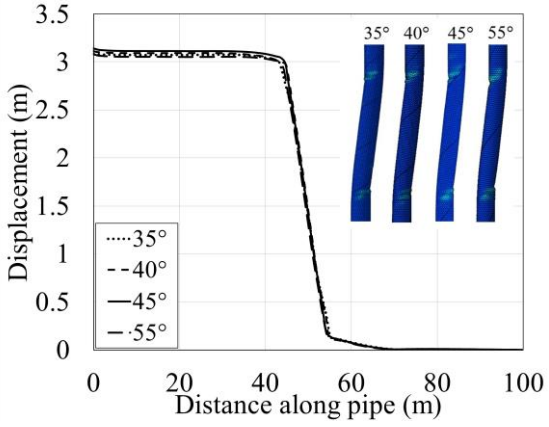

(c)

Figure 4-14. Deformed shape of pipeline considering different helical angle (a) clay, (b) loose sand, (c) dense sand.

Table 4-8. Spiral-welded steel pipeline response under different soils and the intersection angle of 90°.

Pipe helix angle (°)	Soil type	Separation distance between wrinkles (m)	Average axial strain at wrinkles (1&2)	Location of the 3rd minor wrinkle (m)
35	Loose sand	15.56	10-12%	-
	Dense sand	12.93	11-12%	3.08
	Clay	12.21	10-11%	10.96
40	Loose sand	17.20	10-11%	-
	Dense sand	11.65	12-13%	7.68
	Clay	11.62	10-12%	6.54
45	Loose sand	16.39	11-12%	-
	Dense sand	10.64	10-11%	2.94
	Clay	12.41	10-11%	5.12
55	Loose sand	16.58	12-14%	-
	Dense sand	11.14	13-15%	3.51
	Clay	11.34	11-13%	4.10

This can be observed by comparing the maximum axial and compressive strains in Figure 4-15. Furthermore, the comparison of these curves indicates that the helix angle of 45° is favorable for the pipeline due to its smaller compressive and axial strains. Analyzing the maximum axial and compressive strains at wrinkles reveals that when the helix angle ranges from 40° to 45°, both the compressive and axial strains are minimized. Therefore, the most suitable helix angle should be designed within the range of 40° to 45°.

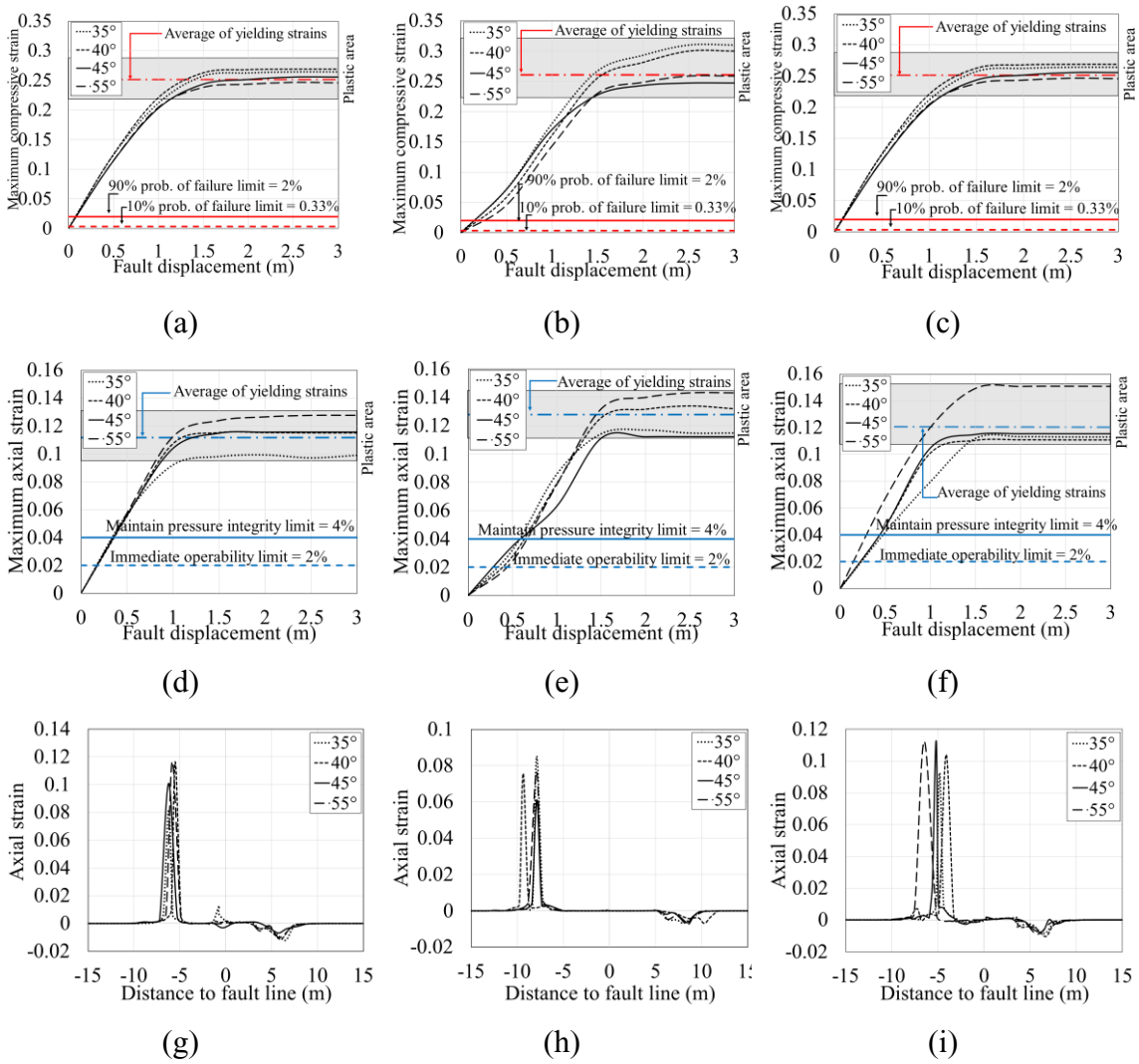

Figure 4-15. Effect of buried pipeline helical angle on the distribution of strain considering the intersection angle of 90°at critical cross-section of pipeline, (a) maximum compressive (buried in clay), (b) maximum compressive strain (buried in loose sand), (c) maximum compressive strain (dense sand), (d) maximum axial strain (buried in clay), (e) maximum axial strain (buried in loose sand), (f) maximum axial strain (buried in dense sand), (g) axial strain distribution along the pipeline (buried in clay), (h) axial strain distribution along the pipeline (buried in loose sand), (i) axial strain distribution along the pipeline (buried in dense sand).

The comparison of the ovalisation parameter for the spiral-welded pipeline at an intersection angle of 90° is presented in Figure 4-16. It is evident from this figure that the ovalisation parameter value is smaller when the helix angle falls within the range of 40° to 45° degrees, compared to other helix angles.

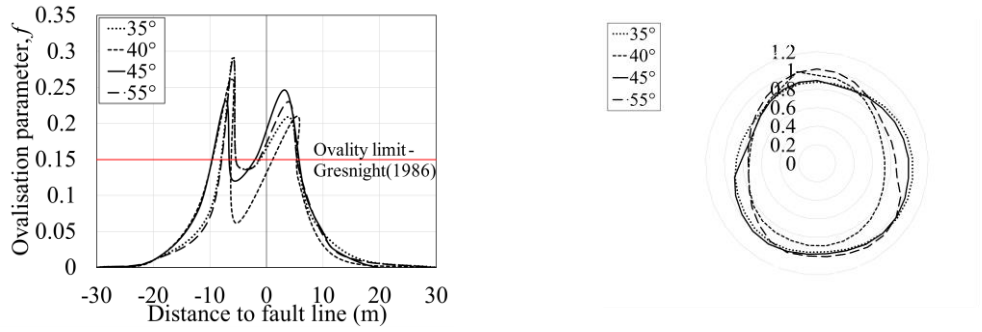

(a)

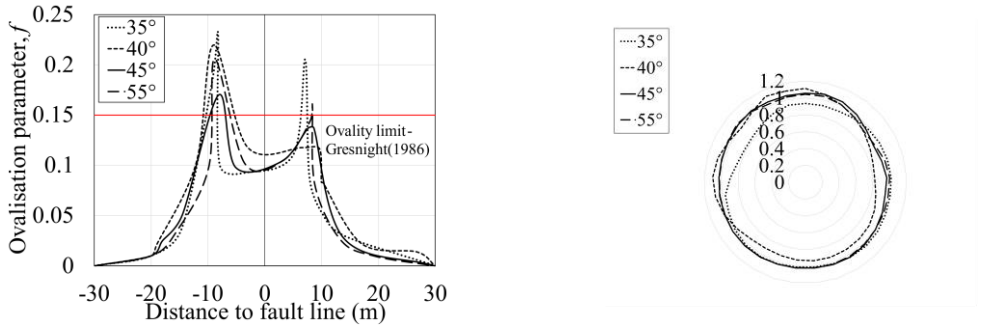

(b)

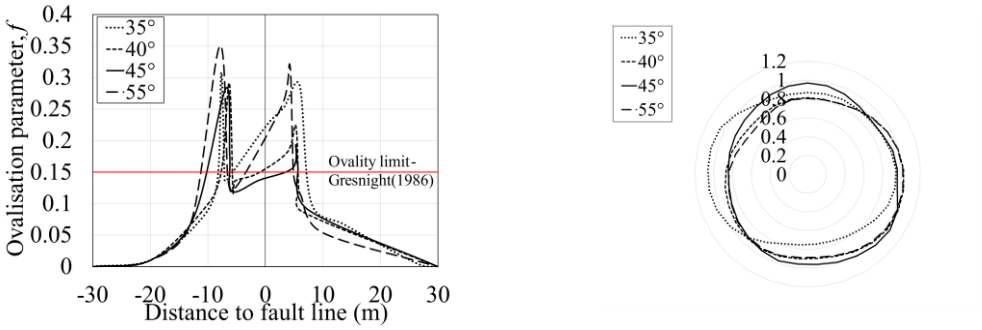

(c)

Figure 4-16. Ovalisation parameter for spiral-welded pipeline considering the intersection angle of 90°, (a) clay, (b)loose sand, (d)dense sand.

4.5. Conclusions

The mechanical behaviour of the buried spiral-welded pipelines subjected to the strike-slip faults was investigated using advanced finite element simulation tools. The study unveiled notable disparities in the bending deformation and strain of the spiral-welded pipeline across various soil conditions. The soil density and stiffness were identified to have as the primary factors influencing the pipeline's response to the strike-slip fault. Specifically, a higher soil density in granular soil led to the occurrence of local buckling of the pipeline at an earlier stage compared to a buried pipeline in loose sand due to the heightened interaction between the soil and the pipeline.

Moreover, the response of the pipeline to fault movement was found to be intensified by reducing the burial depth. In granular soils such as loose sand, the pipeline exhibited wrinkling due to low contact forces. The probability of the formation of a third wrinkle was also found to increase with increasing cohesive and friction forces. Additionally, a decrease in the intersection angle corresponded to an intensified response of the spiral-welded pipeline to fault movement and an increased occurrence of local buckling.

Finally, it was observed that the helix angle played a significant role in affecting the reduction of axial strain and deformation of spiral-welded pipelines. Therefore, the selection of an appropriate angle becomes crucial when dealing with pipeline crossing through faults.

References

ALA, American Lifelines Alliance Guidelines for the Design of Buried Steel Pipes, 2005.

Alrsai M, Karampour H, Albermani F. Numerical study and parametric analysis of the propagation buckling behaviour of subsea pipe-in-pipe systems. Thin-Walled Structures. 2018 Apr 1;125:119-28..

Chen WW, Shih BJ, Chen YC, Hung JH, Hwang HH. Seismic response of natural gas and water pipelines in the Ji-Ji earthquake. Soil Dynamics and Earthquake Engineering. 2002 Oct 1;22(9-12):1209-14.

Demofonti G, Ferino J, Karamanos SA, Vazouras P, Dakoulas P. An integrated experimental-numerical approach to predict strain demand for buried steel pipelines in geo-hazardous areas. InRio Pipeline Conference and Exposition 2013.

DNV, G., 2017. DNVGL-ST-F101, Submarine Pipeline Systems. Standard (DNV GL).

Eidinger JM, O'Rourke M, Bachhuber J. Performance of pipelines at fault crossings. In Proceedings of the 7th US National Conference of Earthquake Engineering, Earthquake Engineering Research Institute (EERI), July 2002 Jul 21 (pp. 21-25).

Gresnigt AM. Plastic design of buried steel pipelines in settlement areas.(1987).

Ha D, Abdoun TH, O'Rourke MJ, Symans MD, O'Rourke TD, Palmer MC, Stewart HE. Centrifuge modeling of earthquake effects on buried high-density polyethylene (HDPE) pipelines crossing fault zones. Journal of geotechnical and geoenvironmental engineering. 2008 Oct;134(10):1501-15.

Jalali HH, Rofooei FR, Attari NK, Samadian M. Experimental and finite element study of the reverse faulting effects on buried continuous steel gas pipelines. Soil Dynamics and Earthquake Engineering. 2016 Jul 1;86:1-4.

Kaya ES, Uçkan E, O'Rourke MJ, Karamanos SA, Akbas B, Cakir F, Cheng Y. Failure analysis of a welded steel pipe at Kullar fault crossing. Engineering Failure Analysis. 2017 Jan 1;71:43-62.

Kennedy RP, Williamson RA, Chow AM. Fault movement effects on buried oil pipeline. Transportation Engineering Journal of ASCE. 1977 Sep;103(5):617-33.

Kokavessis NK, Anagnostidis GS. Finite element modeling of buried pipelines subjected to seismic loads: soil structure interaction using contact elements. InASME Pressure Vessels and Piping Conference 2006 Jan 1 (Vol. 47594, pp. 119-125).

Liu M, Wang YY, Yu Z. Response of pipelines under fault crossing. InISOPE International Ocean and Polar Engineering Conference 2008 Jul 6 (pp. ISOPE-I). ISOPE.

Newmark NM, Hall WJ. Pipeline design to resist large fault displacement. In Proceedings of US national conference on earthquake engineering 1975 Jun 18 (Vol. 1975, pp. 416-425).

NAVFAC. 1986. Foundations, and earth structures. Naval Facilities Engineering Command (NAVFAC) design manual DM7.02. U.S. Government Printing Office, Washington, D.C.

O'Rourke TD, Palmer MC. Earthquake performance of gas transmission pipelines. Earthquake Spectra. 1996 Aug;12(3):493-527.

O'Rourke, M. J., Abdoun, T. H., Ha, D., and Symans, M. D. Factors influencing the behavior of buried pipelines subjected to earthquake faulting. Soil Dynamics and Earthquake Engineering. 2009. 29(3):415-427.

PRCI. 2009. Guidelines for constructing natural gas and liquid hydrocarbon pipelines through areas prone to landslide and subsidence hazards. In Pipeline Research Council International.

Fard SS, Nekooei M, Oskouei AV, Aziminejad A. Experimental and numerical modeling of horizontally-bent buried pipelines crossing fault slip. Latin American Journal of Solids and Structures. 2019 Apr 8;16.

Tang AK, editor. Izmit (Kocaeli), Turkey, earthquake of August 17, 1999 including Duzce earthquake of November 12, 1999: lifeline performance. ASCE Publications; 2000.

Tsai JS, Jou LD, Lin SH. Damage to buried water supply pipelines in the chichi (Taiwan) earthquake and apreliminary evaluation of seismic resistance of pipe joints. Journal of the Chinese Institute of Engineers. 2000 Jun 1;23(4):395-408.

TWI Report, Spiral Welded Pipe for Oil & Gas: State-of-the-Art, PR6161, August 2002.

Vazouras P, Karamanos SA, Dakoulas P. Mechanical behavior of buried steel pipes crossing active strike-slip faults. Soil Dynamics and Earthquake Engineering. 2012 Oct 1;41:164-80.

Vazouras P, Dakoulas P, Karamanos SA. Pipe–soil interaction and pipeline performance under strike–slip fault movements. Soil Dynamics and Earthquake Engineering. 2015 May 1;72:48-65..

Wang LR, Yeh YH. A refined seismic analysis and design of buried pipeline for fault movement. Earthquake engineering & structural dynamics. 1985 Jan;13(1):75-96.

Xie X, Symans MD, O'Rourke MJ, Abdoun TH, O'Rourke TD, Palmer MC, Stewart HE. Numerical modeling of buried HDPE pipelines subjected to strike-slip faulting. Journal of Earthquake Engineering. 2011 Dec 1;15(8):1273-96.

Zhang J, Liang Z, Zhang H. Response analysis of buried pipeline subjected to reverse fault displacement in rock stratum. Transactions of FAMENA. 2016 Nov 22;40(3):91-100.

Zhang J, Liang Z, Han CJ, Zhang H. Numerical simulation of buckling behavior of the buried steel pipeline under reverse fault displacement. Mechanical Sciences. 2015 Sep 22;6(2):203-10.

Chapter 5

The pipeline-backfill-trench wall interaction effect on the accumulation of 2D lateral soil resistance against moving pipeline

Mozhgan Asgarihajifirouz[1], Xiaoyu Dong[2], Hodjat Shiri[3]

1: Department of Civil Engineering
Memorial University of Newfoundland

2: Post-doctoral Fellow, Department of Civil Engineering
Memorial University of Newfoundland

3: Associate Professor, Department of Civil Engineering
Memorial University of Newfoundland

This chapter is under review as a journal manuscript.

5.1. Abstract

Over the past century, onshore buried steel pipelines have been widely regarded as the most cost-effective and efficient means of connecting fuel supply systems. To protect these pipelines from geohazards and environmental loads in these regions, the use of pre-excavated seabed soil has been a common cost-effective practice. The difference in shear strength between the seabed soil and the backfilling soil may have an influence on the interaction between the pipeline and the backfilling soil and the failure mechanism of the surrounding soil due to the strike-slip fault. In this study, a Coupled Eulerian-Lagrangian (CEL) method has been used to evaluate the response of buried steel pipelines. A total of 13 case studies were analyzed to investigate the effects of various parameters on the failure mechanisms of the seabed soils. The results revealed that considering the strain-softening effect with a linear distribution of soil strength in the pipeline-backfilling soil interaction results in a reduction in the ultimate soil strength and upward movement of the pipeline.

Keywords: pipe-backfilling soil interaction; strike-slip fault; large deformation analysis; strain-softening effect; failure mechanism.

5.2. Introduction

Over the past two decades, oil and gas facilities in the offshore area have been extended from deep water floating producing structures to shallow water fixed systems (Strogen et al. 2016). One of the safest ways to transport hydrocarbons from wells to production facilities is using subsea pipelines. These pipelines are commonly buried inside the trench to protect against the external and internal loads in the shallow sea. Recently, the structural

behavior of buried pipelines subjected to permanent ground motion, such as fault movement, has received a lot of attention (Karamitros et al. (2007), Xie et al. (2013), Sarvanis et al. (2017;2018), Banushi et al. (2018), Tsatsis et al. (2019), Talebi et al. (2020)). Permanent ground motion, such as fault crossing and land sliding, may cause large lateral displacement of the trenched pipelines (see Figure 5-1 (a)). It has been recognized that the complicated pipeline-soil interaction in the vicinity of the fault zone has a significant effect on the behaviour of the pipeline. In the design codes, the pipelines are designed inside a uniform seabed, and the effects of trenching (the geometry and material properties) have been ignored (API (2013), ALA (2005), PRCI, DNV. GL (2017)). Therefore, a proper understanding of the pipeline-trenched backfill soil interaction is necessary for engineers to safeguard against lateral movement. Figure 5-1(b) illustrates a schematic shape of a buried pipeline and the surrounding soil deformation.

Continuum numerical models are considered the most efficient way to model the pipe-fault crossing phenomena and assess the local buckling of the pipeline. Most of the research conducted on the evaluation of pipeline-soil interaction under fault crossing has not considered the backfilling effect on the pipeline, and the soil domain has been considered uniform (Liu et al. (2004), Vazouras et al. (2010;2015;2017), Zhang, L. et al. (2016;2017), Zhang, J. et al. (2016), Valsamis et al. (2020)). As mentioned in previous studies, even for excavated trenches in the stiff soil, modelling the trench geometry is required (Cheng et al. (2019), Trifonov et al. (2015)). Modelling a 3D trench pipeline through the Large Deformation Finite Element (LDFE) analysis faces several challenges, including extensive computational effort, difficulties in simulating ground movement, modelling the contact

between the pipe, backfill, and trench wall, etc. These difficulties have led the researchers to assume a Lagrangian soil domain and compromise the accuracy of the analysis.

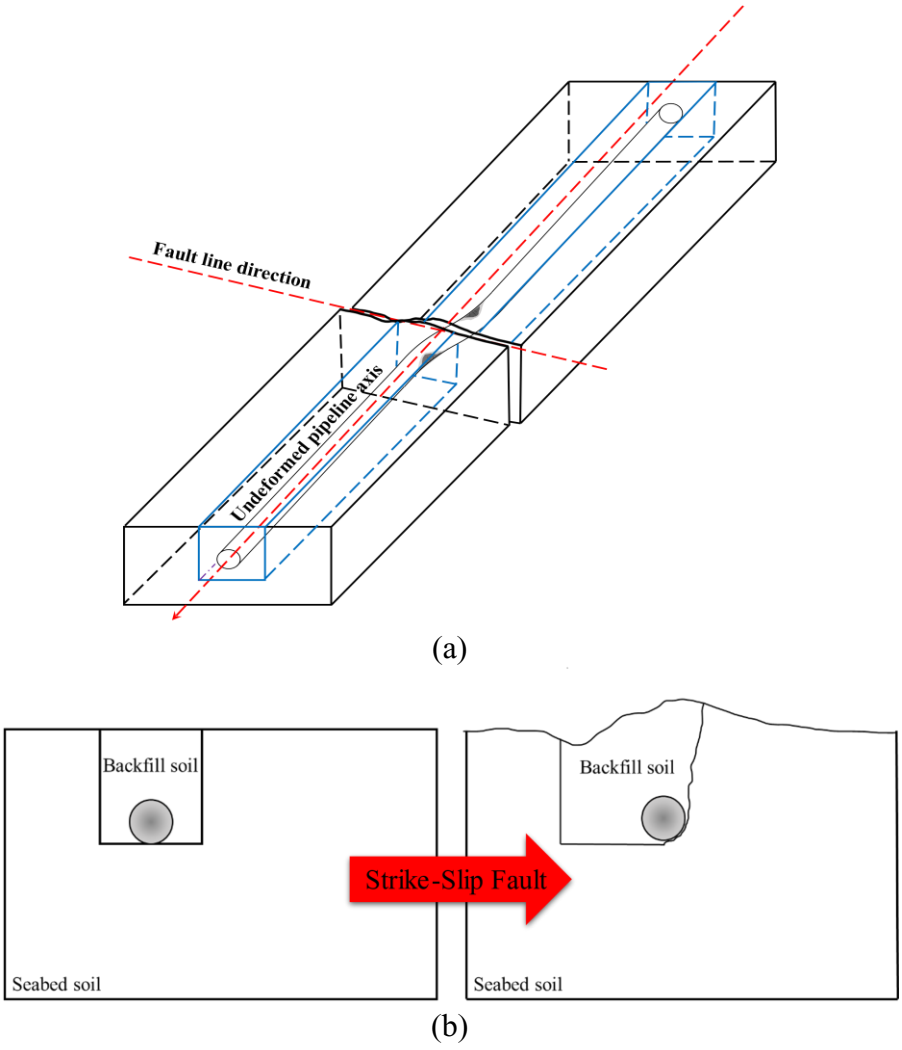

Figure 5-1. Schematic representation of (a) 3D view of a pipeline interaction with strike-slip fault rupture, (b) 2D view of pipeline-backfilling trench interaction.

The existing solutions for predicting lateral soil resistance are usually based on lateral pipeline or pile-soil interaction or plate anchor-soil interactions in uniform soil (Ovesen et al. (1964), Tschebotarioff et al. (1973), Wantland et al. (1979), Ng (1994), Merifield et al.

(2001)). Due to the shear strength difference between the backfilling and seabed soil, the lateral load-displacement response of the pipeline may change. Therefore, the failure mechanism of the surrounding soil and pipe-soil interaction may be affected (Paulin (1998), Kianian et al. (2018), Kianian and Shiri (2020;2021)).

Only a limited number of experimental models have been employed to investigate the pipeline-backfill-trench interaction due to the high costs and time requirements associated with such studies. The experimental studies conducted by Paulin (1998) revealed the impact of trench geometry, backfilling material properties, stress history, and relative displacement rate on lateral pipe-clayey soil interactions. Kianian et al. (2018), and Kianian and Shiri (2020; 2021) conducted a series of centrifuge tests to observe the failure mechanism of the backfill and native seabed soil. In their study, the progressive failure mechanism was visualized using a transparent acrylic sheet, digital camera, and PIV techniques.

In previous studies, there is no accurate plasticity solution for large deformation problems considering the trench effect. However, suggestions proposed by Randolph and Houlsby (1984) have been proposed for circular piles with different depths and failure mechanisms. In this study, this challenge is investigated using the Coupled Eulerian-Lagrangian (CEL) method in the ABAQUS software. A modified Tresca model accounting for strain-softening effects was incorporated to model the surrounding soil (Zhang, 2015; 2019). The numerical model was first verified by comparing the horizontal resistance factors (i.e., the ultimate horizontal resistance normalized by soil strength) of a pipeline embedded in uniform soil with the published analytical and experimental studies (Paulin (1998) and Kianian et al. (2018)). Then, numerical models were developed to simulate the

trenched/backfilled pipelines, where the influence of key factors on the pipeline-backfill-trench interaction was investigated through a parametric study. The numerical model results in undrained conditions show a good agreement with conducted test results. Overall, the study showed that the current design practice that uses uniform soil conditions and neglects the trenching effect overestimates the lateral soil resistance for large pipeline displacements and underestimates it for small (inside the trench) to moderate displacements (approaching the trench wall).

5.3. Material and Methods

In this study, the Coupled Eulerian-Lagrangian (CEL) method in ABAQUS/Explicit software is used to conduct the large deformation analysis. The CEL analysis is a dynamic explicit analysis that is conditionally stable and overcomes the usual convergence issues encountered in unconditionally stable implicit analysis.

The advantage of using the CEL method is the computational speed it offers in dealing with fluid-solid interaction problems. The CEL method effectively addresses issues such as severe mesh distortion and highly localized shear strain that may arise in conventional finite element analysis. Unlike conventional analysis, the CEL method does not involve mesh deformation or nodal displacement. Instead, the boundary condition is defined in terms of velocity. In ABAQUS, the Eulerian volume fraction tool is used to specify the initial conditions of the elements based on the fraction of each element to be occupied by any of the Eulerian materials. The CEL framework is limited to three-dimensional modelling, which means that the analysis will be conducted with only one element in the

pipeline's axial direction. In this analysis, the plane strain condition is adopted, which is commonly used in pipeline cross-sectional analysis.

5.3.1. Model configuration

In the CEL analysis, the entire domain consists of soil as Eulerian material, void space, and a buried Lagrangian pipe. The soil was modelled as an anisotropic continuum domain, considering the Tresca yield criterion to simulate undrained conditions. The soil domain is represented using 8-node linear Eulerian brick elements with reduced integration and hourglass control (EC3D8R). The pipeline was modelled as a 3D discrete rigid body using 4-node 3D bilinear rigid quadrilateral elements (R3D4). To prevent material flow out of the domain, all external faces of the Eulerian domain were restrained in their normal directions. The pipeline ends were extruded out of the front and rear sides of the Eulerian domain (as shown Figure 5-2) to avoid artificial friction between the soil and the pipeline end faces.

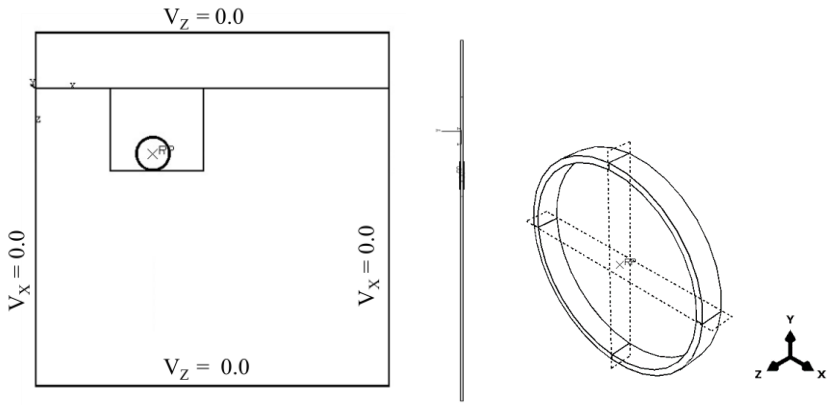

(a) (b)

Figure 5-2. CEL trenched pipeline model (a) Eulerian domain, (b) Lagrangian pipe.

The simulations began with a geostatic step to initialize the prototype stress condition in the soil body. In the second step, the pipe was pushed downward to achieve the specified initial embedment depth with a velocity of 0.05 m/s. Subsequently, in the third step, the pipe was subjected to a constant lateral velocity of 0.046 m/s. The pipe did not have any vertical displacement restraint. The chosen lateral velocity of the pipe in the centrifuge test was set to be sufficiently fast to be considered undrained conditions.

5.3.2. Soil properties and the pipe-soil interaction behavior

The soil was modelled as an isotropic continuum material with the Tresca yield criterion, which is equivalent to the Mohr-Coulomb yield criterion with a friction angle of zero. The soil's elastic behaviour was defined by Young's modulus to shear strength ratio of $E = 500\, S_u$, and Poison's ratio of v = 0.495 to ensure zero volume change. To account for strain-softening effects, the empirical equation proposed by Zhang et al. (2015; 2019) was incorporated as follows:

$$s = s_u + (s_{u,r} - s_u)\frac{\gamma^p}{\gamma_r^p} \tag{5-1}$$

where s_u is the peak undrained shear strength, $s_{u,r}$ is the residual undrained shear strength, γ^p is the accumulated plastic shear strain, and γ_r^p is the value of γ^pthat reduces the shear strength from peak to residual. In this study, the effect of soil strength gradient on the strain-softening was considered to model pipe-soil interaction. This was implemented using a VUSDFLD subroutine for the explicit analysis in the CEL model.

The VUSDFLD subroutine gives access to the material point quantity at the beginning of the time increment, so capturing the effect of the updates during the increment is impossible. Consequently, the accuracy of the results is highly dependent on the length of the time increment. This issue can be significantly resolved using dynamic explicit analysis. It overcomes the limitations of the VUSDFLD subroutine by considering the influence of updates during each time increment and accounting for inertia effects.

The rate effect was ignored in this study because the soil is in undrained condition and under strike-slip fault which is a high-speed incident. Depending on the soil drainage condition, strain rates may affect soil strength during high-speed incidents, such as fault movements. Undrained soils subjected to high strain rates can generate high excess pore water pressures. As a result of high pore pressure, the effective stress and shear strength of the soil may be reduced. This may create instability or liquefaction in saturated soils. On the other hand, in drained conditions, high strain rates can lead to increased soil stiffness or Young's modulus. The soil becomes stiffer and less deformable at higher rates of strains. The trench configuration and soil properties are presented in Table 5-1. It should be noted that the pipe-soil interface strength was limited to half of the soil undrained shear strength at the pipe spring line, considering a total stress friction coefficient of 0.50. Additionally, the parameter γ^p is calculated by the VUSDFLD subroutine, and the assumed values of γ_r^p and $s_{u,r}$ are 10.0 and 6.65 kPa, respectively. The elastic Young's modulus of the rigid steel pipeline is 2.10×10^8 kPa. The weight of pipeline is a crucial factor that significantly affects the pipeline-soil interaction. The consequences of considering or neglecting the mass of the pipe and the inertial effects of either fault or pipe moving vary depending on the particular characteristics of the pipeline system, its intended use, and the goals of the

analysis. Here in this study, the pipe mass is considered to investigate the soil failure mechanisms. To account for the pipeline's self-weight, a mass density of 7850 kg/m^3 was defined for the steel rigid pipeline. This density value ensures that the desired gravity stress level is achieved in the soil domain.

Table 5-1. Trench geometry and soil properties adopted from the centrifuge tests.

Property		Value
Geometry	Burial depth to pipeline center (m)	1.92
	Trench width (m)	2.5
	Initial embedment of pipeline (mm)	4
Native seabed soil	Undrained shear strength at pipeline centerline (kPa)	33.1
	Linear variation of undrained shear strength with depth (kPa)	24.43+6.8z
Backfill soil	Undrained shear strength at pipeline centerline (kPa)	1.6
	Linear variation of undrained shear strength with depth (kPa)	1.26z

*The submerged unit weight (γ') of native seabed soil and backfill soil are used as 9.3 kN/m^3 and 7.5 kN/m^3 respectively.

5.4. Results and discussions

5.4.1. Verification of numerical model

The model configuration was based on the test T4P4 conducted by Paulin (1998) to facilitate comparison with published test results. Figure 5-3 shows the schematic shape of

the finite element model. In this figure, the rigid pipeline represented as a Lagrangian material is placed on the trench bed. The seabed and backfilling soil are modelled as two Eulerian materials that flow through the fixed mesh. The dimensions of the soil domain and the mesh size distribution are presented in Figure 5-3. The pipe diameter in the validated model is 0.95 m.

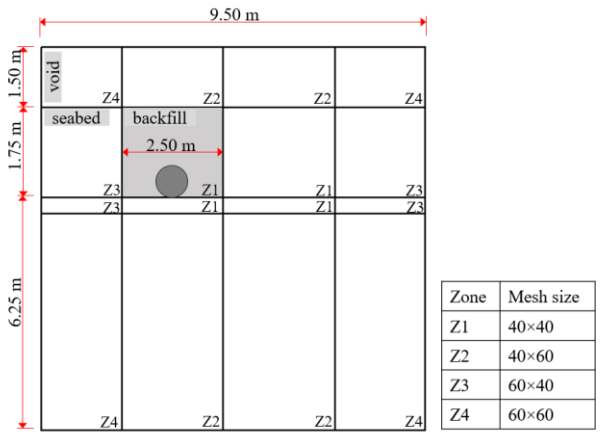

Figure 5-3. Model configurations and initial conditions adopted from the test T4P4.

The properties of the backfilling and seabed soil can be found in Table 5-1. As mentioned before, the analysis began with a geostatic step to establish the desired gravity stress level in the soil domains. In the second step, the pipeline was pushed downward with a velocity of 0.05 m/s to reach the initial embedment. In the third step, a constant lateral velocity was applied to the pipeline. The results obtained from the CEL analysis and centrifuge test are shown in Figure 5-4. Figure 5-4(a) illustrates the comparison of pipeline trajectories between the two models with and without strain-softening effect. It can be observed that the model incorporating strain-softening shows a higher uplift in the soil due to localized strain near the shear bands (see Figure 5-5). Furthermore, Figure 5-4(b) demonstrates the

comparison of pipeline responses obtained from the CEL analysis using the Tresca failure criterion, which reasonably agrees with the results of the centrifuge test conducted by Paulin (1998).

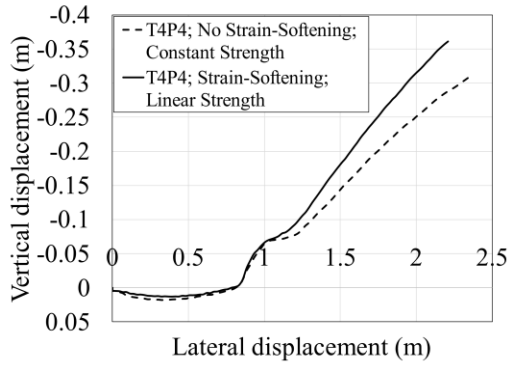

(a)

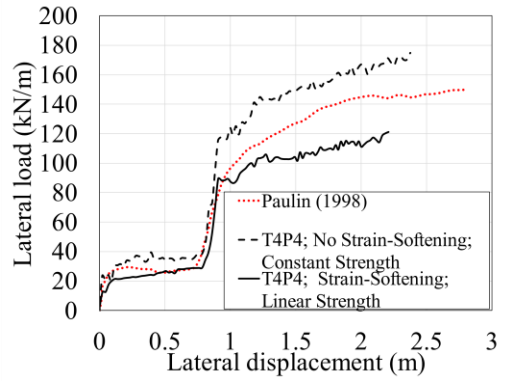

(b)

Figure 5-4. Comparison of the finite element results with the centrifuge test results (a) pipe trajectory (b) load-displacement curve.

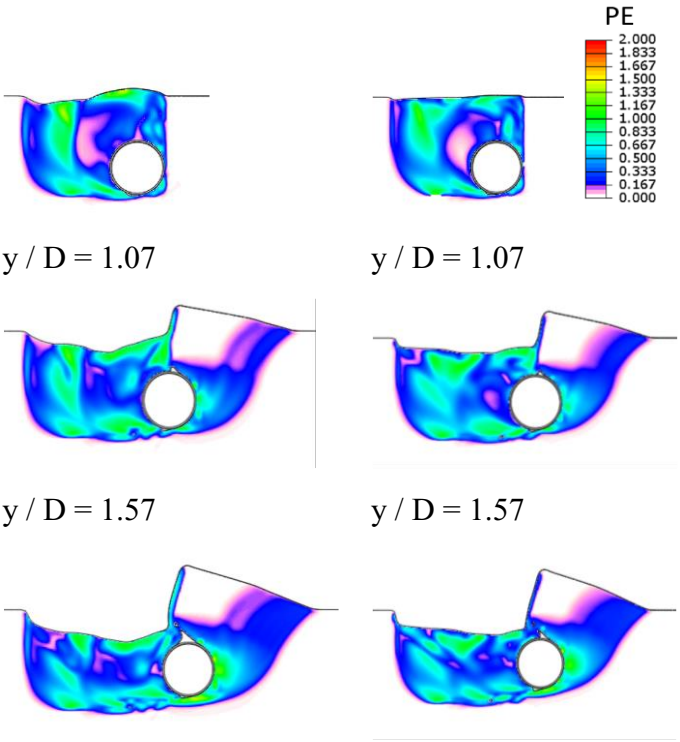

Figure 5-5. The volume fraction average of plastic strain for T4P4 (a) w/o strain-softening, constant soil shear strength, (b) w/ strain softening, linear soil strength.

Table 5-2 summarizes the pipeline's lateral load and vertical displacement at different normalized lateral displacements. This table shows that the model incorporating the strain-softening effect and linear shear strength inside the trench yields results that closely align with those observed in the centrifuge test. In contrast, the model without the strain-softening effect and constant shear strength exhibits discrepancies when compared to the centrifuge test results. Notably, when the pipeline reaches the trench wall (y / D = 1.07), the lateral load values obtained from the model incorporating the strain-softening effect and linear shear strength closely coincide with the results of the centrifuge test. However,

as the pipeline moves into the seabed, the strain-softening effect and constant shear strength results diverge significantly from those observed in the model without the centrifuge test.

Table 5-2. Comparison results of verified models with centrifuge test.

(y / D)	Paulin (1998)	T4P4; No Strain-Softening; constant Strength		T4P4; Strain-Softening; Linear Strength	
	Lateral load (kN/m)	Lateral load (kN/m)	Vertical displacement (m)	Lateral load (kN/m)	Vertical displacement (m)
0.50	25.70	35.85	0.016	25.94	0.012
1.00	89.40	117.79	-0.049	88.31	-0.055
1.50	124.71	147.04	-0.124	102.64	-0.161
2.00	144.54	160.75	-0.232	113.12	-0.291

5.4.2. Parametric studies

To evaluate the effects of trenching/backfilling on the failure mechanisms and the resulting lateral load-displacement curves, a parametric study was conducted. The extracted shear band patterns from the analyses provided good insights into the failure process. Besides, these analyses included an examination of the influence of certain parameters such as the presence of the trench, trench depth, backfill stiffness, and the pipeline-trench bed interface properties on the failure mechanisms and load-displacement curves. A total of 13 case studies were conducted with the configurations adopted from the test T4P4 of Paulin (1998). Table 5-3 provides the properties of the case studies, including the examined parameters and their default values. The impacts of several influential parameters on the lateral response and failure mechanisms of buried pipelines were investigated individually.

Table 5-3. Simulations for assessing the influential parameters.

Case name	Pipe diameter (m)	Burial depth ratio	Soil strength pattern	Backfill su (kPa)	Pipe roughness	Initial embedment (mm)	Strain softening
CS-1	0.9144	1.92	Linear	1.6	Rough	4	Yes
CS-2	0.95	1.92	Linear	1.6	Rough	4	Yes
CS-3	0.9144	2.92	Linear	1.6	Rough	4	Yes
CS-4	0.9144	3.92	Linear	1.6	Rough	4	Yes
CS-5	0.9144	1.92	Constant	1.6	Rough	4	Yes
CS-6	0.9144	1.92	Linear	0.1	Rough	4	Yes
CS-7	0.9144	1.92	Linear	5.0	Rough	4	Yes
CS-8	0.9144	1.92	Linear	1.6	Penalty	4	Yes
CS-9	0.9144	1.92	Linear	1.6	Smooth	4	Yes
CS-10	0.9144	1.92	Linear	1.6	Rough	154	Yes
CS-11	0.9144	1.92	Linear	1.6	Rough	254	Yes
CS-12	0.9144	1.92	Linear	1.6	Rough	4	No
CS-13	0.9144	1.92	Constant	1.6	Rough	4	No

5.4.2.1. The influence of strain softening and soil strength on the soil failure mechanism

The effects of soil strain-softening and shear strength patterns on soil failure mechanism are investigated in this section. Four different case studies are conducted for this investigation: CS-1, CS-5, CS-12, and CS-13. The effect of strain-softening is taken into account in CS-1 and CS-5, and is neglected in CS-12 and CS-13. The material properties of these case studies are presented in Table 5-1.

The lateral load-displacement (p-y) responses and pipe trajectories for the investigations are shown in Figure 5-6. Figure 5-6(a) shows that as the pipe moves laterally in the soil,

uplift is observed along the displacement trajectory. A comparison of the pipe trajectories in different case studies reveals a higher uplift in the soil when the strain-softening effect and linear soil strength are considered. This is attributed to the localization of soil strain along shear bands, as depicted in Figure 5-7. Consequently, the linear soil strength case studies exhibit lower lateral soil resistance due to the higher uplift (see Figure 5-6(b)).

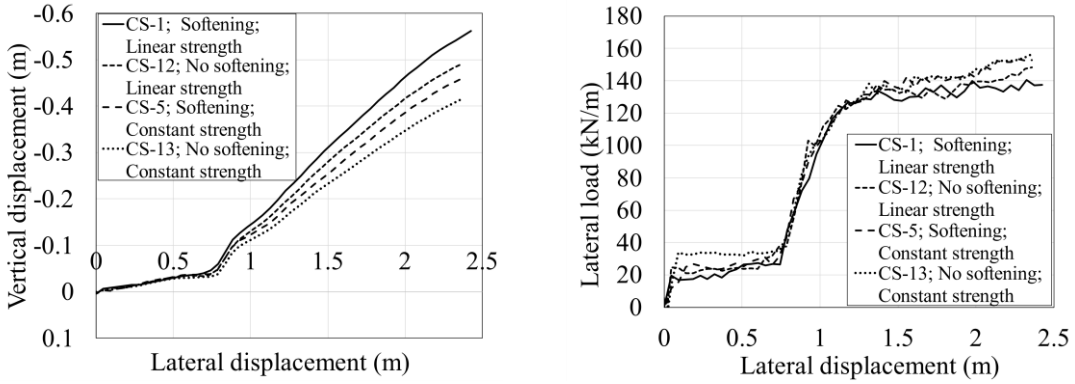

Figure 5-6. Comparison of pipe lateral response considering the effect of strain-softening and with constant and linear soil strength (a) pipe trajectory (b) load-displacement curve.

The plastic strain contours for case studies CS-1 and CS-5 are presented in Figure 5-7. By comparing these contours with the displacement vectors shown Figure 5-8, the significant influence of considering the linear strength of the native soil on the failure mechanism can be observed. In the case studies where the soil strength is constant (CS-5), the plastic strain and shear bands are localized behind the pipeline in the backfilling soil. However, in CS-1, the shear bands reach the top surface of the backfilling soil as the pipeline moves through the it due to the linear distribution of shear strength. Therefore, the upper surface of the trench remains almost plane until the pipeline reaches the trench wall (y / D = 1.07 and y /

D = 1.20). After the pipeline touches the trench wall (y / D = 1.20), shear bands appear in the seabed soil. A comparison of plastic strain reveals that CS-1 exhibits larger plastic strains in the induced shear bands in the seabed soil at y / D = 1.57 and y / D = 1.97. The linear soil strength variation in CS-1 causes a larger uplift due to the localized strain in the backfilling and seabed soils compared to the other cases.

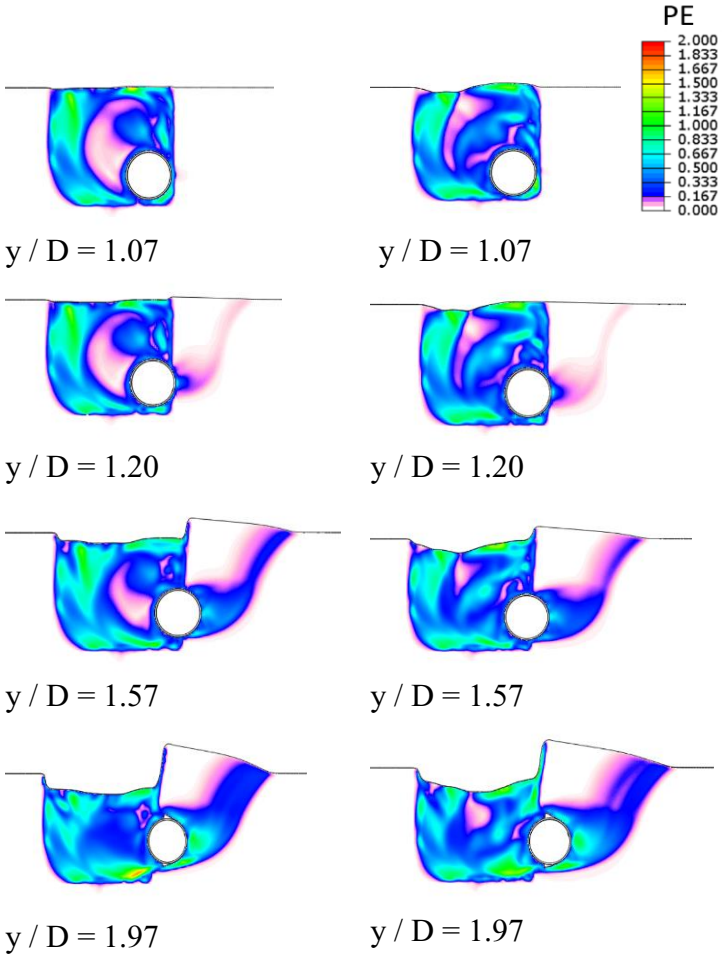

Figure 5-7. Volume fraction average of plastic strain with strain softening (a) CS-1 and (b) CS-5.

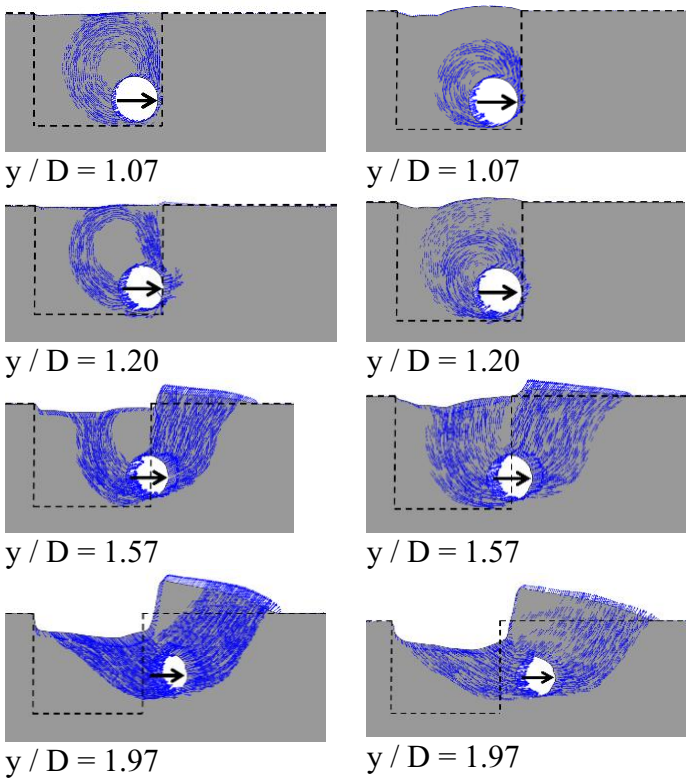

Figure 5-8. Displacement vectors (a) CS-1 and (b) CS-5.

5.4.2.2. The influence of the pipeline's burial depth ratio

The influence of burial depth ratio on the lateral force-displacement responses of pipelines was studied by considering three different burial depth ratios: 1.92, 2.92, and 3.92. The initial embedment, which represents the penetration depth of the pipeline bottom into the trench bed, was 4 mm. The undrained shear strengths of the native soil and the backfill are equal to those shown in Table 5-1. The results of the conducted analyses are presented in Figure 5-9 and Figure 5-10. As shown in Figure 5-9(a), a shallow-depth buried pipeline trajectory exhibits a larger uplift compared to a deep-depth buried pipeline trajectory as the pipeline moves through the seabed soil. However, the uplift of the pipelines is almost the same before reaching the trench wall. Figure 5-9(b) demonstrates that the induced lateral

load in the buried pipeline increases with depth. This can be attributed to the increase in soil weight on the buried pipelines as the height of soil above the pipeline increases as the burial depth ratio rises.

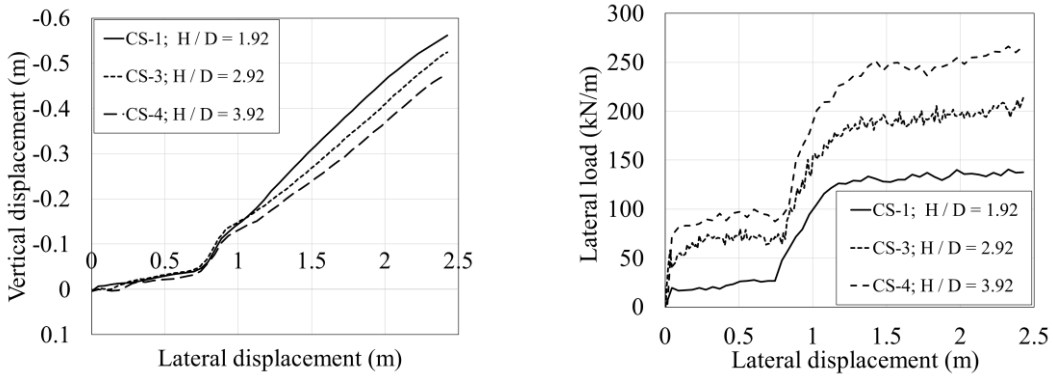

(a) (b)

Figure 5-9. Comparison of pipe lateral response considering different burial depth ratios (a) pipe trajectory (b) load-displacement.

Figure 5-10 illustrates the soil failure mechanism in the three case studies corresponding to different burial depth ratios. It can be observed that the burial depth ratio of the pipeline affects the shape of shear bands around the pipeline. In shallow depths, the shear bands reach the top surface of backfilling soil. The failure mechanism in the deep depth (H / D = 3.92) is predominantly confined to the rear of the pipeline. However, the surrounding soil tends to move upwards (Figure 5-10(c)).

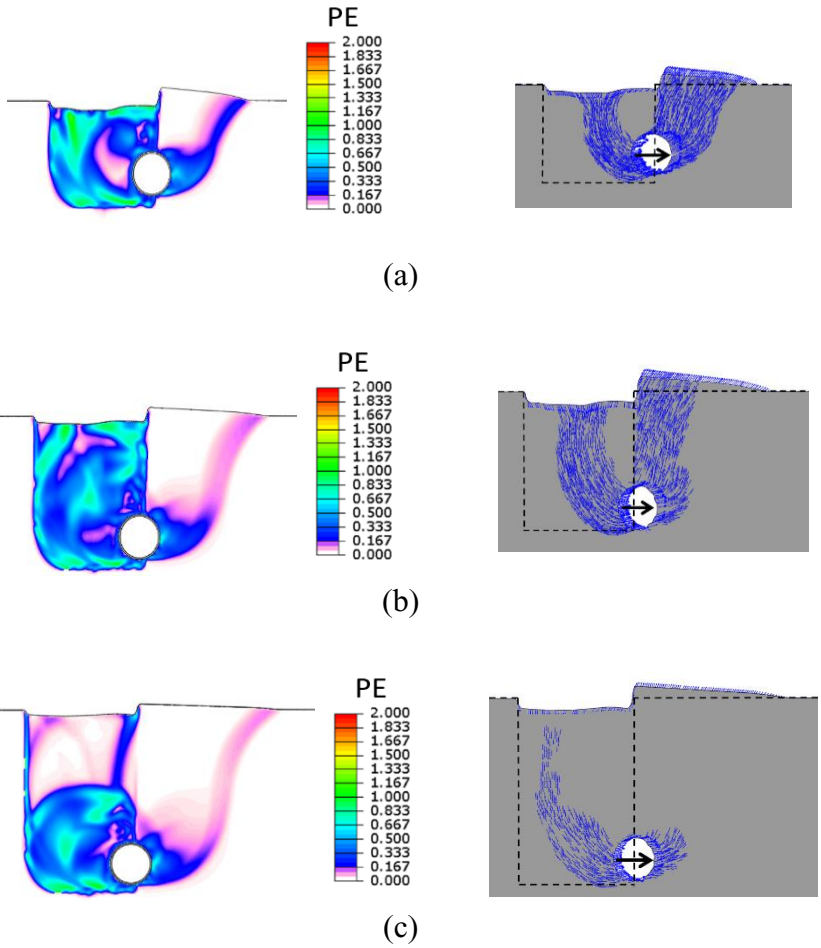

Figure 5-10. Volume fraction average of plastic strain with strain softening and displacement vectors for different burial depth ratios (a) CS-1 (H / D = 1.92), (b) CS-3 (H / D = 2.92), (c) CS-4 (H / D = 3.92).

5.4.2.3. The influence of initial embedment

The initial embedment of the pipeline is a key parameter in the lateral soil resistance against the displacement of the trenched pipeline. To investigate the failure mechanisms during pipeline movement, comparisons were made considering three different initial embedment heights: 4, 154, and 254 mm.

The conducted analyses (CS-1, CS-10, and CS-11) reveal that the uplift of the buried pipeline inside the trench decreases as the initial embedment increases (See Figure 5-11 (a)). Figure 5-11(a) shows that a smaller embedment height results in faster upward movement than the other embedment values. To better understand the reason behind this behaviour, the failure mechanisms of the soil in these three case studies were compared. Figure 5-12 illustrates that a smaller embedment depth induces a larger volume of berm formation in front of the pipe. Additionally, the localized soil plastic strain value increases. Therefore, the pipeline lateral load inside the trench increases as the embedment depth increases.

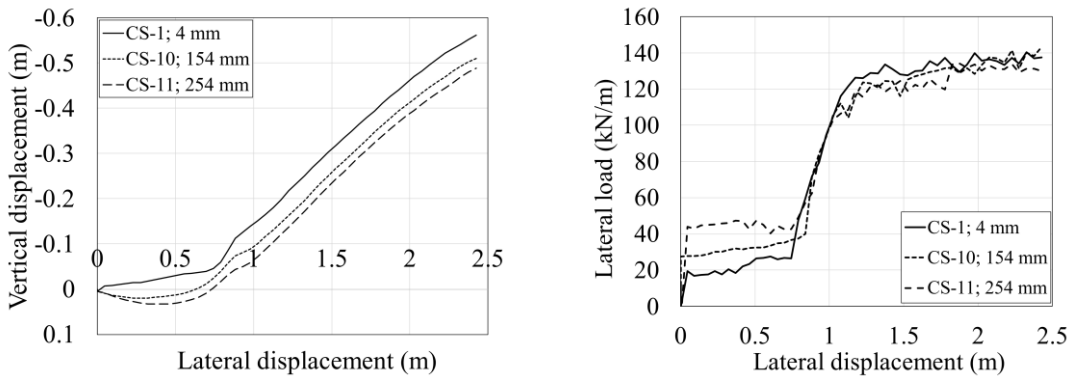

(a) (b)

Figure 5-11. Comparison of pipe lateral response considering different initial embedment heights (a) pipe trajectory (b) load-displacement.

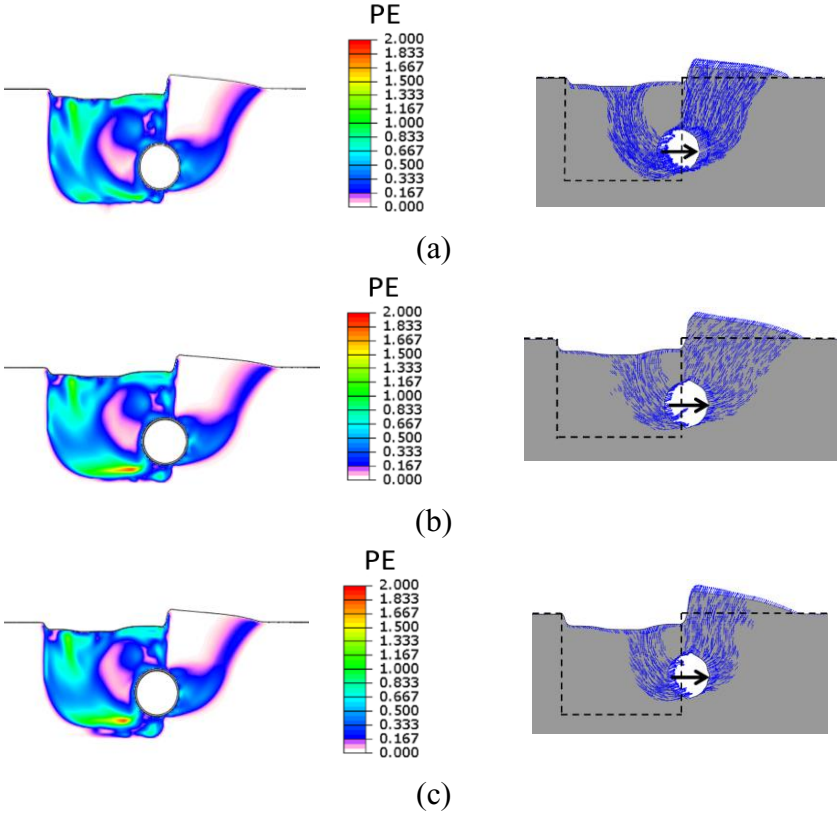

Figure 5-12. Volume fraction average of plastic strain with strain softening and displacement vectors for different initial embedment values (a) CS-1 (4 mm), (b) CS-10 (154 mm), (c) CS-11 (254 mm).

5.4.2.4. The influence of backfilling material strength

Three different backfilling materials were used to evaluate the soil failure mechanism and pipeline displacement trajectory. The results are presented in Figure 5-13 and Figure 5-14. A comparison of the results reveals that the weaker backfilling material leads to smaller uplift compared to the stronger backfilling material. This is attributed to the larger lateral soil resistance inside the trench, resulting in a greater uplift for the pipeline (Figure 5-13). In Figure 5-14, it can be observed that the maximum plastic strain in the trench with weaker backfilling material is concentrated on the surface of the trench because of the larger berm

height in this case study. However, the pipeline lateral load inside the trench with weaker material is smaller than the other backfilling materials. Additionally, this figure indicates that the backfilling soil strength influences the formation of shear bands in the seabed soil. The occurrence of shear bands in the seabed soil indicates that as the backfilling strength increases, the number of shear bands produced in the seabed soil also increases.

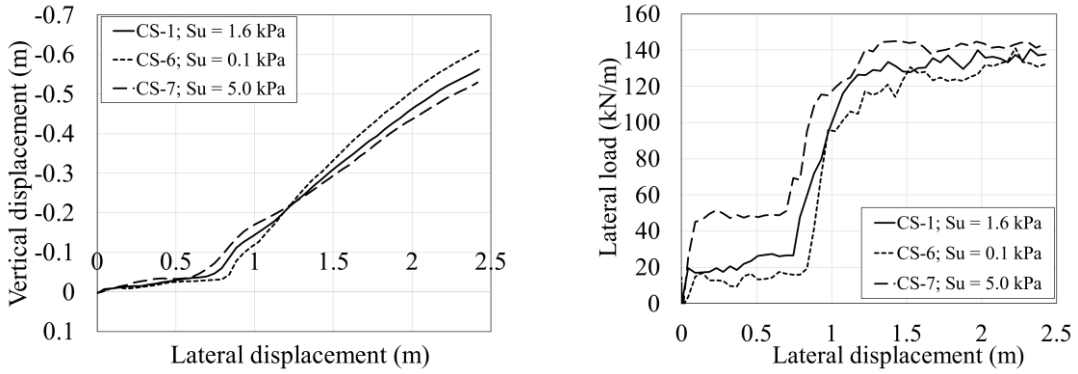

(a) (b)

Figure 5-13. Comparison of pipe lateral response considering different backfilling material (a) pipe trajectory (b) load-displacement.

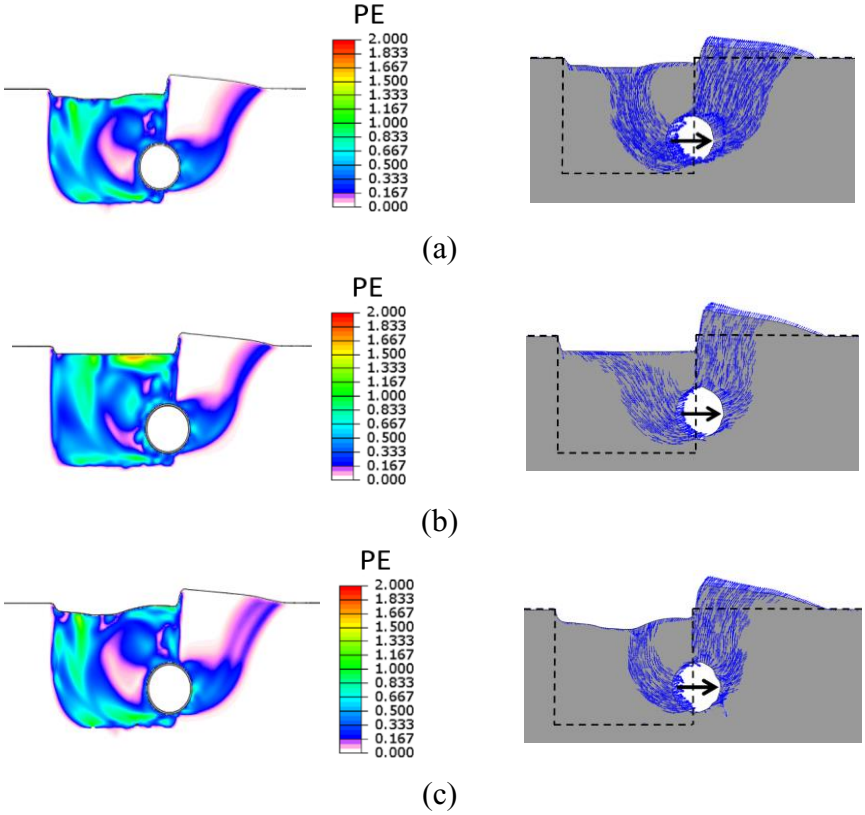

Figure 5-14. Volume fraction average of plastic strain with strain softening and displacement vectors for different backfilling material (a) CS-1 (1.6 kPa), (b) CS-6 (0.1 kPa), (c) CS-7 (5.0 kPa).

5.4.2.5. The influence of pipe diameter

This section investigates the effect of pipeline diameter on the failure mechanism of the soil. Two different pipeline diameters were considered for the analysis. Figure 5-15(a) shows that a larger diameter results in a greater uplift in the pipe trajectory; however, the lateral resistance of the pipe inside the trench decreases (Figure 5-15(b)). The failure mechanism of the soil is presented in Figure 5-16. As shown in this figure, a larger pipe diameter produces a larger berm volume. Consequently, the plastic strain value rises as the berm volume increases.

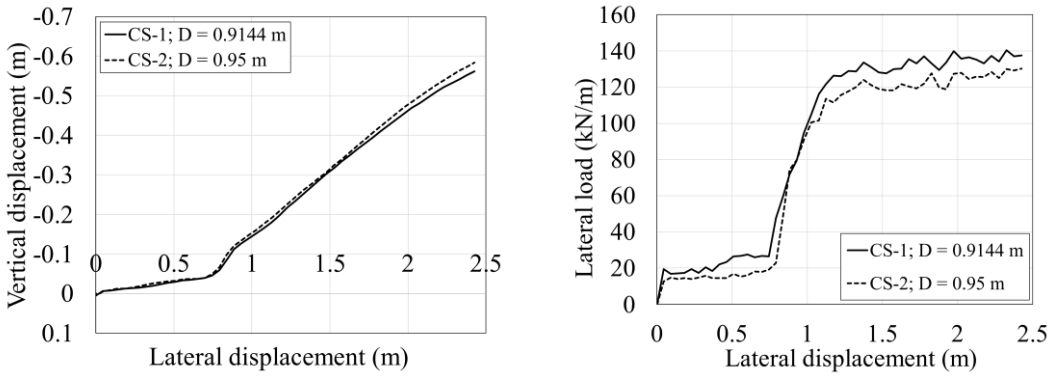

(a) (b)

Figure 5-15. Comparison of pipe lateral response considering different pipe diameters (a) pipe trajectory (b) load-displacement.

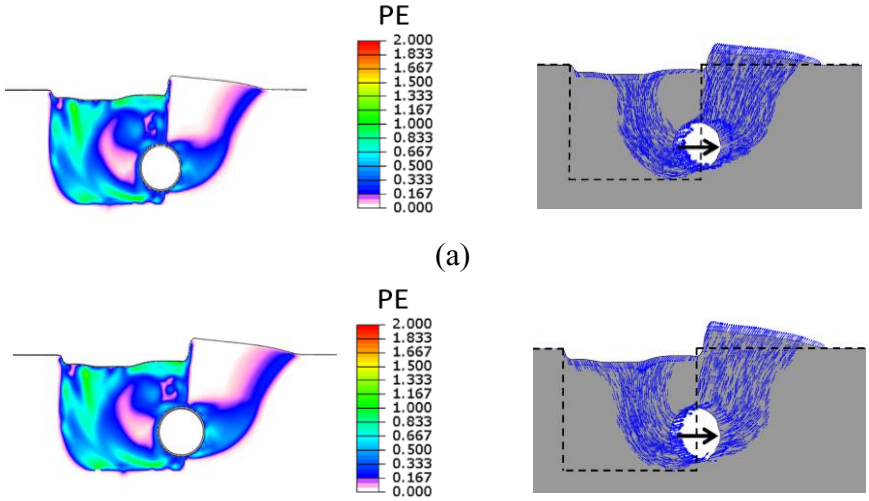

(a)

(b)

Figure 5-16. Volume fraction average of plastic strain with strain softening and displacement vectors for different pipe diameters (a) CS-1 (0.9144 m), (b) CS-2 (0.95 m).

5.4.2.6. Pipeline surface roughness

The surface roughness of the pipeline significantly affects the pipe-soil interaction, failure mechanisms, and resultant lateral soil resistance. Figure 5-17 presents the finite element

results considering rough, penalty, and smooth surface contacts. As shown in this figure, as the surface roughness increases, the lateral soil resistance also increases in both small and large deformation areas (for small displacements inside the trench and large displacements while penetrating the trench wall). Figure 5-18 demonstrates that a rotational flow occurs as the pipe moves inside the trench and interacts solely with the backfilling material. As the pipe interacts with the trench wall, the upper part of the trench wall starts to gradually slide towards the trench. Therefore, the model with smooth surface contact produces a smaller lateral load (Figure 5-17(b)) and larger uplift (Figure 5-17(a)).

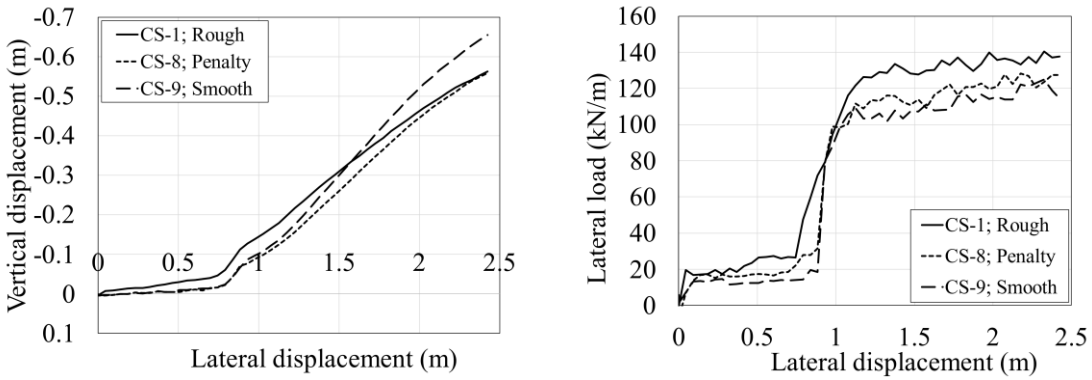

(a) (b)

Figure 5-17. Comparison of pipe lateral response considering different surface roughness values (a) pipe trajectory (b) load-displacement.

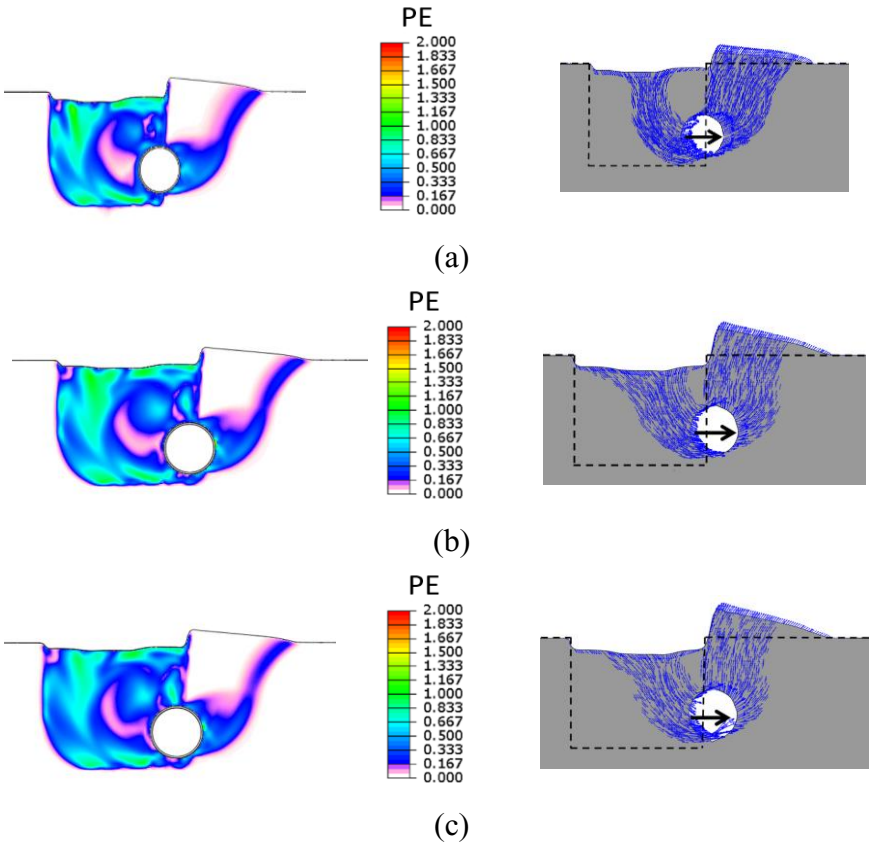

Figure 5-18. Volume fraction average of plastic strain with strain softening for different surface toughness values (a) CS-1 (Rough), (b) CS-8 (Penalty), (c) CS-9 (smooth).

5.5. Conclusions

The pipeline-backfill-trench interaction was investigated using the CEL method implemented in ABAQUS. The strain-softening effects of the seabed soil were incorporated by employing a modified Tresca model proposed by Zang et al. (2015; 2018). The lateral force-displacement response and failure mechanism of the buried pipeline were validated against the published results. Subsequently, a series of parametric studies were conducted to explore the influence of several key properties, including initial embedment,

burial depth ratio, backfilling strength, and pipe diameter. The conducted analyses indicate that:

- Considering strain-softening for the seabed soil leads to an increase in the mobilized soil volume and a decrease in the lateral soil resistance.
- When comparing linear soil strength with constant soil strength, it is observed that the former results in a lower lateral force-displacement response and a greater tendency for the pipeline to move upward.
- The backfilling strength has a significant impact on the lateral soil resistance. A higher backfilling strength (1) increases the intensity of pipeline-trench bed interaction intensity; (2) increases the soil resistance when the pipe moves inside the trench; and (3) by increasing the ultimate lateral soil resistance it produces a passive pressure against the collapsing trench wall and contributes to mobilization of a larger soil volume in front of the moving pipe.
- The initial embedment of the pipeline into the trench affects the lateral load displacement of the pipeline. As the embedment depth increases, the pipeline-trench bed resistance and the earlier propagation of the shear bands beyond the trench wall to the soil surface also increases.
- Pipeline surface roughness plays a significant role in determining lateral soil resistance. A rough surface promotes a strong interaction with the surrounding soil, leading to an increase in soil resistance. The failure mechanism in the trench wall is characterized by a global shear failure for pipelines with a rough surface and a local flow for smooth pipelines.

References

ALA, 2005. Guidelines for the design of buried steel pipe. American Lifelines Alliance, a partnership between FEMA and ASCE.

API-STD-2RD. Standard for riser systems that are part of a floating production system (FPS). American Petroleum Institute, 2013, Washington, DC, USA.

Banushi G, Squeglia N. Seismic analysis of a buried operating steel pipeline with emphasis on the equivalent-boundary conditions. Journal of Pipeline Systems Engineering and Practice. 2018 Aug 1;9(3):04018005.

DNV.GL. (2017). Edition May 2017 Pipe-soil interaction for submarine pipelines.

Karamitros DK, Bouckovalas GD, Kouretzis GP. Stress analysis of buried steel pipelines at strike-slip fault crossings. Soil Dynamics and Earthquake Engineering. 2007 Mar 1;27(3):200-11.

Kianian M, Esmaeilzadeh M, Shiri H. Lateral response of trenched pipelines to large deformations in clay. InOffshore Technology Conference 2018 Apr 30 (p. D032S092R009). OTC.

Kianian M, Shiri H. The effect of backfilling stiffness on lateral response of the shallowly trenched-backfilled pipelines in clay. Marine Georesources & Geotechnology. 2021 May 4;39(5):610-22.

Kianian M, Shiri H. Experimental study of trench effect on lateral failure mechanisms around the pipeline buried in clay. Journal of Pipeline Science and Engineering. 2021 Jun 1;1(2):198-211.

Liu AW, Hu YX, Zhao FX, Li XJ, Takada S, Zhao L. An equivalent-boundary method for the shell analysis of buried pipelines under fault movement. Acta Seismologica Sinica. 2004 Nov;17:150-6.

Merifield RS, Sloan SW, Yu HS. Stability of plate anchors in undrained clay. Geotechnique. 2001 Mar;51(2):141-53.

Ng PC. Behaviour of buried pipelines subjected to external loading (Doctoral dissertation, University of Sheffield).

Ovesen, N.K. Anchor slabs, calculation methods and model tests. Bulletin. 1964, 16, p.39.

Paulin, M.J. An investigation into pipelines subjected to lateral soil loading (Doctoral dissertation, Memorial University of Newfoundland), 1998.

PRCI PR-350-164501-R01 guidance for assessing buried pipelines after a ground movement event.

Randolph MF, Houlsby GT. The limiting pressure on a circular pile loaded laterally in cohesive soil. Geotechnique. 1984 Dec;34(4):613-23.

Sarvanis GC, Karamanos SA. Analytical model for the strain analysis of continuous buried pipelines in geohazard areas. Engineering structures. 2017 Dec 1;152:57-69.

Sarvanis GC, Karamanos SA, Vazouras P, Mecozzi E, Lucci A, Dakoulas P. Permanent earthquake‐induced actions in buried pipelines: Numerical modeling and experimental verification. Earthquake Engineering & Structural Dynamics. 2018 Apr 10;47(4):966-87.

Strogen B, Bell K, Breunig H, Zilberman D. Environmental, public health, and safety assessment of fuel pipelines and other freight transportation modes. Applied energy. 2016 Jun 1;171:266-76.

Talebi F, Kiyono J. Introduction of the axial force terms to governing equation for buried pipeline subjected to strike-slip fault movements. Soil Dynamics and Earthquake Engineering. 2020 Jun 1;133:106125.

Trifonov OV. Numerical stress-strain analysis of buried steel pipelines crossing active strike-slip faults with an emphasis on fault modeling aspects. Journal of Pipeline Systems Engineering and Practice. 2015 Feb 1;6(1):04014008.

Tsatsis A, Loli M, Gazetas G. Pipeline in dense sand subjected to tectonic deformation from normal or reverse faulting. Soil Dynamics and Earthquake Engineering. 2019 Dec 1;127:105780.

Tschebotarioff, G.P. Foundations: retaining and earth structures: the art of design and construction and its scientific basis in soil mechanics. McGraw-Hill Companies. 1973.

Valsamis AI, Bouckovalas GD. Analytical methodology for the verification of buried steel pipelines with flexible joints crossing strike-slip faults. Soil Dynamics and Earthquake Engineering. 2020 Nov 1;138:106280.

Vazouras P, Karamanos SA, Dakoulas P. Finite element analysis of buried steel pipelines under strike-slip fault displacements. Soil Dynamics and Earthquake Engineering. 2010 Nov 1;30(11):1361-76.

Vazouras P, Dakoulas P, Karamanos SA. Pipe–soil interaction and pipeline performance under strike–slip fault movements. Soil Dynamics and Earthquake Engineering. 2015 May 1;72:48-65.

Vazouras P, Karamanos SA. Structural behavior of buried pipe bends and their effect on pipeline response in fault crossing areas. Bulletin of Earthquake Engineering. 2017 Nov;15:4999-5024.

Wantland GM, O'Neill MW, Kalajian EH, Reese L. Pipeline lateral stability in soft clay. Journal of Petroleum Technology. 1982 Jan 1;34(01):217-20.

Xie X, Symans MD, O'Rourke MJ, Abdoun TH, O'Rourke TD, Palmer MC, Stewart HE. Numerical modeling of buried HDPE pipelines subjected to normal faulting: a case study. Earthquake Spectra. 2013 May;29(2):609-32.

Zhang J, Liang Z, Zhang H, Feng D, Xia C. Failure analysis of directional crossing pipeline and design of a protective device. Engineering Failure Analysis. 2016 Aug 1;66:187-201.

Zhang L, Zhao X, Yan X, Yang X. A new finite element model of buried steel pipelines crossing strike-slip faults considering equivalent boundary springs. Engineering Structures. 2016 Sep 15;123:30-44.

Zhang L, Zhao X, Yan X, Yang X. Elastoplastic analysis of mechanical response of buried pipelines under strike-slip faults. International Journal of Geomechanics. 2017 Apr 1;17(4):04016109.

Zhang W, Wang D, Randolph MF, Puzrin AM. Catastrophic failure in planar landslides with a fully softened weak zone. Géotechnique. 2015 Sep;65(9):755-69.

Zhang W, Randolph MF, Puzrin AM, Wang D. Transition from shear band propagation to global slab failure in submarine landslides. Canadian Geotechnical Journal. 2019;56(4):554-69.

Chapter 6

Incorporation of pipeline-backfill-trench wall interaction into the structural analysis of fault-induced steel pipeline deformation using a decoupled approach

Mozhgan Asgarihajifirouz[1], Hodjat Shiri[2]

1: Department of Civil Engineering
Memorial University of Newfoundland

2: Associate Professor, Department of Civil Engineering
Memorial University of Newfoundland

This chapter is under review as a journal manuscript.

6.1. Abstract

Over the past few years, there has been an increased focus on offshore pipeline safety due to the development of offshore oil and gas resources. Both onshore and offshore pipelines may face significant geological hazards resulting from active faults. Pre-excavated soil can be used as backfill for trenches to prevent major pipeline deformations. Since these backfill materials have been heavily remolded, they are softer than the native soil. Therefore, the difference in shear strength between the backfill and native ground may have an effect on the interaction between the pipeline and the backfill. In this paper, the pipeline-backfill-trench interaction has been investigated using a hybrid beam-spring model. The p-y curves obtained from CEL analysis are incorporated into a 3D beam-spring model to analyze the pipeline's response to lateral strike-slip faults. Additionally, the nonlinearity of pipeline materials is considered to study pipeline failure modes under strike-slip fault movements. A series of parametric studies were conducted to explore the effects of fault intersection angle, pipe diameter, buried depth of the pipe, and soil conditions on the failure modes of buckling pipelines. The developed method can be used to analyze and assess pipeline-backfill-trench interaction when subjected to strike-slip fault displacements.

Keywords: Pipeline-backfill-trench interaction, force-displacement curves, beam-spring model, Coupled Eulerian-Lagrangian (CEL) method, strain-softening, strike-slip fault

6.2. Introduction

Buried pipelines play a significant role in the worldwide economy and society by facilitating the transmission of oil, gas, and other fluids over long distances. However, these pipelines are often susceptible to considerable damage caused by different sources of permanent ground displacement (PGD), such as surface faulting, landslides, seismic settlement, and soil liquefaction caused by lateral movement.

Throughout history, earthquakes such as the 1906 San Francisco, 1976 Tang-shan, 1983 Nihonkai-Chubu, 1989 Loma Prieta, 1995 Kobe, and 1999 Kocaeli earthquakes have caused significant damage to pipeline systems, including water pipelines. The fault displacement resulting from these earthquakes exposes the pipeline to substantial axial and bending stresses, which can lead to pipeline buckling or rupture.

Newmark and Hall (1975) and Kennedy (1977) made significant contributions to the mechanical analysis of pipelines subjected to fault displacement. Following their pioneering work, researchers such as Wang and Yeh (1985), Takada et al. (2001), Karamitros et al. (2007), and Trifonov (2010) have proposed improved analytical techniques for strain analysis. However, it is important to note that these analytical methods rely on several assumptions and can calculate only tensile strains.

Advanced numerical simulation tools have emerged as the most effective approach for analyzing pipelines under compression. In recent years, researchers have utilized these tools to investigate the behavior of steel pipelines crossing active faults and their response to fault movement. Takada et al. (2001) developed a beam-shell hybrid finite element (FE) model to study the correlation between maximum strain and bending angle. Building upon Takada et al.'s model, Karamitros et al. (2011) improved the simulation by incorporating

pipe-soil interactions through a series of springs. Vazouras et al. (2010), Shokouhi et al. (2013), Uckan et al. (2015) and Melissianos et al. (2017) investigated the mechanical behavior of onshore steel pipes subjected to fault movement. Furthermore, Ha et al. (2008), Xie et al. (2011), and Jalali et al. (2017) performed numerical studies on buried polyethylene (PE) pipes under normal, strike-slip, and reverse fault movement, respectively. Recently, Qin et al. (2019) conducted numerical simulations to examine the behavior of rigid pipes buried in granular soil under downward movement. The authors discovered that the existing code expressions tend to overestimate the bearing capacity. As an alternative, they proposed a new force-displacement relationship based on the local shear failure theory, deviating from the general shear failure theory adopted by the existing codes.

The previous studies did not account for the variable stiffness of the backfill and native soil. Buried pipelines are commonly placed in excavated trenches with pre-existing soil used as a protective measure against environmental forces. However, the pre-excavated backfill material is often extensively remolded and exhibits lower stiffness compared to the surrounding native soil. This study aimed to fill this gap in the literature by conducting a systematic examination of the buckling failure modes of steel pipelines under strike-slip faults. To achieve this, a hybrid FE model utilizing a highly efficient algorithm was employed to investigate the buckling behavior of buried pipelines under various conditions.

6.3. Numerical model and material properties

This chapter investigates the pipeline-backfill-trench interaction by employing a hybrid method utilizing the commercial FE software ABAQUS. The investigation begins by

developing a Coupled Eulerian-Lagrangian (CEL) method to determine the mobilized soil resistance (p-y curves) against the significant lateral displacement of the trenched/backfilled pipe. Subsequently, the p-y curves obtained from the CEL analysis are incorporated into a 3D beam-spring model to evaluate the pipeline's response to lateral strike-slip faults.

Two parameters are used to assess the impact of fault displacement on pipelines: fault displacement (δ), and the crossing angle (β) between the pipeline and the fault. The schematic shape of the developed beam-spring model is illustrated in Figure 6-1.

The assumed length of the pipeline is 1200 m. It is necessary for the pipe length on both sides of the fault line to be significantly longer than the unanchored length (L). The unanchored length is calculated using the using the following formula (IITK-GSDMA 2007):

$$L = \frac{\sigma_u \pi D t}{T_u} \tag{6-1}$$

where D and t represent the diameter and thickness of pipeline in meters, σ_u is the ultimate strength in Pa, and T_u denotes the maximum axial soil friction force in N. Considering the native soil friction force and the dimensions and material properties of an X80 pipeline, the maximum unanchored length is determined to be 1008 m.

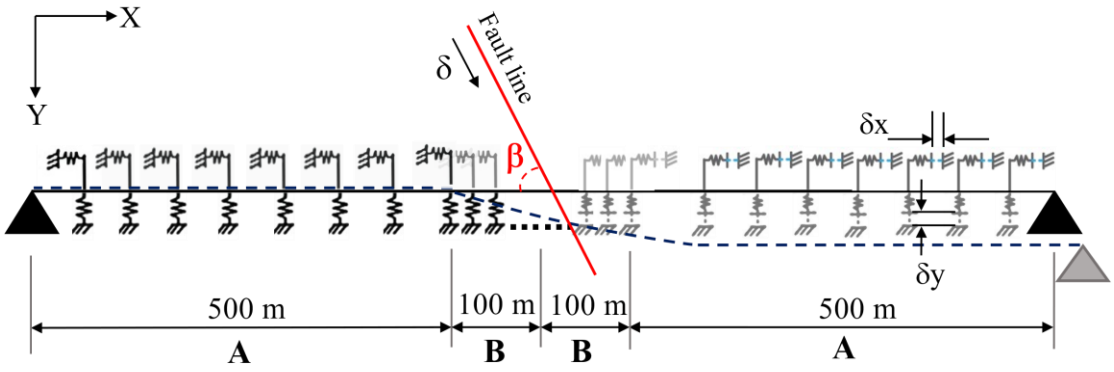

Figure 6-1. Schematic shape of for buried pipeline subjected to strike-slip fault.

In ABAQUS, the nonlinear soil springs that describe pipe-soil interaction are represented by pipe soil elements (PSI 34). The PSI element consists of four nodes, with two of these nodes connecting to the soil nodes and the other two connecting to the pipeline nodes. To ensure accurate results near the fault line areas, a fine mesh of PIPE elements (PIPE31) with a size of 0.1 m was employed for the two adjoining pipeline sections, each spanning 100 m on either side of the fault line. Conversely, for the 500 m sections closer to the two pipeline ends, a coarse mesh with a size of 1.0 m was utilized. A set of 3001 soil nodes, representing the pipe nodes, were established, and connected using 3000 pipe-soil interaction elements (PSI 34) to simulate the nonlinear soil constraints on the pipeline.

In the beam-spiring analysis, two nonlinear steps were utilized to simulate the effects of fault displacement on the pipeline. The non-linear buckling analysis of pipelines subjected to strike-slip fault movement involves geometric and material non-linearities. Therefore, a non-linear stabilization algorithm was deemed appropriate for this study. The first step involved applying internal pressure to the entire pipeline. In the second step, the soil nodes on the left side of the fault line are fixed, while fault displacements are imposed on the soil

nodes on the right side. The fault displacement consists of two components: one in the axial direction and the other in the transverse direction ($\delta_x = \delta cos\beta \; and \; \delta_y = \delta sin\beta$, respectively).

The required p-y curves for the nonlinear beam-spring model were obtained through a 2D CEL analysis. The schematic configuration of the CEL model is presented in Figure 6-2. In Figure 6-2(a), the entire domain in the CEL analysis consists of soil as the Eulerian material, void space, and a buried Lagrangian pipeline.

The simulation process involved three steps. It begins with a geostatic step. The second step entailed pushing the pipeline downwards, with a velocity of 0.05 m/s, until it reaches the specified embedment depth. In the third step, the pipeline was subjected to a constant lateral velocity of 0.046 m/s. The boundary condition properties are illustrated in Figure 6-2(b).

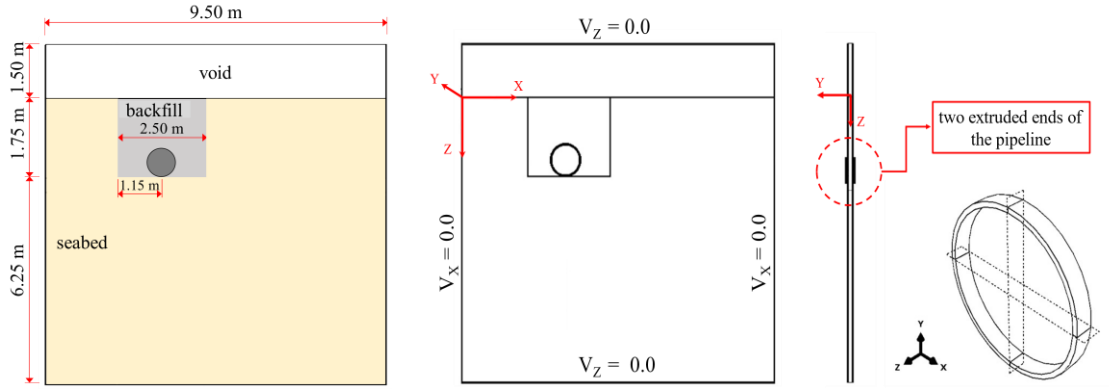

(a) (b)

Figure 6-2. Schematic representation of the CEL model, (a) CEL domain dimensions, (b) boundary conditions properties.

6.3.1. Steel pipeline properties

In this study, the steel pipeline stress-strain relationship is described by Ramberg-Osgood model. Eq. (6-2) represents the Ramberg-Osgood model.

$$\varepsilon = \frac{\sigma}{E}[1 + \frac{\alpha}{1+r}\left(\frac{\sigma}{\sigma_s}\right)^r] \quad (6\text{-}2)$$

In this Equation, E is the initial elastic modulus (in MPa), ε denotes strain, σ and σ_y represent stress and yield stress (in MPa), respectively. Additionally, α and r are the parameters of the Ramberg-Osgood model.

6.3.2. Pipe-soil interaction

According to the requirements of the Canadian Standard Association for oil and gas pipeline systems, CSA (2007), the analysis of soil-pipe interaction necessitates adherence to the guidelines for seismic design and assessment of natural gas and liquid hydrocarbon pipelines established by the Pipeline Research Council International (PRCI) as outlined in Honegger and Nyman (2004). Therefore, the soil spring characteristics were derived following the guidelines provided by both PRCI (Honegger and Nyman, 2004) and the American Lifeline Alliance (ALA, 2001).

ALA-ASCE guidelines define the force-displacement relationship for soil springs as elastic-perfectly plastic, characterized by two parameters (the maximum soil resistance per unit length and the soil yield displacement). Figure 6-3 represents a schematic representation of pipe-soil interaction.

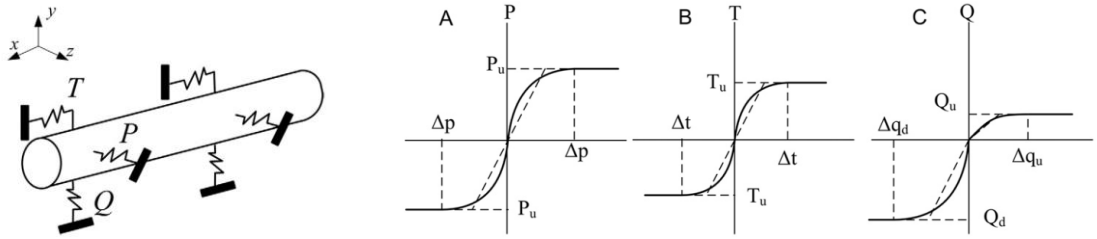

(a) (b)

Figure 6-3. Schematic pipe-soil interaction in ALA-ASCE, (a) nonlinear soil springs, (b) force-displacement relationships: (A) lateral, (B) axial, (C) vertical.

- *Longitudinal soil spring*

In accordance with the ALA guideline, the maximum transferable axial force per unit length (T_u) can be calculated as:

$$T_u = \pi D \alpha c + \pi D H \bar{\gamma} \frac{1 + K_0}{2} tan\delta \tag{6-3}$$

where D represents the pipe diameter, H is the burial depth (measured from the ground surface to the pipe center), and $\bar{\gamma}$ denotes the unit weight of the pipeline, K_0 is the lateral soil pressure coefficient at rest, and δ represents the friction interface angle between the pipe and soil.

The corresponding displacement at T_u, depending on the soil type, is 3-5 mm for dense to loose sand and 8-10 mm for stiff to soft clay.

- *Transverse horizontal soil spring*

The maximum transverse horizontal force per unit length along the pipeline can be calculated as:

$$P_u = N_{ch} cD + N_{qh} \bar{\gamma} HD \tag{6-4}$$

The expression of N_{ch} and N_{qh} can be found in the ALA code.

Δ_p, the displacement at P_u can be obtained by

$$\Delta_p = 0.04\left(H + \frac{D}{2}\right) \leq 0.1D \; or \; 0.15D \tag{6-5}$$

- *Vertical uplift and bearing soil springs*

ALA-ASCE describes the maximum uplift and bearing soil spring forces per unit length, as well as their corresponding yield displacement for sand, as follows:

$$Q_u = N_{cv} cD + N_{qv} \bar{\gamma} HD \tag{6- 6}$$

$$\Delta_{qu} = (0.01H - 0.02H) < 0.1D \tag{6-7}$$

$$Q_d = N_c cD + N_q \bar{\gamma} HD + N_\gamma \gamma \frac{D^2}{2} \tag{6-8}$$

$$\Delta_{qu} = 0.1D \tag{6-9}$$

The expressions of N_{cv}, N_{qv}, N_c, N_q and N_γ are specified in the ALA-ASCE code.

In this study, the p-y curves obtained from the CEL analysis are used as the transverse soil springs, and the ALA-ASCE soil spring equations are used to calculate the vertical and axial soil spring properties.

6.3.3. Pipeline internal pressure and failure criteria

The pipeline internal pressure, p ,can be obtained by the following equation considering the safety factor of 0.72 according to ASME.

$$p = 0.72\frac{2t\sigma_s}{D} \tag{6-10}$$

There have been several studies aiming to determine the critical compressive strain, ε_{cr}, that leads to wrinkles and decreased load carrying capacity in pipelines. The proposed ε_{cr} by Gresnigt A. M. (1987) (Eq. (6-11)) has been adopted by CSA Z662 and is widely used in the industry due to its reasonable and conservative value. This criteria constitutes the basis of the local buckling failure of trenched pipelines investigation conducted in this study.

$$\varepsilon_{cr} = 0.5\left(\frac{t}{D}\right) - 0.0025 + 3000(\frac{\sigma_h}{E})^2 \tag{6-11}$$

In this equation, σ_h is the hoop stress that can be calculated as:

$$\sigma_h = \begin{cases} \frac{pD}{2t}, \ \frac{pD}{2t\sigma_s} \leq 0.4 \\ 0.4\sigma_s, \frac{pD}{2t\sigma_s} > 0.4 \end{cases} \tag{6-12}$$

The pipeline internal pressure, p ,can be calculated using the following equation, considering the safety factor of 0.72 as recommended by ASME.

6.3.4. Validation basis

To verify the accuracy of the proposed FE model, the experimental and FE studies conducted by Rofooei et al. (2015) were used. In this study, the proposed beam-spring model was validated by obtaining soil-spring parameters based on the sand properties used in the experiment. Figure 6-4 illustrates the properties of the soil springs.

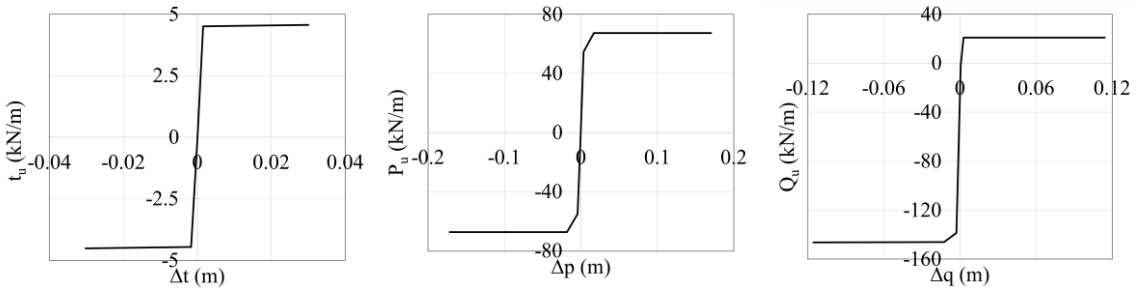

(a) (b) (c)

Figure 6-4. Soil spring characteristics of the Rofooei et al. (2015): (a) axial, (b) horizontal, and (c) vertical soil springs.

The true stress-strain curve (See Figure 6-5) of the API-5L Grade B material used in the experiment was also considered. The steel pipeline diameter, thickness, and length are 114.3 mm, 8.6 mm and 8.0 m, respectively. An internal pressure of 413 kPa (60 psi) was applied to the model. Regarding the given fault, displacement components in the axial, vertical and transverse directions are -0.08 m, 0.35 m and -0.18 m, respectively.

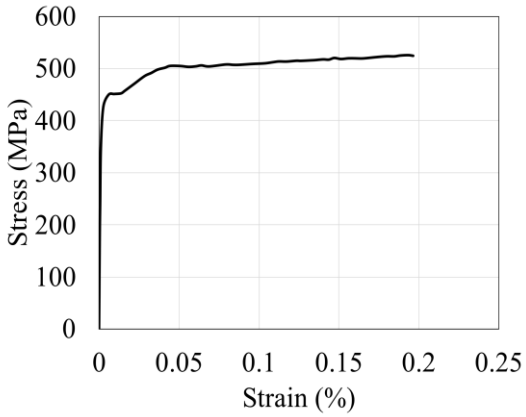

Figure 6-5. Steel pipeline stress-strain curve (Rofooei et al. (2015)).

The numerical results obtained by the proposed model were compared with the experiment and simplified FE model results obtained by Rofooei et al. (2015). As shown in Figure 6-6, the proposed numerical model exhibits a closer match with the FE results reported by Rofooei et al. (2015).

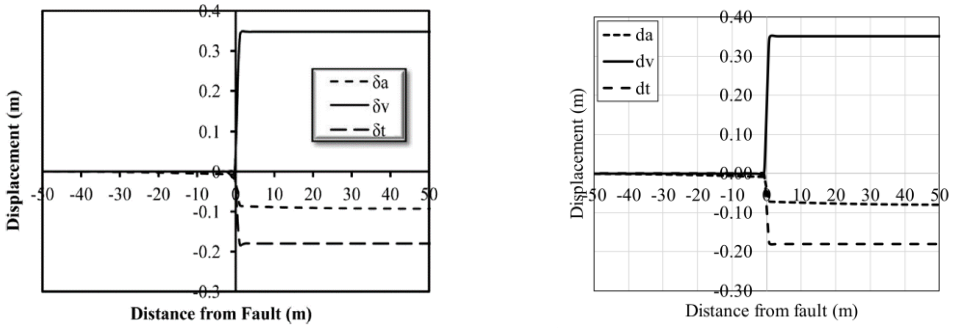

(a) (b)

Figure 6-6. Pipe displacement in three orthogonal directions. (a) the conducted FE model by Rofooei et al. (2015), (b) verified FE model.

Figure 6-7 illustrates the distribution of invert and crown strains along the pipeline in the region of large deformation. In the proposed model, the oval deformation of the pipeline

was ignored due to the limitations of the PIPE31 elements in simulating the local buckling. However, the results obtained from the proposed model closely match the FE and experimental findings reported by Rofooei et al. (2015).

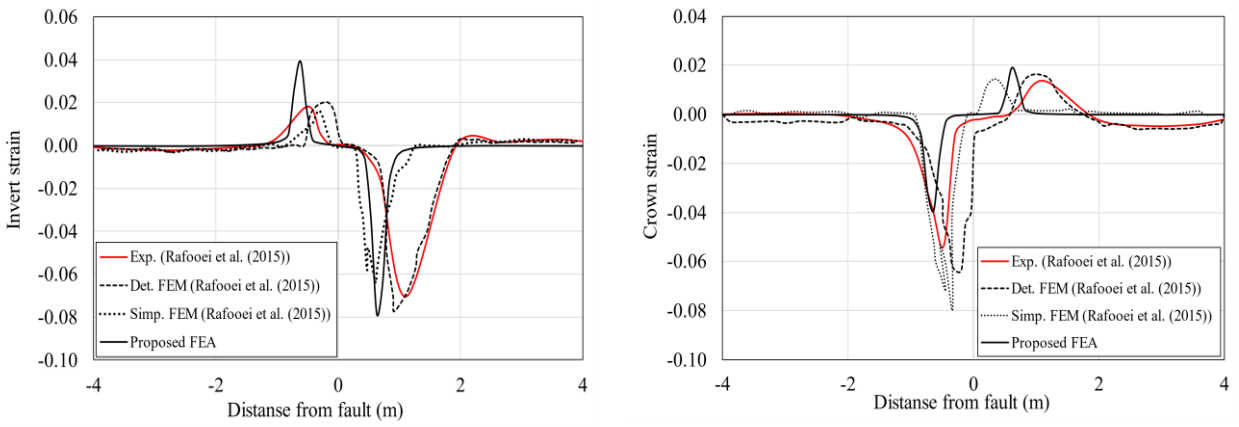

(a) (b)

Figure 6-7. (a) Invert and (b) crown strains of FE and experimental models.

6.4. Results and discussion

A series of numerical studies were conducted in this research to investigate the influence of factors such as fault intersection angle, pipeline diameter, burial depth, initial embedding, and properties of backfilling soils on the buckling behavior of X80 steel pipelines under strike-slip faults.

The stress-strain curve for the X80 pipeline material is presented in Figure 6-8. This material exhibits a Young's modulus of 2.07×10^5 MPa and a yielding stress of 530 MPa. The Ramberg-Osgood parameters α and r are determined as 15.94 and 15.95, respectively. For a pipeline with a diameter of 0.9144 m and a thickness of 0.027 m, the internal pressure

is calculated as 22.5 MPa according to Eq. (6-10). Additionally, the critical compressive strain is 2.24 % (using Eq. (6-11)).

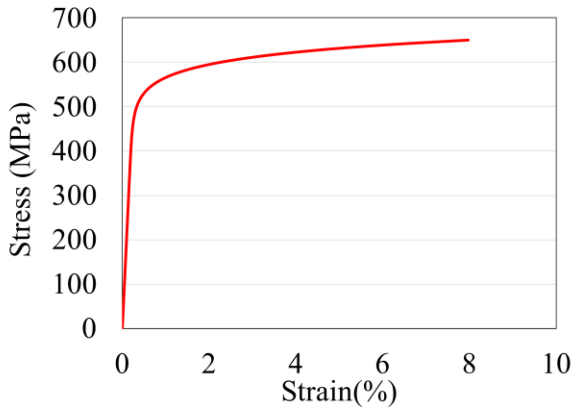

Figure 6-8. X80 stress-strain curve.

Using the configurations of Paulin's (1998) T4P4 test, a total of 13 case parametric studies were conducted. The trench configurations and soil properties are presented in Table 6-1, while Table 6-2 presents the parametric study properties. The submerged unit weight (γ') of native seabed soil and backfill soil are used as 9.3 kN/m^3 and 7.5 kN/m^3, respectively. Based on these properties, a series of CEL analyses were conducted to extract the required p-y curves.

Table 6-1. Trench geometry and soil properties adopted from the centrifuge tests.

Property		Value
Geometry	Burial depth to pipeline center (m)	1.92
	Trench width (m)	2.5
	Initial embedment of pipeline (mm)	4
Native seabed soil	Undrained shear strength at pipeline centerline (kPa)	33.1
	Linear variation of undrained shear strength with depth (kPa)	24.43+6.8z
Backfill soil	Undrained shear strength at pipeline centerline (kPa)	1.6
	Linear variation of undrained shear strength with depth (kPa)	1.26z

Table 6-2. Case studies properties.

Case name	Pipe diameter (m)	Burial depth ratio	Soil strength pattern	Backfill su (kPa)	Pipe roughness	Initial embedment (mm)	Strain softening
CS-1	0.9144	1.92	Linear	1.6	Rough	4	Yes
CS-2	0.95	1.92	Linear	1.6	Rough	4	Yes
CS-3	0.9144	2.92	Linear	1.6	Rough	4	Yes
CS-4	0.9144	3.92	Linear	1.6	Rough	4	Yes
CS-5	0.9144	1.92	Constant	1.6	Rough	4	Yes
CS-6	0.9144	1.92	Linear	0.1	Rough	4	Yes
CS-7	0.9144	1.92	Linear	5.0	Rough	4	Yes
CS-8	0.9144	1.92	Linear	1.6	Penalty	4	Yes
CS-9	0.9144	1.92	Linear	1.6	Smooth	4	Yes
CS-10	0.9144	1.92	Linear	1.6	Rough	154	Yes
CS-11	0.9144	1.92	Linear	1.6	Rough	254	Yes
CS-12	0.9144	1.92	Linear	1.6	Rough	4	No
CS-13	0.9144	1.92	Constant	1.6	Rough	4	No

6.4.1. Effect of strain-softening and soil strength on the pipeline failure mechanism

In this section, the effects of soil strain-softening and shear strength pattern effects on pipeline failure are studied through four different case studies: CS-1, CS-5, CS-12, and CS-13. The soil spring characteristics for these models are presented in Figure 6-9. Soil spring characteristics for investigating strain-softening and soil strength (a) axial, (b) horizontal, and (c) vertical soil springs.

.

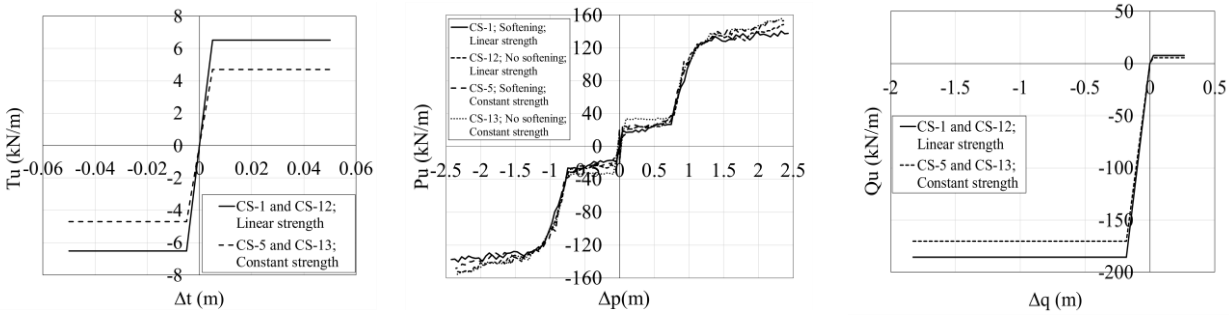

(a) (b) (c)

Figure 6-9. Soil spring characteristics for investigating strain-softening and soil strength (a) axial, (b) horizontal, and (c) vertical soil springs.

Figure 6-10 shows the FE analysis results for the four case studies. A comparison of pipeline deflection curves in Figure 6-10(a) reveals that the length of the large deformation area in soil with the strain-softening effect and linear soil strength is greater compared to the other cases. The results indicate that strain-softening with linear shear strength pattern induces a higher uplift due to the localized shear bands. Consequently, the pipeline can move easily in the fault direction, and the axial strain on the pipeline decreases (See invert and crown strain curves in Figure 6-10). Furthermore, Figure 6-10 shows that the maximum axial strain in CS-1 is lower than the other cases. Therefore, CS-1 and CS-5 exhibit a

greater distance between two wrinkles due to the strain-softening effect. Additionally, a comparison of invert and axial strains considering two different intersection angles reveals that linear shear strength patterns reduce axial strain by approximately 5%.

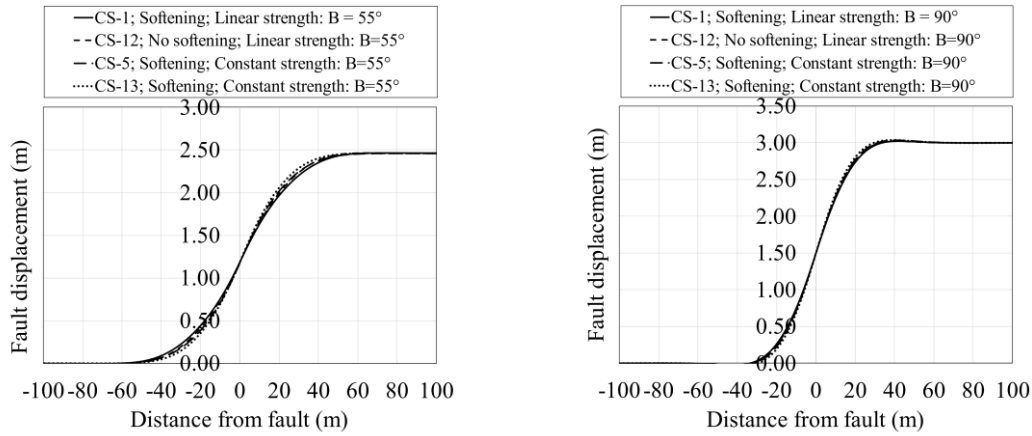

(a)

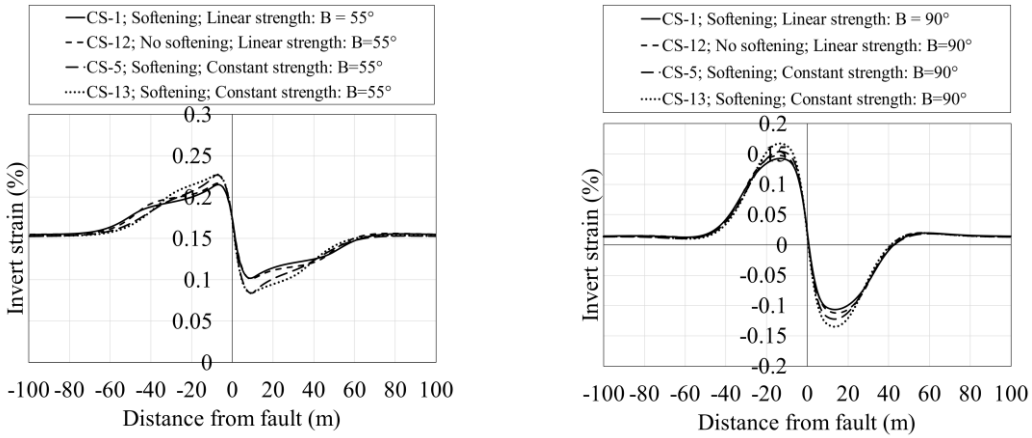

(b)

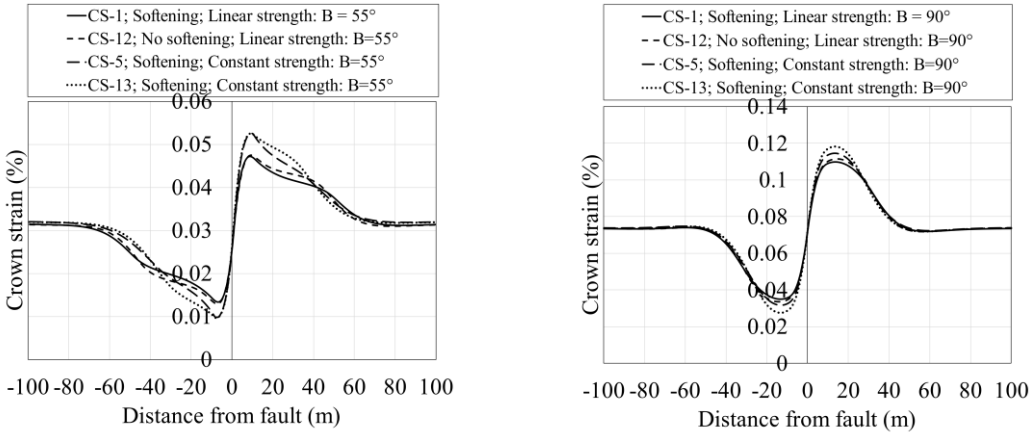

(c)

Figure 6-10. Strain-softening and soil strength pattern effect on the deformation and axial strain of the pipeline, (a) distribution of vertical displacement, (b) invert axial strain, (c) crown axial strain.

6.4.2. The influence of the pipeline burial depth ratio

In this section, the influence of burial depth ratio on the pipeline behavior is investigated. Three different burial depth ratios, namely 1.92, 2.92, and 3.92, were investigated in this study. Figure 6-11 presents the corresponding soil spring properties used in this analysis.

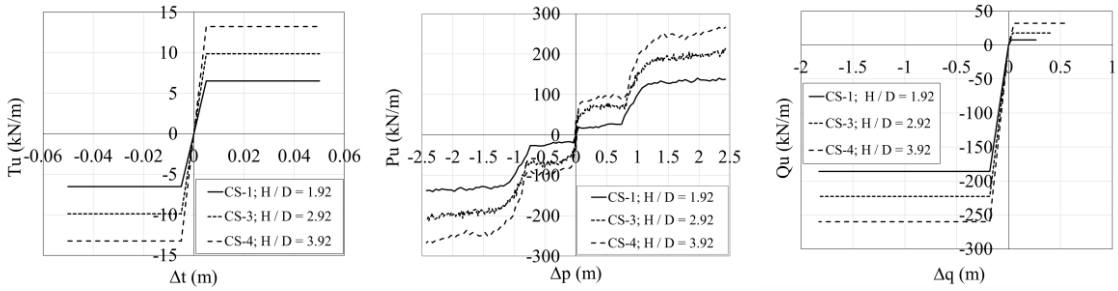

(a) (b) (c)

Figure 6-11. Soil spring characteristics for different burial depth ratio (a) axial, (b) horizontal, and (c) vertical soil springs.

According to the analytical study conducted by Asgarihajifirouz et al. (2023), the axial strain of the pipeline decreases significantly in presence of backfilling soil, and the maximum axial strain does not vary significantly with increasing burial depth ratio. Figure 6-12 clearly demonstrates the effect of burial depth ratio on the deflection and axial strain curves. In Figure 6-12(a), it is evident that bending deformations decrease with increasing burial depth ratios. This is because the burial depth ratio of the pipeline affects the shape of shear bands around the pipeline. At shallow depths, shear bands reach the top surface of

backfilling soil. Moreover, comparing Figure 6-12(a) highlights the influence of the intersection angle on the reduction of the deflection curve. It can be observed that an increase in fault crossing angle and burial depth ratios has a minor effect on bending deformation. Comparing the invert and crown strain in Figure 6-12 reveals that as the burial depth increases, the axial strain also increases. The position of the maximum axial strain remains constant at great depths. However, at shallow depths, it is near the fault line because the pipeline can easily fold up. Buried pipelines in shallow depths experience smaller forces compared to those in greater depths due to the thickness of the overlying soil. The parametric studies indicate that the induced axial strain in trenched pipelines is 10 times less than the critical strain (2.24%). Consequently, the buried pipeline does not experience local buckling if it is buried within the trench.

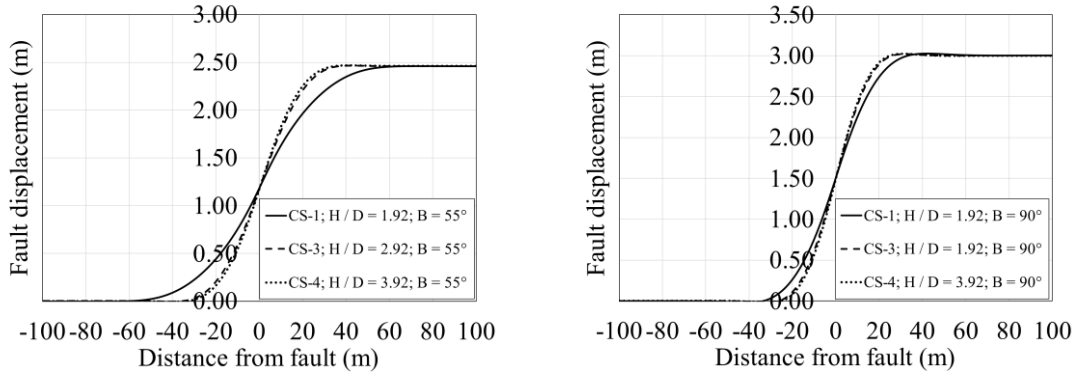

(a)

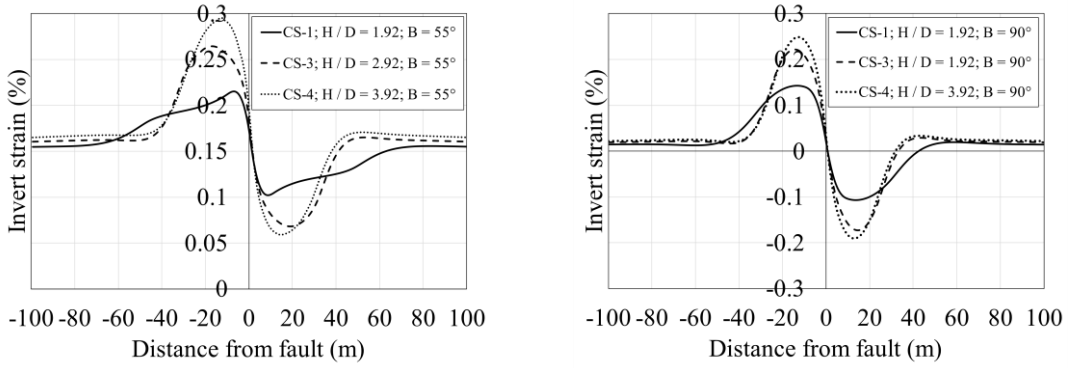

(b)

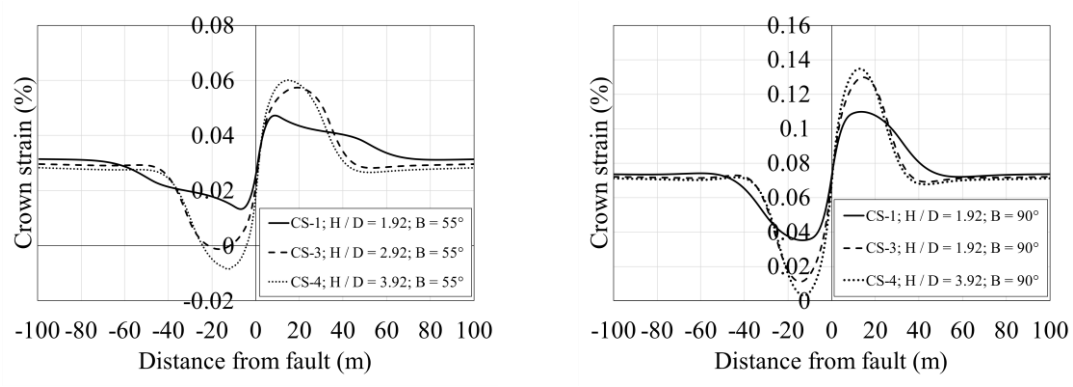

(c)

Figure 6-12. Burial depth effect on the deformation and axial strain of the pipeline, (a) distribution of vertical displacement, (b) invert axial strain, (c) crown axial strain.

6.4.3. The influence of initial embedment

In this section, the nonlinear response of the pipeline is studied by considering three different initial embedment depths :4 mm, 154 mm, and 254 mm. Figure 6-13 illustrates the soil spring properties for these case studies.

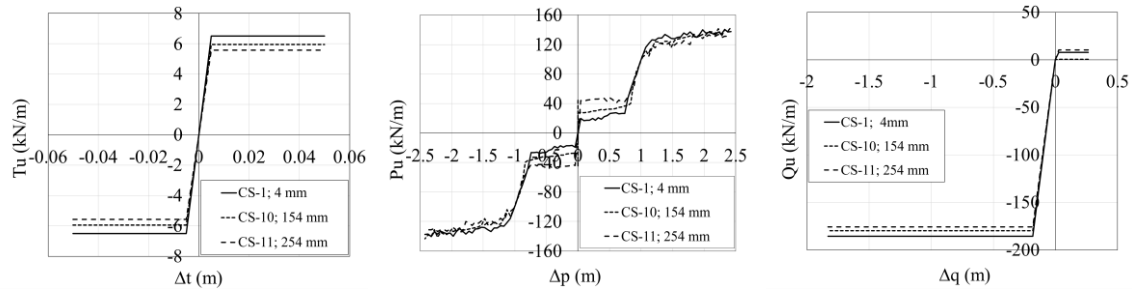

(a) (b) (c)

Figure 6-13. Soil spring characteristics of case studies with different initial embedment (a) axial, (b) horizontal, and (c) vertical soil springs.

Figure 6-14 presents the FE analysis results. The deflection curves in Figure 6-14(a) demonstrates that as embedment height decreases, the pipeline is more prone to moving towards the seabed, resulting in the formation of wrinkles in the region near the fault.

The axial strain curves in Figure 6-14 illustrate that the location of the maximum axial strain shifts as the initial embedment height increases. Additionally, the magnitude of the maximum axial strain increases with higher initial embedment heights.

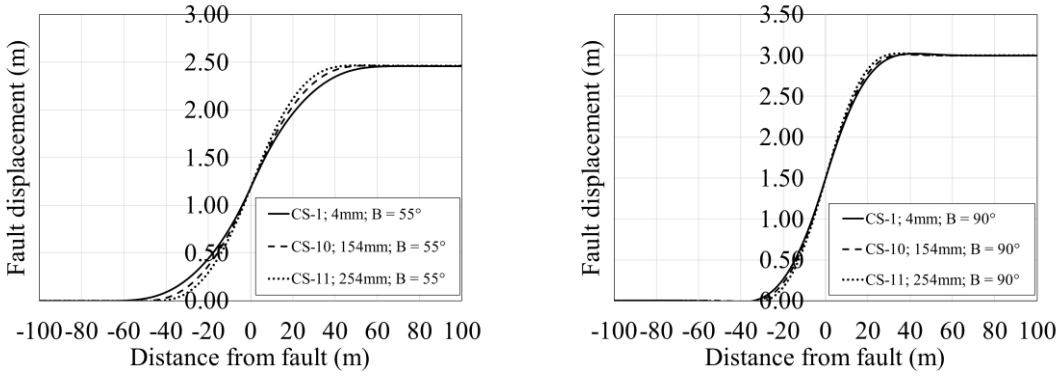

(a)

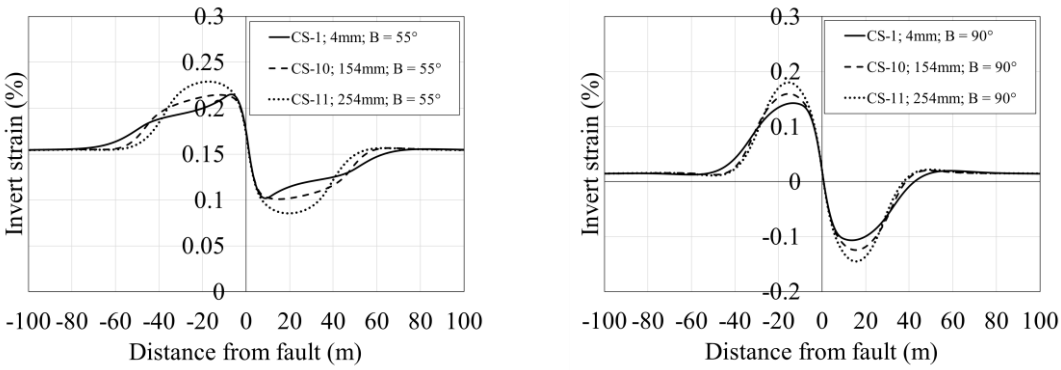

(b)

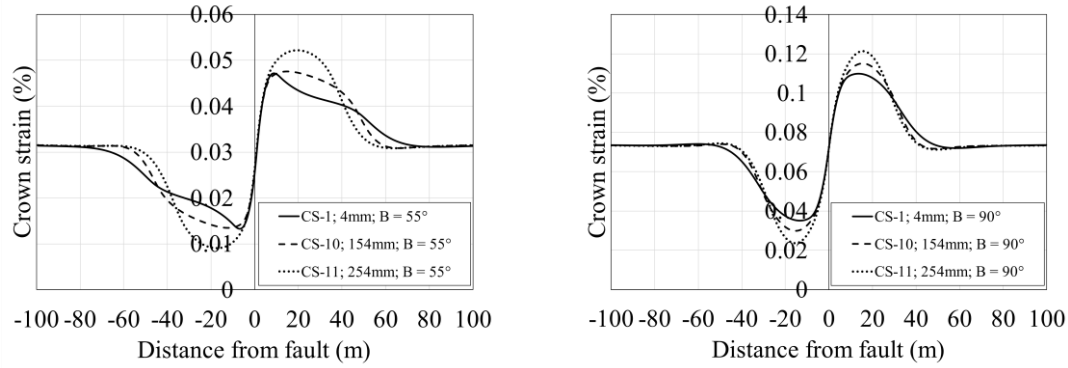

(c)

Figure 6-14. Initial embedment effect on the deformation and axial strain of the pipeline, Initial embedment effect on the deformation and axial strain of the pipeline, (a) distribution of vertical displacement, (b) invert axial strain, (c) crown axial strain.

6.4.4. The influence of backfilling material strength

This section provides an analysis of the pipeline deformation under three different undrained shear strengths of the backfill soil. The soil spring properties are presented in Figure 6-15.

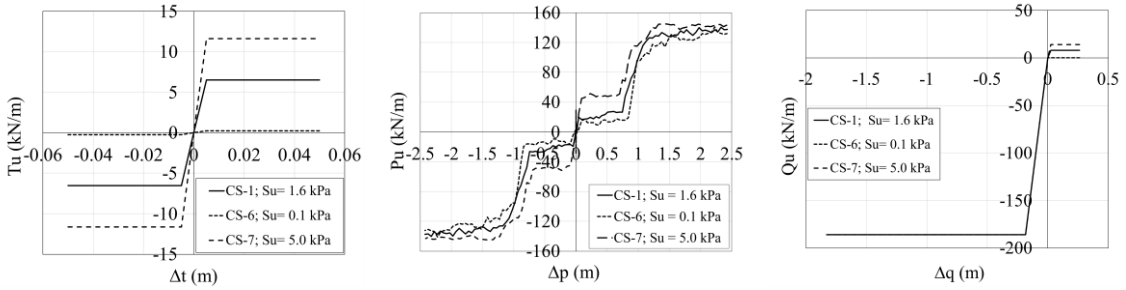

(a) (b) (c)

Figure 6-15. Soil spring characteristics for different backfilling soil strength (a) axial, (b) horizontal, and (c) vertical soil springs.

Figure 6-16 illustrates the FE results for pipeline deformation under three different undrained shear strengths of the backfill soil. It shows that as the friction force between the pipeline and the soil increases, the axial force also increases. In Figure 6-16 (a), it can be observed that when the backfill soil shear strength changes from soft to stiff, the length of the large deformation area decreases. Consequently, the maximum axial strain, including invert and crown strains increases. Moreover, Figure 6-16, demonstrates that the maximum axial strain is located near the fault line, and the magnitude of the axial strain has no effect on this location.

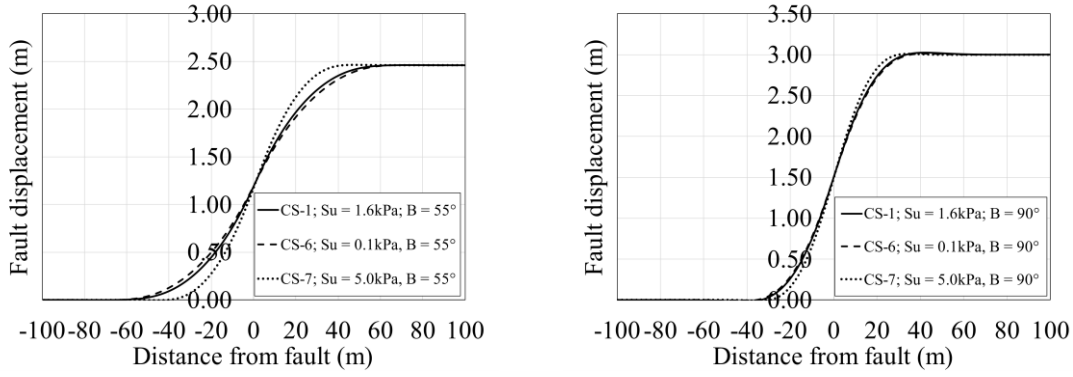

(a)

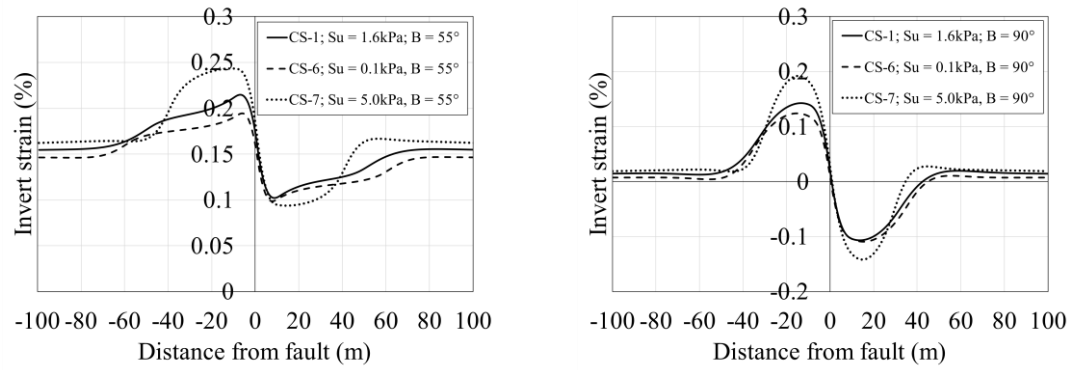

(c)

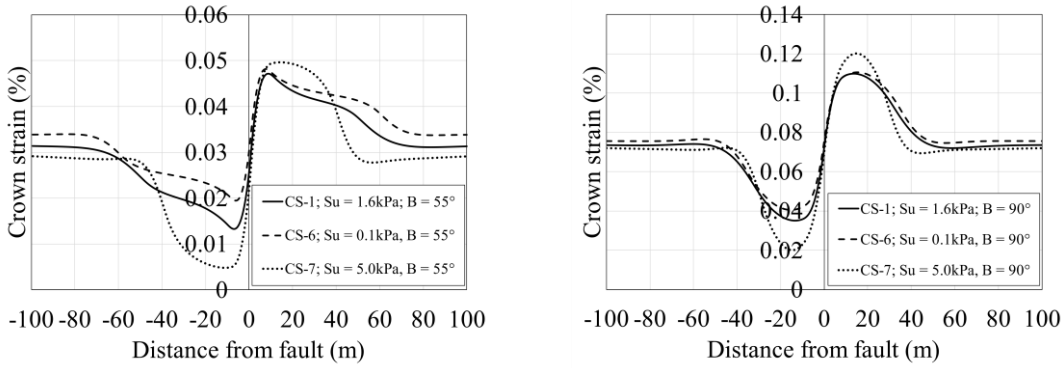

(c)

Figure 6-16. Backfilling soil strength effect on the deformation and axial strain of the pipeline, (a) distribution of vertical displacement, (b) invert axial strain, (c) crown axial.

6.4.5. The influence of pipe diameter

The capacity and deformability of a pipeline are directly influenced by its diameter. This section aims to investigate the impact of pipeline diameter on the interaction between the pipeline, backfill, and trench soil. Two pipelines with outer diameters of 0.9144 m and 0.95 m were considered, corresponding to D / t ratios of 33.87 and 35.18, respectively. Both pipelines have the same thickness (t = 0.027 m). The Pipeline with a diameter of 0.9144 m can withstand a maximum internal pressure of 22.5 MPa and has a critical compressive strain of 2.24%. The pipeline with a diameter of 0.95 m, on the other hand, can withstand a maximum internal pressure of 22.5MPa and has a critical compressive strain of 2.19%. The soil spring properties for these two case studies are presented in Figure 6-17.

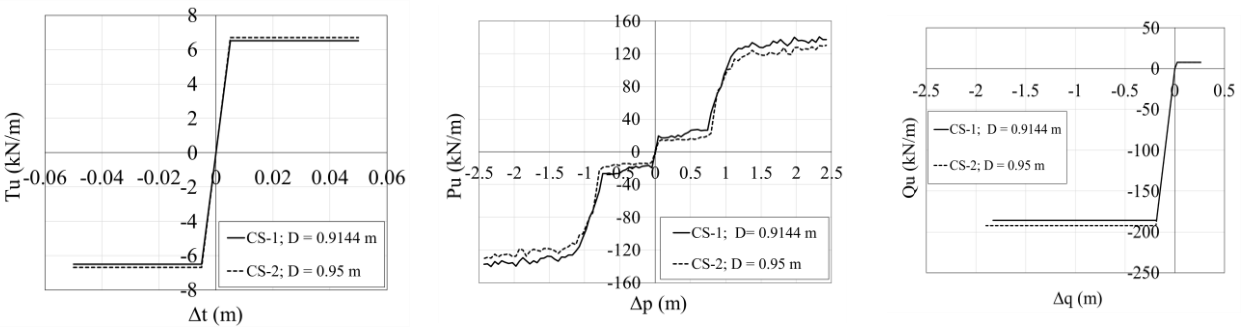

(a) (b) (c)

Figure 6-17. Soil spring characteristics of case studies with different pipeline diameters (a) axial, (b) horizontal, and (c) vertical soil springs.

Figure 6-18(a) depicts the deflection curve of the buried pipeline under different diameter-thickness ratios and fault intersection angles. The Y-axis denotes the vertical displacement of the fault, and the X-axis represents the distance from the fault. It is worth noting that the deflection curve remains constant at point C regardless of the diameter value. However, Figure 6-18(a) shows that the point C is located at a higher vertical position (1.5 m) when the fault intersection angle is 90°.

Figure 6-18(b) and (c) illustrate the maximum axial strain at the invert and crown points, indicating that the most vulnerable section of the pipeline is the one with a larger diameter (D = 0.95m). The results indicate that the maximum compressive strain experienced by the buried pipeline is below the critical strain value. Additionally, as the fault intersection angle increases, the axial strain decreases, even though the vertical displacement is greater compared to that of the fault with a 55° intersection.

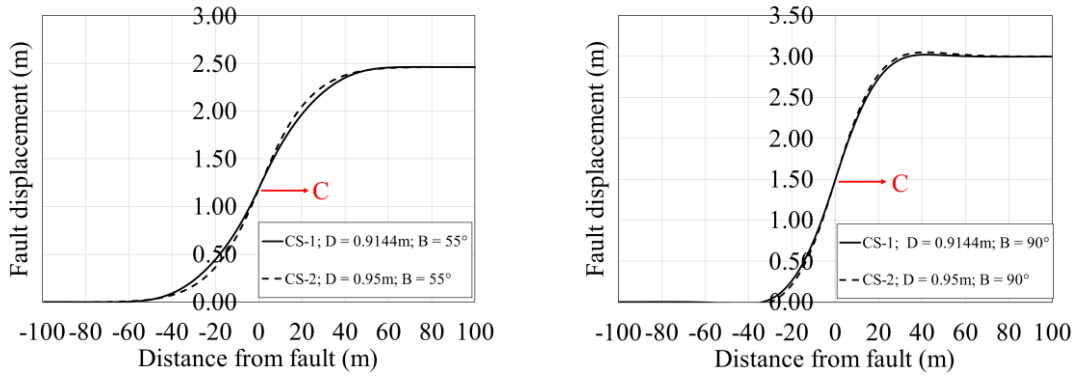

(a)

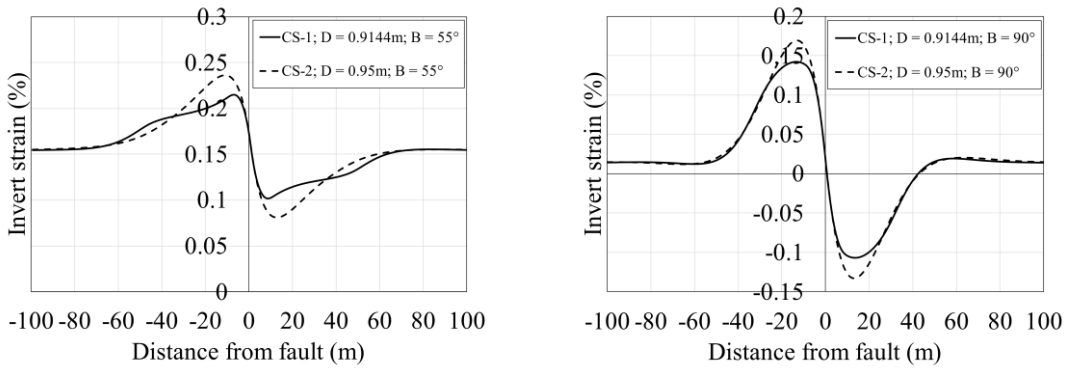

(b)

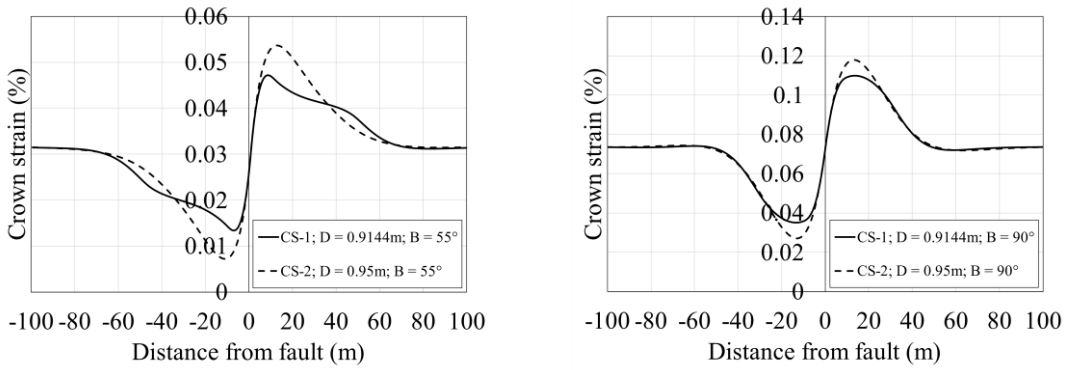

(c)

Figure 6-18. pipe diameter effect on the deformation and axial strain of the pipeline, (a) distribution of vertical displacement, (b) invert axial strain, (c) crown axial strain.

6.4.6. Pipeline surface roughness

The impact of pipeline surfaces was considered in three p-y curves obtained from the CEL analysis. It should be noted that the axial and vertical soil springs are determined using force-displacement equations in ALA, which already account for the effect of surface roughness. Consequently, there are no changes in these curves for the three case studies mentioned above. The force-displacement curves presented in Figure 6-19 are utilized to derive the deflection and axial strain curves were derived for the pipeline under a strike-slip fault.

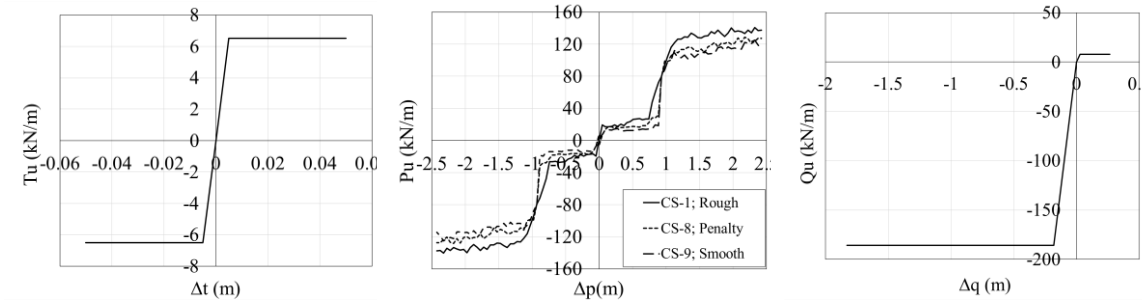

(a) (b) (c)

Figure 6-19. Soil spring characteristics of case studies with different pipeline surface roughness (a) axial, (b) horizontal, and (c) vertical soil springs.

Figure 6-20 presents the FE analysis results. In Figure 6-20(a), it can be observed the deflection curves remain unchanged when the fault crossing angle is 90 degrees. However, a small reduction in the deflection and axial strain curves can be seen when the surface roughness is smooth. The axial strain curves in Figure 6-20 show that near the fault line, the use of rough contacts results in higher axial invert and crown strains compared to the penalty and smooth contact. However, at a distance approximately 2/3 of the length of large

deformation area from the fault line, the axial strain induced by a model with smooth contact is larger than others.

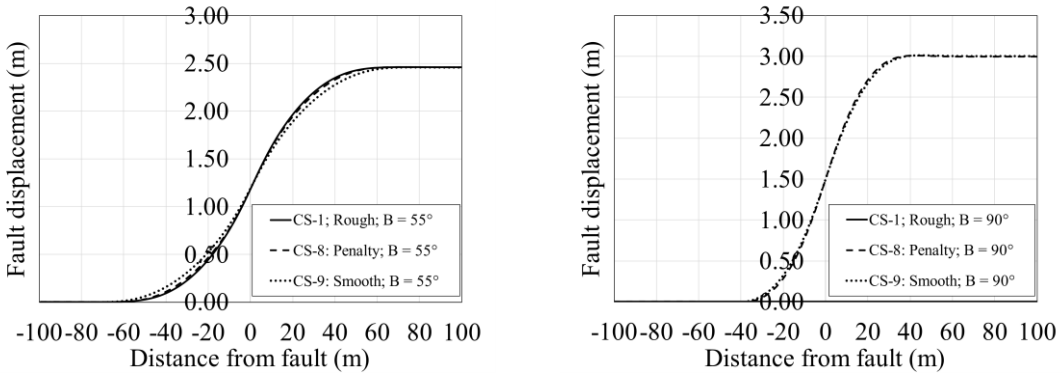

(a)

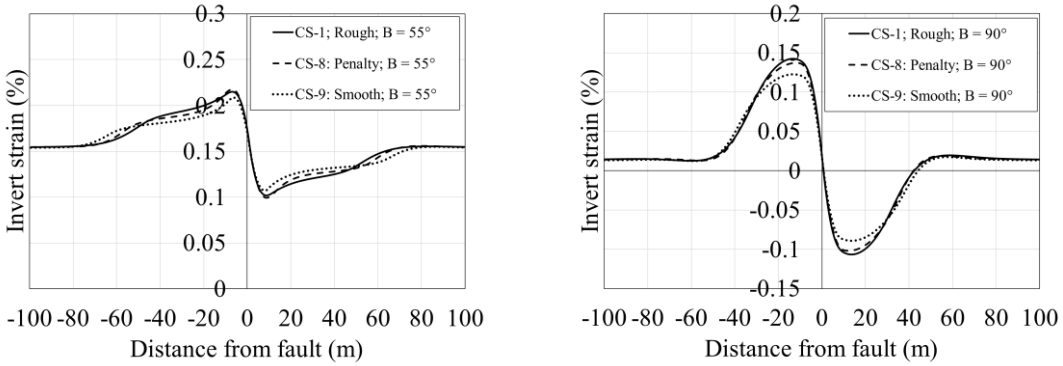

(b)

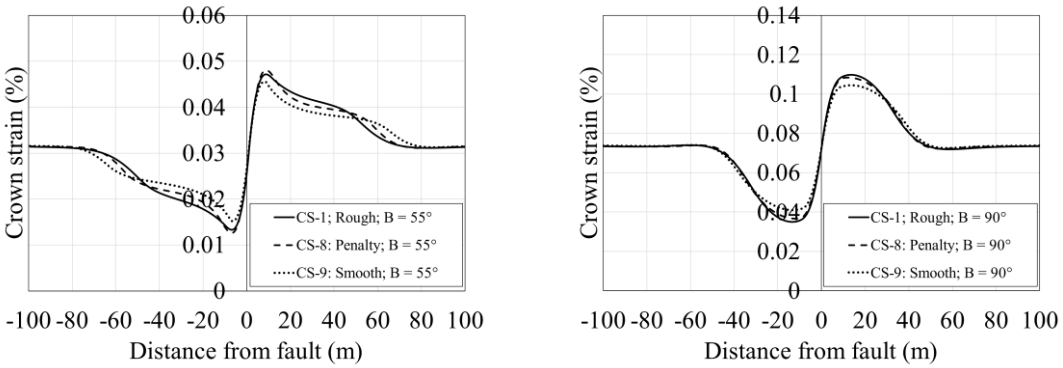

(c)

Figure 6-20. Surface roughness effects on the deformation and axial strain of the pipeline, (a) distribution of vertical displacement, (b) invert axial strain, (c) crown axial strain.

6.5. Conclusions

The pipeline-backfill-trench interaction under strike-slip faulting was investigated through parametrical study using a decoupled beam-spring FE model. The 3D beam-spring model, despite simplifying complexity to prioritize computational efficiency and user-friendliness, serves specific purposes effectively. Nevertheless, it may not be appropriate for all analysis conditions and usually necessitates extra adjustments and the use of specialized material models to account for creep effects. In spite of these limitations, the results of the methodology presented were in excellent agreement with the recent analytical method results in the case of pipe-backfill-trench interactions under strike-slip fault conditions. Both material and geometry nonlinearity were considered in this study. Parameters that were considered in this study were strain-softening and soil shear strength, burial depth, initial embedment, backfilling material strength, pipe diameter, and pipeline surface roughness. Based on these parametric studies the following results are made:

- The use of backfilling soil decreases the probability of local buckling decreases.
- When strain-softening and linear shear strength are considered by soil, the induced axial strains in the pipeline decrease.
- The use of stiffer backfilling material does not significantly affect the location of the maximum axial strain.
- Higher initial embedment's result in higher axial strain on the pipeline.
- As the burial depth increases, the axial strain in the pipeline also increases.

References

ABAQUS, ‘User's Manual’, Version 6.11. Dassault Systemes. Hebbit, Karlsson and Sorensen Inc, 2011.

American Lifelines Alliance, Guidelines for the Design of Buried Steel Pipe, American Society of Civil Engineers, US, 2001.

Asgarihajifirouz M, Dong X, Shiri H. Assessment of the Response of Trenched–Backfilled Pipelines to Strike-Slip Faults: An Analytical Approach. Geosciences. 2023 Jan 31;13(2):47.

ASME, Gas Transmission and Distribution Piping Systems, American Society of Mechanical Engineers, 2007.

A.M. Gresnigt, Plastic design of buried steel pipelines in settlement areas, Heron 31 (1987) 1–113.

Canadian Standards Association, Oil and Gas Pipeline SystemsCSA Z662-07, Canada 2007.

Rofooei FR, Jalali HH, Attari NK, Alavi M. Full-scale laboratory testing of buried pipelines subjected to permanent ground displacement caused by reverse faulting. In Proceedings of the 15th World Conference on Earthquake Engineering, Lisboa, Portugal 2012 Sep 24 (pp. 24-28).

Rofooei FR, Jalali HH, Attari NK, Kenarangi H, Samadian M. Parametric study of buried steel and high density polyethylene gas pipelines due to oblique-reverse faulting. Canadian Journal of Civil Engineering. 2015;42(3):178-89.

Honegger DG, Gailing RW, Nyman DJ. Guidelines for the seismic design and assessment of natural gas and liquid hydrocarbon pipelines. InInternational Pipeline Conference 2002 Jan 1 (Vol. 36207, pp. 563-570).

IITK-GSDMA. 2007. Indian Institute of Technology Kanpur, IITKGSDMA guidelines for seismic design of buried pipelines. Gandhinagar: Gujarat State Disaster Management Authority.

Liu X, Zhang H, Chen Y. Strain Prediction for X80 Steel Pipeline Subjected to Strike-Slip Fault Under Compression Combined With Bending. InPressure Vessels and Piping Conference 2015 Jul 19 (Vol. 56987, p. V005T09A006). American Society of Mechanical Engineers.

Liu X, Zhang H, Han Y, Xia M, Zheng W. A semi-empirical model for peak strain prediction of buried X80 steel pipelines under compression and bending at strike-slip fault crossings. Journal of Natural Gas Science and Engineering. 2016 May 1;32:465-75..

Karamitros DK, Bouckovalas GD, Kouretzis GP. Stress analysis of buried steel pipelines at strike-slip fault crossings. Soil Dynamics and Earthquake Engineering. 2007 Mar 1;27(3):200-11.

Karamitros DK, Bouckovalas GD, Kouretzis GP, Gkesouli V. An analytical method for strength verification of buried steel pipelines at normal fault crossings. Soil Dynamics and Earthquake Engineering. 2011 Nov 1;31(11):1452-64.

Kennedy RP, Williamson RA, Chow AM. Fault movement effects on buried oil pipeline. Transportation Engineering Journal of ASCE. 1977 Sep;103(5):617-33.

M.J. O'Rourke, X. Liu. Seismic Design of Buried and Offshore Pipelines,Multidisciplinary Center for Earthquake Engineering Research, University at Buffalo, Buffalo New York. 2011.

Newmark NM, Hall WJ. Pipeline design to resist large fault displacement. In Proceedings of US national conference on earthquake engineering 1975 Jun 18 (Vol. 1975, pp. 416-425).

Ramberg W, Osgood WR. Description of stress-strain curves by three parameters. 1943 Jul 1.

Takada S, Hassani N, Fukuda K. A new proposal for simplified design of buried steel pipes crossing active faults. Earthquake engineering & structural dynamics. 2001 Aug;30(8):1243-57.

Trifonov, O.V. and Cherniy, V.P. A semi-analytical approach to a nonlinear stress–strain analysis of buried steel pipelines crossing active faults. Soil Dynamics and Earthquake Engineering. 2010; 30(11), pp.1298-1308.

Vazouras P, Karamanos SA, Dakoulas P. Finite element analysis of buried steel pipelines under strike-slip fault displacements. Soil Dynamics and Earthquake Engineering. 2010 Nov 1;30(11):1361-76.

Vazouras P, Karamanos SA, Dakoulas P. Mechanical behavior of buried steel pipes crossing active strike-slip faults. Soil Dynamics and Earthquake Engineering. 2012 Oct 1;41:164-80.

Vazouras P, Dakoulas P, Karamanos SA. Pipe–soil interaction and pipeline performance under strike–slip fault movements. Soil Dynamics and Earthquake Engineering. 2015 May 1;72:48-65.

Wang LR, Yeh YH. A refined seismic analysis and design of buried pipeline for fault movement. Earthquake engineering & structural dynamics. 1985 Jan;13(1):75-96.

Chapter 7

Conclusions and recommendations

7.1. Overview

In this research project, a new decoupled methodology was developed by combining the advanced continuum modelling of the pipeline-backfill-trench wall interaction using CEL analysis and a 3D beam-spring pipeline model to overcome the limitations of existing models. First, a Coupled Eulerian-Lagrangian (CEL) model was used for LDFE analysis of the trenched/backfilled pipeline in a 2D planar fashion to obtain the lateral soil resistance involving pipeline-backfill-trench interaction effects. Later, the extracted lateral soil resistance for various displacements was transferred to a 3D beam-spring pipeline structural model to obtain the pipeline response to the fault-induced large displacements. The results were compared with analytical and Lagrangian models to assess the improved model performance. The study contributed to a deeper insight into this challenging engineering problem and resulted in a set of key observations that are shortly listed below:

- The study showed the significance of incorporation of the pipeline-backfill-trench wall interaction effects into the structural analysis of pipelines attacked by fault. It was observed that pipeline structural response is rather dependent on pipeline-backfill-trench interaction than the backfill stiffness alone.
- Analytical solutions were found to be improvable by incorporation of the trenching/backfilling effects into the structural response. The enhanced analytical solutions can be remarkably beneficial in performing design optimization studies and initial analysis at the construction planning stages of the project. The analytical

results showed that if it is inevitable that a pipeline crosses a fault line, the distributed axial strain and deflection may be reduced by using a trench containing softer material.

- The 3D Lagrangian analysis showed a significant difference in the bending deformation and strain of the spiral-welded pipeline under different soil conditions. The soil density and stiffness were the most influential factors in determining how the pipeline responded to the strike-slip fault. In granular soils, an increase in soil density led to earlier local buckling of the pipeline compared to a pipeline buried in loose sand due to a greater interaction between the soil and the pipeline.
- It was observed that the helical angle in spiral-welded pipelines considerably influences the nonlinear response of the pipeline. The results showed that depending on the soil type and the fault crossing angle, any helical angles between 40°- 45° would be appropriate to reduce the axial and compressive strain through the spiral-welded pipeline.
- The 2D Coupled Eulerian-Lagrangian analysis showed that the mobilized lateral soil resistance against the laterally displaced pipeline is significantly affected by the pipeline-backfill-trench wall interaction, which intern is governed by the trench configuration.
- The 2D CEL analysis showed the significance of the incorporation of strain-softening effects that result in enlarging of the mobilized soil volume and decreasing the lateral soil resistance.
- The developed decoupled analysis method was found effective in resolving the existing limitations of the pipeline-fault interaction analysis including the

computational burden, challenges in simulating ground movement in LDFE analyses, and inadequate modelling of the pipeline-backfilling-trench soil interaction, etc.

- The decoupled analysis showed that the probability of local buckling failure of in the buried pipeline was significantly reduced when subjected to a strike-slip fault displacement of a few pipe diameters. Furthermore, the consideration of strain-softening effect resulted in decreasing in the axial strain of the pipeline.
- The study resulted in developing a set of analysis tools particularly the decoupled method that can be effectively used in daily engineering practice by the pipeline industry to incorporate the pipeline-backfill-trench interaction effects into the pipeline-fault interaction analysis. These tools have combined the accuracy of the continuum CEL analysis and the simplicity of the beam-spring structural models.

7.2. Recommendations for future studies

The developed decoupled analysis for 3D modeling of the pipeline-fault interaction with incorporation of trenching/backfilling effects is new its kind. The following recommendations are made to improve the developed model in the future studies: Incorporation of the remolding and consolidation effects into the 2D CEL analysis of lateral pipeline-backfill-trench wall interaction. This will enable capturing time-dependant response of the soil for the cases when the ground displacement happens gradually and slow enough to have partially drained or drained condition.

- In the current study, an implicit approach was used to incorporate the trenching/backfilling effect into the analytical methods. Mathematical

improvement and re-solving of the differential equations are recommended in analytical solution to enable proposing a set of explicit equations for incorporation of non-linear hyperbolic pipeline-backfill-trench wall interactions.

- Performing 3D large scale experimental studies with accurate modelling of the trenching/backfilling configurations are recommended for a more accurate validation and improvement of the developed model.
- The performance of the developed decoupled method is suggested to be examined in a wider range of applications including the upheaval buckling of trenched pipelines in different fault crossings.
- To further assess the performance of the decoupled method and improve its functionality, it is recommended to redo the current fault-crossing analysis using the sub-modelling module of ABAQUS, where the 2D CEL analysis of lateral pipeline-backfill-trench interaction can be defined as a local sub-model linked to the global 3D beam-spring model.